MANUFACTURING SYSTEM PARAMETER OPTIMIZATION FOR SPECIFIED SURFACE PROPERTIES OF THE MACHINED PART

By

DONG YOUNG JANG

A DISSERTATION PRESENTED TO THE GRADUATE SCHOOL
OF THE UNIVERSITY OF FLORIDA IN PARTIAL FULFILLMENT
OF THE REQUIREMENTS FOR THE DEGREE OF
DOCTOR OF PHILOSOPHY

UNIVERSITY OF FLORIDA

1990

ACKNOWLEDGEMENTS

The author thanks God for his blessing and grace to my life and wishes to extend his gratitude to the many individuals who contributed to the completion of this work. In particular, he wishes to thank his advisor, Dr. Ali Seireg, for his advice, guidance and creativity throughout the course of the research. He would like to express his appreciation to the other members of his supervisory committee, Dr. G. Sandor, Dr. G. Matthew, Dr. U. Kurzweg and Dr. B. Edwards, for their help and encouragement. He would like to thank Dr. M. Jaeger for his help. Additionally, he wishes to thank Siva, Chen and Tarng for their good friendship. Special thanks are given to the author's family and to his wife, Hyemin, for her love, confidence and understanding. Finally he wishes to thank his son, Kukjin.

TABLE OF CONTENTS

page

ACKNOWLEDGEMENTS ii

LIST OF TABLES vi

LIST OF FIGURES vii

ABSTRACT x

CHAPTER 1 INTRODUCTION 1

CHAPTER 2 LITERATURE REVIEW 6

2.1 Cutting Force Relations 6
2.2 Surface Residual Stress 8
2.3 Surface Roughness in the Cutting Process 10
2.4 Surface Accuracy Models 11
2.5 Tool Failures 14
2.6 Adaptive Control in Machining Operation 16

CHAPTER 3 DYNAMIC MODEL OF SURFACE ROUGHNESS GENERATION 19

3.1 Introduction 19
3.2 Model Predicting Surface Error and Surface Roughness 21
3.2.1 Basis for Predicting Surface Error and Surface Roughness 21
3.2.2 Dynamic Cutting Force Model 22
3.2.3 Evaluation of Cutting Stiffness 31
3.2.4 Dynamic Cutting Model for Surface Generation 38
3.3 Prediction of Surface Roughness and from the System Response 46
3.4 Results 47
3.4.1 Numerical Example 47

3.4.2 Development of a Generalized Surface Roughness Equation 51
3.5 Conclusions 55

CHAPTER 4 PREDICTION OF HEAT GENERATION IN THE CUTTING PROCESS 60

4.1 Introduction 60
4.2 Heat Generation in the Cutting Process 62
4.2.1 Heat Generation in the Primary Shear Plane 64
4.2.2 Heat Generation in the Tool/Chip Interface 68
4.2.3 Heat Generation in the Tool-Workpiece Contact 73
4.3 Numerical Calculation 78
4.4 Conclusions 82

CHAPTER 5 PREDICTION OF SURFACE RESIDUAL STRESS 83

5.1 Introduction 83
5.2 Residual Stress Prediction Model 86
5.3 Stress Analysis during Cutting 88
5.3.1 Perfectly Sharp Edge Cutting Tool Effect 88
5.3.2 Effect of Tool Radius 92
5.3.3 Effect of Flank Wear on the Cutting Forces 95
5.3.4 Thermal Stresses at the Tool-Workpiece Interface 96
5.4 Calculation of Residual Stress in the Machined Surface 99
5.4.1 Procedure of Residual Stress Formation 99
5.4.2 Calculating Procedure of Residual Stress 100
5.5 Numerical Examples 104
5.6 Conclusions 108

CHAPTER 6 OPTIMIZATION ALGORITHM FOR USE IN ADAPTIVE CONTROL OF THE MACHINING PROCESS 114

6.1 Introduction 114
6.2 Formulation of the Optimization Model 117
6.2.1 Constraints Identification and Mapping onto the Decision Space 118
6.3 Optimization Procedure 130
6.4 Numerical Calculations 132
6.4.1 Cutting Conditions 132
6.4.2 Tool Fracture Constraints 132
6.4.3 Tool Plastic Deformation Constraints 133
6.4.4 Tool Wear Failure Constraints 133
6.4.5 Surface Integrity Constraints 134
6.5 Conclusions 142

CHAPTER 7 SUMMARY, CONCLUSIONS AND RECOMMENDATIONS. 157

7.1 Summary 157
7.2 Conclusions 159
7.3 Recommendations 160

APPENDIX A MERWIN-JOHNSON METHOD 162

APPENDIX B STATIC ANALYSIS OF SIMPLE SPINDLE MODEL 166

REFERENCE LIST 168

BIOGRAPHICAL SKETCH 176

LIST OF TABLES

Table	page
3.1 Constants for the calculation of cutting forces	37
3.2 List of test data	48
3.3 Simulation results	49
6.1 Softening points of tool materials and melting points of workpiece materials	127
6.2 Results of case 1	137
6.3 Results of case 2	138
6.4 Results of case 3	139
6.5 Results of case 4	140
6.6 Results of case 5	141
6.7 Results of case 6	142
6.8 Results of case 7	143
6.9 Results of case 8	143

LIST OF FIGURES

Figure page

3.1 Schematic view of the cutting zone 25

3.2 Source of damping 29

3.3 Cutting resistance variation with cutting speed 33

3.4 Diagram of the cutting zone 35

3.5 Dynamic model of the system 39

3.6 Simple spindle model 41

3.7 Correlation between Eq. (3-45) and (3-44) 52

3.8 Relationship between the response surface and cutting parameters for turning 53

3.9 Surface geometry generated from the simulation along the axis of workpiece 54

3.10 Values for parameter C in Eq. (3-47) 57

3.11 Coefficient value of K_1 and K_2 from the equation (3-47) 58

3.12 Coefficient value of K_3 and K_4 from the equation (3-47) 59

4.1 The geometry of orthogonal cutting 65

4.2 Variation of β with R$\tan\varphi$ 67

4.3 Flank wear development curves 72

4.4 Effect of flank wear land length on temperature distribution in workpiece and chip 74

4.5 The variation of cutting force with wear land for mild steel at 225 ft/min 77

4.6 Isothermal curves according to varying feed rate and cutting speed at the primary deformation zone 80

4.7 Isothermal curves according to varying feed rate and cutting speed at the tool and interface zone 81

5.1 Diagrammatic representation of residual stress generation 85

5.2 Force components acting in the lower boundary of the primary deformation zone 89

5.3 Appearance of a compressed zone in the surface layer 91

5.4 Elliptically distributed stresses in the cutting zone 94

5.5 Loading and unloading process 99

5.6 Residual stress distribution compared with experimental data from Ref. [100] 106

5.7 Residual stress variation with feed 109

5.8 Residual stress variation with depth of cut 110

5.9 Residual stress variation with speed 111

5.10 Residual stress variation with tool radius 112

6.1 Basic model of adaptive system 116

6.2 Acting force diagram in the tool face 119

6.3 Compressive yield strength of tool material against temperature 124

6.4 Results of case 5 145

6.5 Results of case 6 148

6.6 Results of case 7 151
6.7 Results of case 8 154

Abstract of Thesis Presented to the Graduate School
of the University of Florida in Partial Fulfillment of the
Requirements for the Degree of Doctor of Philosophy

MANUFACTURING SYSTEM PARAMETER OPTIMIZATION FOR SPECIFIED SURFACE PROPERTIES OF THE MACHINED PART

By

Dong Young Jang

May, 1990

Chairperson: Dr. Ali Seireg
Major Department: Mechanical Engineering

Technological developments make it possible that very efficient machining conditions can be implemented for the purpose of increasing the productivity of machine tools. However, such machining conditions may cause undesirable surface properties which have recently become the most critical quality factor in terms of reliability and strength-to-weight ratio. The surface condition is generally characterized by surface integrity, which is defined by the mechanical, metallurgical, chemical and topological states. It plays an important role in all areas of tribology and precision manufacturing and is directly related to the reliable performance or failure of mechanical components.

In this thesis, an optimum design methodology is developed for selecting the design variables of a lathe and the machining parameters which maximize the productivity of the system, while providing the required dimensional accuracy and

surface specifications for the machined parts. Computer-based simulation models for predicting the surface roughness and residual stresses are developed. The models take into consideration the dynamic interaction between the tool and the workpiece. The simulation results show good agreement with published experimental data.

Regression analysis is used to develop generalized equations for predicting surface roughness in turning, covering the practical range of cutting conditions and machine tool dynamic characteristics. Regression equations are also developed for predicting the surface residual stress, the plastically deformed depth and the maximum tensile stress as a function of the cutting parameters and cutting tool edge radius.

The relationship between the temperature in the cutting zone and the cutting parameters is developed and used to define the constraints on tool wear in the optimization procedure.

The optimization algorithm can be readily used in the adaptive control of the machining process. It maximizes the metal removal rate and takes into consideration tool wear and surface integrity based on the physical behavior of the machining process.

CHAPTER 1
INTRODUCTION

One of the most important manufacturing processes used in the production of mechanical components is metal cutting. This involves the systematic removal of layers of material from a workpiece in the form of chips by a wedge-shaped cutting tool for the generation of a new surface. In this machine tool operation, some forces always come into play. These forces may be either an action intentionally provided for shaping the part (as in mechanical working) or a reaction as a result of the relative motion between the job and the tool (as in metal cutting). In both cases, however, the shaping of the job is a consequence of its plastic deformation.

It is well recognized that this process can introduce into the surface region (which includes both the actual surface and subsurface) of a workpiece a wide variety of geometrical and metallurgical alternations that make it different in nature from the bulk material. This surface region is called the surface layer, which is the layer of material bounded by the actual geometrical surface of the machined component. It represents the part of the material--from the geometrical surface inward--where the physical and sometimes the chemical properties are altered as a result of the machining process.

It is the aim of manufacturing to produce parts with prespecified quality. The quality of a product is evaluated according to

a) the degree of reliability with which it functions and fulfills its tasks,

b) its total life or service life, i.e., the time during which the useful features of the machine do not change,

c) outer appearance, and particularly the so-called surface finish,

d) the suitability and the quality of material of which the product is made.

The surface integrity (defined below) has recently become the most important quality factor as a result of the advances made in alloy developments and heat treatment which led to the production of materials with increased strength and strength-to-weight ratios. In turn, this has led to a reduction in the section thickness of many components used in weight-sensitive situations and a corresponding increase in the surface area-to-volume ratio. In addition, advances in engineering design in recent years have necessitated the use of new and existing materials under increasingly severe service conditions with respect to stress, temperature, and environment. These trends dictate that increased attention must be paid to the possibilities of severe failures produced by fatigue, creep, and stress corrosion cracking. Such failures invariably start at the surface of components and depend to a great extent on the condition of the surface.

The surface condition of machined components is characterized by the so-called surface integrity, which is generally defined by its mechanical, metallurgical, chemical and topological states. It is interpreted as including those elements which describe the actual structure of both the surface and subsurface.

The physical properties of the machined surface are affected by

a) microstructure or fibrous structure as well as its distribution and size within the surface layer,

b) plastic deformation or compression and the resulting changes of hardness and strength, and

c) residual stresses and their distribution within the surface layer and in the bulk material.

Changes of the bulk material properties and of the surface layer formation are attributed to

a) the stress field created by the cutting forces,

b) the temperature field generated during the cutting operation,

c) the external and internal friction during the machining process.

The geometrical properties of the machined surface are characterized by

a) surface irregularities such as surface roughness and waviness, and

b) geometrical structure of the surface of the part including tool mark array and possible surface defects such as scratches, cracks, chipping and gaps.

The geometric properties of the machined surface result from

a) geometrical and kinematic reproduction of tool point shape in the material being machined (taking into account system vibrations),

b) external friction between tool edge and workpiece material,

c) built-up edge formation in the machining of certain materials within certain ranges of machining conditions.

If the surface of a component possesses integrity, then it is unimpaired or enhanced by the action of the machining process used in its fabrication. Conversely, if integrity is lacking, then surface and subsurface damage has occurred as a result of the machining process as explained in the previous section.

Therefore, the design engineer must have complete information on the characteristics of the surface region of a component as produced in order to ascertain whether or not a particular machining process adversely affects the quality of the surface region. In addition, the effect of machining on the mechanical

properties of the surface layer must be understood so that remedial machining procedures can be introduced if necessary.

Generally, the cutting variables such as cutting speed, feed rate and depth of cut, work material, tool material, tool geometry and lubricant have direct effects on the surface conditions of the machined parts. Therefore, the relationships between the state of a component after machining, or its technological quality and the cutting variables should be identified in order to insure that the specified surface conditions are met.

Machining conditions for a specified purpose are generally selected based on empirical approaches formed by past experience, experimental data, or trial and error. The empirical approach has a number of drawbacks, the most serious among them are

a) The knowledge gained about the process may not provide for a complete understanding of the mechanics of the process. A particular process may be observed, but it is difficult to identify what characteristics or variables in the process are responsible for the observed response.

b) It is difficult to extrapolate data from one set of conditions. Experiments must be run for every combination of tool, workpiece, and cutting condition that is of interest. Laboratory testing is time consuming and expensive.

A different approach may be taken by developing mathematical models for the responses of interest based on the mechanics of the cutting process. This requires that the model builder carefully considers the mechanics of the process and the interaction between the significant parameters affecting it and decides what assumptions may be made to simplify the analysis of the process. Once these models

are developed, the effect of varying one or more of the process variables on the response may be studied without actually performing experiments. The models can also be used for the process design, which includes the selection of the machining conditions to satisfy certain constraints or optimize some performance index.

In this thesis, a design methodology is developed for selecting the design variables of a lathe and the machining parameters which maximize the productivity of the system, while providing the required tolerance and specifications for the machined parts. To attain the purpose of this research, analytical models are developed for the dynamic cutting forces, dynamic surface roughness and surface residual stress distribution for the turning process. Thermal effects on tool wear and residual stress distribution are considered, and the Merwin-Johnson theory is used to calculate the plastic stress and residual stress distribution inside the workpiece. In the formulation of the dynamic cutting forces and dynamic surface roughness, the regenerative cutting effect is considered.

CHAPTER 2
LITERATURE REVIEW

A review of the literature pertaining to the cutting forces, dynamics and optimization of the cutting process as related to this study can be divided into six sections: cutting force relations for the turning process, surface roughness, surface accuracy, surface residual stress, tool failure, and adaptive control of the cutting operation.

2.1 Cutting Force Relations

Reliable knowledge of cutting forces and cutting power makes it possible to properly design machine tools and to choose cutting conditions for a given machining process. Cutting force measurement is an essential means for evaluating some of the basic elements of developing the cutting theory such as chip formation, kinematics and kinetics of the cutting process, frictional phenomena between the tool and workpiece, and metallurgical changes within the tool or workpiece. The cutting force must be able to overcome the resistance of the material to elastic and plastic deformation, the frictional resistance, and the cohesive resistance during the creation of a new material surface.

There have been many attempts in the past at providing a suitable model for predicting the cutting forces from process parameters and work material properties [1]. Most of these used empirical and statistical methods and showed that the cutting forces are related to the chip area on the tool.

$$F_c = C_c \cdot f^{mc} \cdot d^{nc} \qquad (2\text{-}1)$$

$$F_t = C_t \cdot f^{mt} \cdot d^{nt} \tag{2-2}$$

$$F_f = C_f \cdot f^{mf} \cdot d^{nf} \tag{2-3}$$

where F_c is the cutting force,

F_t is the thrust force which influences the surface accuracy and roughness of the machined part,

F_f is the feed force, and

f is the feed and d is the depth of cut.

The values of the parameters C, m and n vary with tool geometry and work material. Kronenberg [1] derived an empirical cutting force equation as follows.

$$F_c = \frac{C_c(G/5)^{g_p}(1000 \cdot f \cdot d)^{1-z_p}}{1000} \tag{2-4}$$

(pound-force)

where

G = slenderness ratio = d/f and

C_c, g_p and z_p = empirical constants.

The statistically established relationships between average values of the cutting force components in the tool system are

a) in turning steel:

$$F_t = (0.4 - 0.6) \cdot F_c \tag{2-5}$$

$$F_f = (0.2 - 0.3) \cdot F_c \tag{2-6}$$

b) in turning cast iron:

$$F_t = (0.3 - 0.6) \cdot F_c \tag{2-7}$$

$$F_f = (0.15 - 0.3) \cdot F_c \tag{2-8}$$

K. Nakayama [2] proposed a theoretical cutting force equation using the shear stress on the shear plane, the chip hardness and the shear angle calculated from the chip thickness ratio. E. Usui and A. Hirota [3] proposed a theoretical

method for predicting the three components of the cutting forces from two dimensional experiments. Nakayama and Ari [4] proposed a semi-empirical approach for calculating the cutting resistance. In this work, Nakayama and Ari's approach will be followed to estimate the cutting resistance which will be used to derive the dynamic cutting forces.

2.2 Surface Residual Stress

The residual stress distribution can greatly affect material stability and resistance to deformation. Fatigue life is generally increased by the presence of compressive residual stress and is decreased by the presence of tensile residual stress.

According to Osgood's definition [5], residual stress can be classified according to the way it is generated, that is, mechanical residual stress or contingent residual stress. Mechanical residual stresses are generated following inhomogeneous plastic flow caused by external forces or thermal gradients, glide, twinning, kinking, grain boundary effects, orientation effects, dislocations, etc. Contingent residual stresses are those stresses that are contingent on the coexistence of the source from which they are derived. They are produced by chemical or structural effects, alloying, precipitation, phase transformation, thermal effects causing relative expansion between different constituents, etc. The major difference between the two types of residual stresses is whether or not there are chemical or structural changes in the new material states.

Many studies on the residual stress distribution produced in the workpiece by a machining process have been carried experimentally and theoretically.

Henriksen [6] presented empirical data on residual stress distribution. He suggested that residual stresses are generated by the mechanical rather than the

thermal effects of the cutting process. The experimental method used is of the destructive type which is time consuming and does not reveal the loading history by which a particular residual stress pattern is produced. Okushima and Kakino [7] used the elastic-plastic finite element method to calculate the residual stress in the machined surface from the ploughing force and the temperature distribution in the workpiece. They speculated that at a cutting speed higher than 50 m/min, residual stresses are produced mainly by thermal effects. Lojczok [8] used shear and normal stress distribution exerted by the tool rake face on the chip to calculate the plastic deformation using the finite element method. The results showed poor agreement between the experimentally and analytically determined depths of the plastic deformation. Liu and Barash [9] found experimentally that the length of the shear plane in the chip formation correlated with subsurface deformation and residual stress formation. They suggested that it is reasonable to use the shear plane as a boundary and disregard the chip and hence, the complicated and unclear chip-tool interface boundary conditions, for finite element analysis. Barash and Schoech [10] suggested a slip-line model with varying yield stress which extends below the machined surface to account for the depth of the deformed layer. This model can place an upper bound on the depth of the strained hardened layer. Recently, an excellent review of previous work on the residual stresses has been given by Field, Kahles and Cammett [11]. In this study, Merwin and Johnson's model [12] will be used to calculate the stresses in the plastically deformed region and to obtain the residual stress distribution in the machined surface. Originally, the model was developed in order to explain the residual stress produced during rolling contact.

2.3 Surface Roughness in the Cutting Process

A machined surface is created as a result of geometric and kinematic reproduction of the tool edge as it moves relative to the workpiece. The surface roughness is a factor of great importance in the evaluation of workshop production. From a large number of theoretical analyses and experimental studies on the surface roughness of turning operations, it has been generally accepted that the cutting conditions such as cutting speed, feed rate, depth of cut and tool nose radius have effects on the surface geometry of the machined parts.

Several investigators have reported that the surface roughness improves with increasing cutting speed and tool nose radius and with decreasing feed [13-15]. Other researchers [16] have found that at slow speeds less than 75 fpm, discontinuous or semi-discontinuous chip and built-up-edge formation occurred which gave a poor surface finish. At speeds above 75 fpm, the built-up-edge size decreased and the surface finish improved. Of the factors influencing the surface roughness, the depth of cut was found to be have the least effect. This was found to confirm the findings of Sata [16].

The effect of tool wear was studied by Solaja [17] who showed an undulating type of surface finish-time (or wearland) curve. The surface deteriorated with cutting time and tool wear. Similarly, the principal cutting edge and Brinell hardness number of the workpiece material also affect the surface roughness [18].

In general, it appears that the ideal surface finish may be achieved when the cutting speed is increased sufficiently. Unfortunately this condition may not always be obtained in practice and theoretical values of surface finish derived from geometric analysis show considerable difference with the experimental values.

Theoretically, for a lathe with zero nose radius the peak-to-valley height, as shown by Chisholm [19] can be calculated as

$$h = \frac{f}{\tan C_s + \cot C_e} \tag{2-9}$$

where

C_s is the side cutting edge angle of tool and

C_e is the relief angle of tool.

For a radiused tool the peak-to-valley roughness in the case of small values of feed can be shown to be

$$h = \frac{f^2}{8 \cdot r_\beta} \tag{2-10}$$

where

r_β is the tool edge radius and

f is the feed rate.

Recently, statistical techniques developed by Box and Wilson have been applied to establish a predictive equation for the relationship between tool life or surface finish and cutting parameters [20,21].

2.4 Surface Accuracy Models

Machining accuracy is evaluated by considering the difference between the desired (nominal) dimensions and properties and those of the finished product. The smaller the machining errors, the greater is the accuracy.

Deflection of the tool and workpiece generates inaccuracies in the dimensions of the part produced, and have to be limited to acceptable tolerances. In the case of the turning operation, if the processing system is absolute by rigid, the part produced would be a perfectly accurate cylinder. However, it is virtually impossible to achieve this absolute rigidity and if an attempt is made to approach it, the cost involved would be too high.

Many investigations into the accuracy of the surface produced by turning have been made [22,23]. From the point of view of analysis, the different errors can be subdivided into random and variable systematic errors [24]. Deflections of the different parts of the processing system as a result of the operational cutting force are expected to produce variable systematic errors. This means that the extent of the error changes nonuniformly along the workpiece axis. Investigations of the non-uniformly variable error has been reported, but only the uncoupled effects of the cutting force were considered.

When machining cylindrical pieces, there exists a definite relationship between the compliance of the machine tool assemblies, which directly influences the relative positions of workpiece and tool, and the machining errors.

The following equations can be used to calculate the displacements in the direction of the cutting force acting on the spindle assembly (spindle axis displacement y_{sp}), tailstock assembly (displacement of tailstock center axis y_t), saddle assembly (y_s) and the elastic deformation of a constant diameter workpiece shaft (y_w), as a function of the tool position along the machined length between centers:

$$y = 2\,(y_{sp} + y_t + y_s + y_w) \qquad (2\text{-}11)$$

where

y_{sp}, y_t, y_s and y_w are functions of the position of the cutting force F,

$$y_{sp} = m_{sp} \cdot F\left(\frac{x}{l}\right)^2 \tag{2-12}$$

$$y_t = m_t \cdot F\left(\frac{l-x}{l}\right)^2 \tag{2-13}$$

$$y_s = m_s \cdot F \tag{2-14}$$

$$y_w = \frac{F \cdot (l-x)^2}{3 \cdot E \cdot I \cdot l} x^2 \tag{2-15}$$

where

E = Young's modulus

I = moment of inertia

l = workpiece length

m_{sp} = spindle compliance

m_t = tailstock compliance

m_s = saddle assembly compliance

Taking all these conditions into account yields the following equation:

$$y = 2F\left[m_{sp}\left(\frac{x}{l}\right)^2 + m_t\left(\frac{l-x}{l}\right)^2 + m_s + m_w x^2\right] \tag{2-16}$$

where

m_w = workpiece compliance = $(l-x)^2/(3 \cdot E \cdot I \cdot l)$

These equations are used to predict surface error and dimensional inaccuracies when the functional relationship is known between the compliances and the position of the load in relation to the origin of the reference coordinates.

2.5 Tool Failures

A tool material must fulfill two fundamental requirements: it must be resistant to brittle fracture and to plastic deformation when subjected to the cutting forces. If these requirements are met, the tool tip will maintain its integrity and resistance to wear becomes the primary concern.

The brittle failure of a tool is defined as the break-away of the tool edge. Published theoretical and experimental studies [25] show that the "dangerous" point where the tensile principal stress has its maximum value is located at the rake surface of the cutting tool. It is therefore expected that the most probable area where cracking and brittle failure begins is the rake surface region. Thermal stresses can play a significant role in the brittle failure of the working part of the tool. During interrupted cutting such as milling and hobbing, the value of the thermal stress is higher than in the case of continuous cutting such as turning and boring.

The effect of increasing cutting speed is not necessarily associated with increased cutting force and tendency to fracture. An increased cutting speed often results in a decrease in chip thickness and a corresponding decrease in cutting force [26]. Therefore, when employing tool materials of high wear resistance and limited fracture resistance, such as aluminum-based tooling, the solution to problems with tool fracture is often to increase the cutting speed.

Plastic deformation has been identified as a major mode of failure for high-speed steel and carbide tools [27]. This effect is directly related to the cutting temperature and the melting point of the tool material.

When machining aluminum based alloys at any speed, extreme cutting temperatures are usually not encountered because of the high thermal conductivity of aluminum. The maximum cutting speed for cemented carbides will be limited by

this effect in the machining of steel and exotic alloys. Tungsten carbide-cobalt alloys melt at the Co-WC eutectic temperature of 1325 C degree, and the strength of cemented carbides falls off precipitously above 1100 C degree [28]. Therefore, plastic deformation is directly related to the cutting speed.

As the cutting speed increases, the stress near the tool edge probably doesn't increase and may decrease. However, the temperature will rise and consequently the yield stress of the tool material is reduced, and deformation starts when the tool is critically weakened. Therefore, to avoid plastic deformation, the temperature at the tool tip should be kept lower than some critical value.

Tool failures due to fracture or deformation are sudden and catastrophic. Such tool failures are disruptive in a conventional factory and can not be tolerated in an automated machining system. After the requirements for adequate fracture and deformation resistance are met, the failure of the cutting tool is determined by the progressive development of characteristic wear scars in two different regions on the tool. Wear will appear on the flank of the tool and also on the tool rake face, forming a characteristic cavity known as "crater." The flank wear is important because it has a direct effect on the quality of the product. The onset of crater wear produces a change in the mechanics of the cutting process (the effective rake angle and chip tool contact) and reduces the amount of force that the tool can withstand. Flank wear has a three-fold influence [29-31]. It causes

(a) change in the mechanics of the process,

(b) an increased tendency for chatter, and

(c) changes in the dimensions of the part.

The mechanism of tool wear can be classified into two main types, namely, mechanical and thermochemical. The mechanical type of wear includes the minute

breakdown or chipping of a cutting edge and the abrasion due to ploughing of the tool flank by hard constituents, including fragments of the built-up-edge from the work material as they are swept over the tool surface. This effect is dominant only when the cutting temperature is relatively low. Adhesive wear [30] predominates in the intermediate steady state stages. Chemical reaction between some constituents of the tool material and the material being cut, and diffusion between the tool and work material can generate thermochemical wear processes [31]. This effect causes accelerated wear in the regions where the temperature is higher than a critical temperature which is called "burn-out" temperature.

It has been considered that diffusion wear plays a major role in the crater wear formation [32]. This is attributed to the fact that a high tool-chip interface temperature occurs there. Evidence by Dawihl [33], Trent [34], Venkatesh [35], and others confirm that diffusion wear occurs on the tool rake face. Colding [36] presents evidence that a larger crater can weaken the tool and lead to total failure. In carbide tools, which are temperature sensitive, the predominant mechanism of wear is diffusion.

2.6 Adaptive Control in Machining Operation

In the machining process, adaptive control is defined as a system that allows machine tools equipped with sensors to detect a changing environment (e.g., tool wear, working material hardness, and chattering) and to take adaptive actions accordingly (e.g., change speed or feed).

Since 1960, adaptive control of machining has been analyzed using several different concepts which can be categorized into two groups: the adaptive control of optimization (ACO) and the adaptive control of constraints (ACC). The ACO

method utilizes the well-known Taylor equations (or extended ones) for the particular tool-workpiece combination and economic criteria to optimize the cutting parameters such as speed, feed and depth of cut [37-41].

The ACC method, realizing the difficulty associated with optimization (see below), focuses attention on maintaining a safe operation under certain physical constraints [42-49].

Many ACO and ACC systems have been investigated in various ways, including the use of minimum cost and maximum production rate [50] or maximum profit [51] as a performance index. Geometric programming is also used in the optimization problem with constraints [52,53] in multipass turning [54] and in multiple production stages [55]. However, there is no evidence to suggest that these methods have been successfully introduced in industry.

The first method, ACO, presents the problem that an extensive database is needed before it can be applied. Furthermore, the reliance on Taylor's tool life equation to obtain the optimum working condition makes it difficult to implement with on-line real time control. The second method, ACC, is also associated with problems such as how to justify the "objective" or criterion for the control strategy, in the general sense. Another difficulty is how to approach the global optimum working condition with incomplete knowledge of the relationships among the machining variables.

Consequently, there has been increased interest in recent years not only in advanced ACC systems [56-58], but also in more advanced ACO systems [48-49]. Yen and Wright [58] presented an in-depth analysis of the ACC concept, modelling the constraint parameters based on the physics of the cutting process. Another important aspect studied by Ulsoy, Koren and Rasumussen [57] is the stability of the

machine tool adaptive control system with respect to the controller algorithms, parameter estimation, and controller adaptation algorithms for variable gain AC systems. The cost of computing, storing, and transmitting information for controlling the machine tool, which are considered as part of the performance index in ACO, was calculated by Schlueter et al [49].

Summary:

The literature review presented in this chapter gives an overview of a representative example of the published research related to this study. Because of the wealth of publications on the subject and the relatively wide scope of the problem, it is understandably difficult to refer to all of the excellent publications which investigate in greater detail specific aspects of the study reported in this thesis.

CHAPTER 3
DYNAMIC MODEL OF SURFACE ROUGHNESS GENERATION

3.1 Introduction

Surface roughness plays an important role in all area of tribology. During the metal cutting operation, a machined surface is created as a result of geometric and kinematic reproduction of the tool point. The forces coming into play due to the relative motion between the tool and the workpiece cause deflections and vibrations between tool and workpiece, producing inaccuracies in dimensions and undesirable effects on the finished surface of the machined part.

Usually, the real mean total height of surface irregularities is greater, to a varying degree, than the theoretical value calculated according to reproduction formulae. The difference between the real and theoretical mean total height is attributed to the influence of physical and dynamic phenomena such as built-up edge, friction of cut surface against tool point and vibrations, etc. The influence of the built-up edge on the tool point is very distinct and this depends mostly on the cutting speed. Therefore, the influence of built-up edge on the finished surface can be reduced by choosing appropriate speeds and lubricants. When the effect of built-up edge is excluded, vibrations occurring during cutting generally exert a stronger influence on the accuracy and surface finish of a machined part.

Since the machine tool and workpiece are always compliant to some extent, deviations from the true shape can be expected, and these errors cause variations in the pre-set cutting conditions such as depth of cut. These variations give rise to

a fluctuating force which causes tool and workpiece to oscillate, performing a relative motion of some complexity. This unwanted relative vibration between tool and workpiece is called "chattering" and this phenomenon produces undesirable effects on the dimensional accuracy and the surface conditions of the machined part.

In this work, surface errors are defined to be deviations of the finished surface dimension from those of the surface that would be produced by a rigid machining system. These errors are considered to be macroscopic and caused by the deflection of the cutting tool and the workpiece system.

In addition to these errors, the relative vibrational effects on the finished surface are significant. These are called microscopic errors. In order to investigate the finished surface properties of a machined part, microscopic and macroscopic errors of the surface must be considered.

In this chapter, a generalized computer based simulation model for predicting surface roughness and surface error for any given condition which can take into consideration all the important parameters influencing the vibratory behavior of the machine tool-workpiece system is developed. The model considers the interaction between the vibratory characteristics of the workpiece/machine structure/cutting tool as well as the regenerative and damping effects in the dynamic cutting process. The contact point reactions where the cutting edge of the tool touches the surface of the workpiece are considered in the formulation of the dynamic cutting model. The forces which cause the dynamic instability between the tool and workpiece are assumed to be activated by disturbances in the cutting process and friction in the cutting zone.

3.2 Model Predicting Surface Error and Surface Roughness

3.2.1 Basis for Predicting Surface Error and Surface Roughness

An analysis of surface error and roughness in the turning operation requires an understanding of the surface generation mechanism. Because the surface is created by a wedge-shaped cutting tool, there always exist cutting forces between the tool and the workpiece. These forces cause deflection of the tool and workpiece, and when combined with the geometric shape of the tool point, generate roughness of the machined surface.

When the surface conditions are considered, the vibrations which occur between the tool and workpiece must be included, because the surface state gets worse due to these vibrations. The vibrations which are activated during the cutting operations may be generally divided into two groups:

- vibrations independent of the cutting process,
- vibrations dependent on the cutting process.

The second group of vibrations, which are related to the cutting process, include vibrations caused by variations in the cutting force and self-excited vibrations. In this analysis, the first group of vibrations will be negligible under the assumption of homogeneous cutting conditions.

In order to fully analyze the surface generation mechanism, it is necessary to develop mathematical expressions for

1) the cutting force system,
2) the dynamic characteristics of the cutting tool,
3) the dynamic properties of the workpiece, and
4) the dynamic characteristics of machine structure.

3.2.2 Dynamic Cutting Force Model

For formulating the dynamic cutting force model, the following assumptions are made:

(a) The surface finish in steady state machining operations will depend on the type of chip formation. In general, the continuous chip with no built-up edge is most desirable, since steady cutting conditions prevail, with little or no force fluctuations and their associated difficulties.

(b) The effect of the radius of curvature of the work on the chip geometry is negligible.

(c) The change in the uncut chip cross-sectional area induced by the nose radius is negligible.

(d) The regenerative effect will be used in calculating the dynamic cutting force.

(e) The frictional effect at the tool-workpiece interface will be included in the dynamic cutting force model.

In the analysis of the turning operation, the principal direction of the relative vibration is not necessarily constrained to be in the direction of the tangential or radial projection of the cutting force. However, the analysis will be restricted to the transverse movement [59] and the equation of motion in this direction will be formulated.

It is well known that the cutting force under steady state conditions may reasonably be assumed to be directly proportional to the uncut chip cross-sectional area [1]. That is,

$$F = K_c \cdot A \tag{3-1}$$

where F = the cutting force on a tool,

K_c = specific cutting force (cutting resistance) and

A = area of the chip being removed.

The cutting resistance, denoted by K_c is a fundamental property of the material being cut and is represented by the quotient of the main cutting force and the cross-sectional area of the undeformed chip. The value of K_c is changeable, depending on the cutting conditions such as depth of cut, feed rate, cutting speed, etc.

From a knowledge of the cutting process under steady state conditions it is expected that any fluctuations in the cutting process may give rise to fluctuations in the forces on the tool tip. Depending on how these fluctuations are directed and phased, relative to the vibratory motion, they may either damp or excite the vibration. Normally if the system is disturbed by some sudden force pulse it will vibrate, then the damping characteristics of the machine will eliminate the vibration after a finite number of oscillations.

If, however, the cutting force fluctuations are large and are opposing the damping effect they may cause the vibration amplitude to grow and reach a limit cycle when the damping and exciting forces are in balance. This is a self-excited vibration.

There are three mechanisms associated with self-excited vibration in machining [59]: velocity dependent effect, regenerative effect, and mode coupling. The velocity-dependent effect is due to a self-induced mechanism based on the negative slope of the cutting force variation with respect to the cutting speed. [59,60] The difference in the average magnitude of the cutting forces generated during the upward and downward strokes of tool motion causes net energy to be fed into the system. The regenerative effect is caused by the overlap of waves in the tool motion

and work surface during the successive cuts [61,62]. The modulation of the uncut chip thickness creates a continuous variation in the cutting forces, and excites the machine structure at one of its natural frequencies. The mode coupling effect occurs when the principal natural modes of the vibratory system are closely matched. Since vibration in the transverse direction only is considered in this work, the mode coupling effect will be excluded in the formulation of the dynamic cutting forces.

3.2.2.1 Regenerative effect on dynamic cutting forces

A basic assumption is made that the dynamic cutting force is proportional to the chip load. This chip load can be obtained by multiplying the instantaneous depth of cut by the feed rate. This calculation is based on evaluating the geometry in the cutting process. It can be seen that in the regenerative vibration mode, the instantaneous forces acting on the tool and workpiece depend not only on the present state of relative motion of the tool and the workpiece but also on its motion in the preceding motion history.

The geometry of the conventional turning operation is shown in Fig. 3.1. The chip thickness has a mean component and a variable component as a result of the relative vibration between the tool and the workpiece in the horizontal direction. The trace of the vibration displacement of the tool and the workpiece in the preceding turns is left on the uncut chip thickness. The mean chip thickness is determined by the preset depth of cut.

Let the amplitude of the relative vibration between tool and workpiece be $z(t)$ at any instant during the turning operation, depending on the relative displacement between tool and workpiece. This displacement represents the deviation from

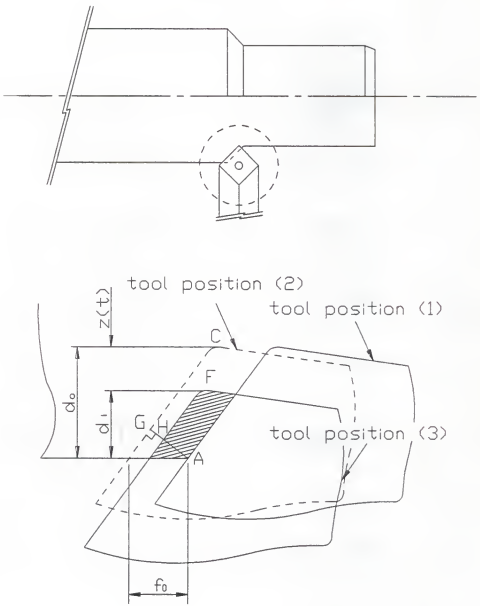

Fig. 3.1 Schematic view of the cutting zone

equilibrium position between tool and workpiece. As can be seen in Fig. 3.1, the instantaneous depth of cut is given by

$$d_i = d_0 - z(t) \tag{3-2}$$

where d_0 is the originally set depth of cut. Position 3 represents the tool location after one revolution of the workpiece from position 1. Position 2 represents the tool location, if there were no forces acting on the tool.

$$CF = z(t) \tag{3-3}$$

$$GH = z(t)\cdot\sin(C_s)$$

Therefore, the instantaneous uncut chip width, f_i is given by

$$AH = f_i = f_0\cdot\cos(C_s) - z(t)\cdot\sin(C_s) \tag{3-4}$$

where f_0 = originally preset feed rate and

C_s = side cutting angle.

This relation can be applied when the tool cuts the workpiece for the first time. As shown in Fig. 3.1, the surface of the workpiece, which is the trace of the tool motion of the previous turn, is influenced partly by that of two turns before, and there is a period in each cycle in which the tool edge is separated from the workpiece surface, and the chip generated would be broken at the trace of the previous turn. Then, the cutting force becomes zero for a short period during which the vibrational amplitude grows. This is induced by the trace left by the tool during the previous two or more turns on the work and is the cause for the variations of the uncut chip thickness. This effect is called the multiple regenerative effect on the dynamic cutting force and chip formation and depends on the vibrational amplitude, the cutting conditions and the shape of the cutting tool. Therefore, the mean depth of cut d_0, the current relative vibration z(t), and the relative undulation of the surface previously produced by the relative vibration $z_{min}(t-L)$ must be considered together in order to give the

total chip thickness d_i and chip width f_i. As a result of this effect on the dynamic chip formation, equation (3-4) will be changed as follows:

$$f_i = f_\phi \cdot \cos(C_s) - (z(t) - z_{min}(t-L)) \cdot \sin(C_s) \quad (3\text{-}5)$$

where $z_{min}(t-L)$ = minimum value among the vibration amplitudes during the previous cuts and

L = time for one complete rotation of the job.

$z_{min}(t-L)$ is given as follows:

$z_{min}(t-L)$ = minimum value among

$\{ z(t-L), f_\phi \cdot \cos(C_s) + z(t-2L), ..., z(t-n \cdot L) + (n-1) \cdot f_\phi \cdot \cos(C_s) \}$

This consideration is important when the feed rate is less than the depth of cut or in the case of plunge cutting. If the feed rate is relatively high as in the thread cutting case, then only the previous cut has an effect on the present cut. Therefore, the relationship for the instantaneous feed rate can be expressed as following equation.

$$f_i(t) = f_\phi \cdot \cos(C_s) - (z(t) - z(t-L)) \cdot \sin(C_s) \quad (3\text{-}6)$$

where $z(t-L)$ = amplitude of vibration of the previous cutting.

In the conventional turning operation, the instantaneous chip area during cutting can be expressed as follows:

$$A_i(t) = \frac{d_i(t) \cdot f_i(t)}{\cos(C_s)} \quad (3\text{-}7)$$

As mentioned earlier, a nonlinearity occurs as a result of the interactions among the previous cuts. It is possible that vibrations between tool and workpiece may become so large that they actually cause a loss of contact with the workpiece during a segment of the cut. In such an instance, when $z > z_{min} + d_\phi$, Eq. (3-1) would produce a negative value. This is not physically possible, and the stipulation must be

added that if $F < 0$, then $F = 0$. It is this basic nonlinearity that limits the vibrations to finite values although they may be uncomfortably large.

3.2.2.2 Effect of damping in the dynamic cutting force

In addition to the basic regenerative nonlinearity, there is another less powerful nonlinearity, which is related to the damping mechanism in the cutting process. When the cutting tool meets the wavy surface, it removes the chip in a wavy form and leaves behind another wavy surface. This leads to the regeneration of waviness which becomes the source of the self excited oscillation. Damping may also be generated in the cutting process, and it is generally known that at low cutting speeds cutting is stable at much larger chip width than at high cutting speeds due to damping. It is generally accepted [59,60,62] that there exists a resistive force which works in the horizontal direction and which is related to damping. It is caused by the interference of the flank of cutting tool with the slope of its motion in the cut. The clearance angle of the cutting tool can therefore have a very strong effect on the damping as explained in the Fig. 3.2 [63].

In position 1 the tool is moving upwards and there is enough clearance between it and the surface it has just cut. In position 2 it moves into the material and the clearance is diminished. The increased cutting force acts against the velocity of the motion and generates damping. The slope of the wave is proportional to the amplitude of the vibration, the frequency of the wave and is inversely proportional to the cutting speed [62,63].

$$\text{slope} = \frac{\omega_r \, 2 \cdot \pi \cdot A}{v} \tag{3-8}$$

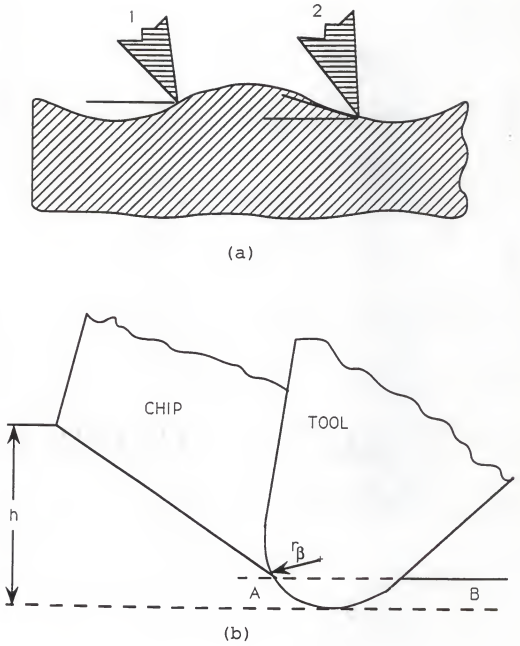

Fig. 3.2 Source of process damping
(a) Regeneration of waviness
(b) Rounded cutting edge

where A = amplitude of surface vibration,

v = cutting speed and

ω_t = frequency of wave.

The characteristics of the damping force are similar to those of the penetration force [59-63]. Although the fundamental aspects of the nonlinear effect are not yet fully understood, if the tool motion is restricted to a small amplitude of vibration, then the penetrating force on the tool nose region is found to be substantially independent of the uncut chip thickness. The penetration effect was analytically studied by Kondo et al. [62] and Sisson and Kegg [60]. The penetration force shows the following fundamental properties: It is inversely proportional to the cutting speed and proportional to the relative velocity between the tool and the work. Therefore, the damping force can be expressed by

$$F_d(t) = \frac{\alpha \cdot \dot{z}(t)}{v} \tag{3-9}$$

$$v = \frac{\pi \cdot D \cdot \Omega}{60} \tag{3-10}$$

where α = damping factor in the dynamic cutting force,

$z(t)$ = relative velocity between the tool and workpiece,

D = diameter of the workpiece and

Ω = rotational speed of the workpiece (RPM).

The constant α for orthogonal cutting was analytically derived by Sisson and Kegg [60] and is given by the following equation.

$$\alpha = \frac{f \cdot r_\beta \cdot C \cdot \sigma_y}{\beta^2} \tag{3-11}$$

where r_β = radius of cutting tool tip,

C = constant related with the contact between the tool and the workpiece,

f = width of cut,

β = clearance angle and

σ_y = workpiece yield strength.

In the formulation of this relation, the flank surface of the cutting tool which comes into contact with the workpiece material will cause a very high interference force, which can be evaluated by multiplying the contact area by the yield stress of the work material. It can also be expected that the tool motion will cause the effective rake and clearance angles to be time-dependent.

3.2.3 Evaluation of the Cutting Stiffness

The cutting resistance, K_c is defined as the cutting force per unit uncut chip cross-sectional area. The value of K_c can be obtained by dividing the steady state cutting force by the chip area and depends on several factors:

(a) factors connected with the cutting point,

(b) factors connected with the workpiece material and

(c) factors connected with the cutting conditions.

These are external factors whose influence on the cutting resistance is of an indirect character. They depend on such basic parameters as cutting temperature, the external and internal friction and the magnitude, direction and rate of any resulting deformation.

According to Kronenberg [1], the general equation for the unit cutting force in which feed f and depth of cut d are taken as separate quantities can be expressed as follows:

$$K_c = \frac{C_p\,(G/5)^{g_p}}{(1000\,A)^{z_p}} \text{ psi} \qquad (3\text{-}12)$$

where C_p = empirical constant when d = 1.in. and
f= 1. in. G = 5.,
G = slenderness ratio = d/f,
A = uncut chip area = d·f,
g_p = empirical constant and
z_p = empirical constant.

This equation shows that the unit cutting force K_c for the same chip cross sectional area A increases when the slenderness ratio G (= depth/feed) increases, i.e. when the ratio of depth of cut to feed/rev increases.

Actually the geometry of the cutting tool and the tensile strength of the workpiece have direct effects on the value of C_p. The recommended values for C_p for steel and cast iron are given as follows [1]:

$$C_p = 134\,K_z^{.455}\,(80 - \alpha)^{.67} \text{ for steel} \qquad (3\text{-}13)$$

$$C_p = 1360\,(BHN)^{.4}\,(80 - \alpha)^{.67} \text{ for cast iron} \qquad (3\text{-}14)$$

where K_z = tensile strength of material,
BHN = Brinell Hardness Number and
α = Rake angle.

These equations however are based on old cutting data and may not be applicable to present cutting operations.

It is generally assumed that a direct relationship exists between the cutting force and the cutting speed. Actually, however, these two quantities can be practically independent of each other within the cutting speed limits of the various tool materials. The cutting force depends on one hand, directly on the speed of deformation and on the other hand, indirectly on the cutting temperature [14].

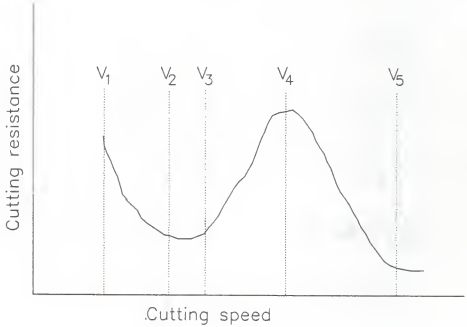

Fig. 3.3 Cutting resistance variation with cutting speed [19]

According to Rozenberg and Eremin [19], as illustrated by the typical curves shown Fig. 3.3, a reduction of cutting resistance occurs within the range of cutting speed between v_1 and v_2 due to an increase of the actual rake angle (as a result of built-up edge) which causes the magnitude of deformation (chip area compression) to decrease. Within the range v_2 - v_3, the cutting resistance rises as a result of the disappearance of BUE (built-up edge) and the reduction of actual rake angle to the value of the tool point rake angle. Further increase in the

cutting resistance in the speed range v_3 - v_4 is caused by a rise in the coefficient of external friction. After reaching a maximum at speed v_4, the cutting resistance decreases because of the diminishing coefficient of friction as a result of the rising temperature. A critical cutting speed v_5 is then reached above which the cutting resistance is stabilized. At these speeds, a thin liquid film develops along the face causing the frictional resistance to be almost independent of the temperature.

In practice, the applied cutting speeds using sintered carbide tools usually exceed 50 m/min. Since speeds of this order are in most cases higher than v_4, the cutting resistance generally decreases with increasing cutting speed.

The simplest case among the cutting operations is known as orthogonal cutting. In this case, the cutting edge is perpendicular to the relative cutting velocity between the tool and the workpiece. Since most practical cutting operations are geometrically complex, the simplest case in cutting will be chosen in order to simplify the evaluation of the cutting resistance, K_c.

In the analysis of the orthogonal cutting operation, many workers such as Piispanen [64], Merchant [65], and Kobayashi and Thomson [66] have assumed a thin-plane (or thin-zone) model and others such as Palmer and Oxley [67], and Okushima and Hitomi [68], have based their analyses on a thick deformation model. Nakayama and Ari [4] also calculated the forces in conventional cutting operations using the orthogonal cutting approximation.

In orthogonal cutting as shown in Fig. 3.4, the cutting force F_c and thrust force F_t are calculated as:

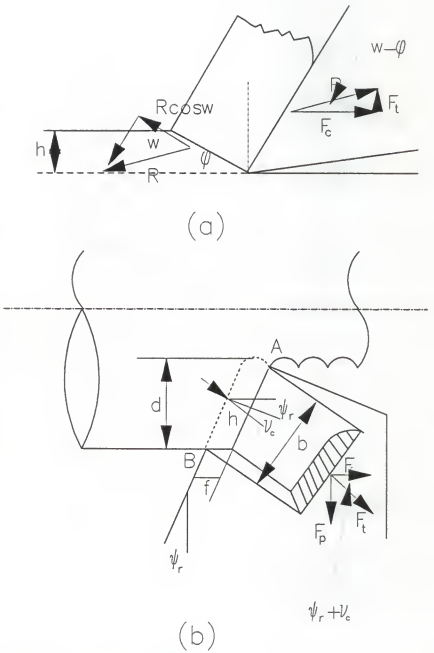

Fig. 3.4 Diagram of the cutting zone
(a) Orthogonal cutting
(b) Conventional cutting

$$F_c = R \cdot \cos(w - \phi) = S \cdot f \cdot d \cdot (\cos \phi + \tan w) \quad (3\text{-}15)$$

$$F_t = R \cdot \sin(w - \phi) = S \cdot f \cdot d \cdot (\cot \phi \cdot \tan w\text{-}1) \quad (3\text{-}16)$$

where R = resultant cutting force,

f = chip width = feed rate,

d = chip thickness = depth of cut,

w = angle between the shear plane and the direction of resultant cutting force,

ϕ = shear plane angle and

S = shear flow stress of workpiece.

In conventional cutting, when the side cutting edge angle C_s and the angle of the chip flow θ_c are as shown Fig. 3.4, the cutting force F_v, feed force F_f, and thrust force F_p are calculated as

$$F_v = F_c = S \cdot f \cdot d \cdot (\cot \phi + \tan w) \quad (3\text{-}17)$$

$$F_f = F_t \cdot \cos(\theta_s + \theta_c) = S \cdot f \cdot d \cdot (\cot \phi \cdot \tan w\text{ -}1) \cdot \cos(C_s + \theta_c) \quad (3\text{-}18)$$

$$F_p = F_t \cdot \sin(\theta_s + \theta_c) = S \cdot f \cdot d \cdot (\cot \phi \cdot \tan w\text{-}1) \cdot \sin(C_s + \theta_c) \quad (3\text{-}19)$$

where S = shear flow stress or workpiece,

R = resultant force,

w = angle between the shear plane and the direction of the resultant force R,

ϕ = shear plane angle,

Cs = side cutting edge angle and

θ_c = angle of chip flow.

The undeformed chip thickness h and the width of cut are given as

$$h = \frac{f \cdot \cos(C_s)}{\cos(\theta_c)} \tag{3-20}$$

$$b = \frac{d \cdot \cos(\theta_c)}{\cos(C_s)} \tag{3-21}$$

The friction angle w, the shear angle ϕ, and the chip flow angle θ_c are related to the cutting process parameters using empirical equations based on experimental data as follows:

$$w = w_0 - K_1 \cdot \alpha_n \tag{3-22}$$

$$\phi = \phi_0 + K_2 \alpha_n - A/\sqrt{v \cdot f \cdot \cos(C_s)} \tag{3-23}$$

$$\theta_c = \tan^{-1}((r_\beta + f_0/2)/d_0) \tag{3-24}$$

All the constant values which are needed for Eqs. (3-22), (3-23) and (3-24) are listed in the Table 3.1 and the results obtained by Nakayama and Ari will be used in calculating the cutting resistances.

Table 3.1 Constants for the calculations of cutting forces [4]

Material	S45C	S25C	SCM3
K_1	.25	.25	.25
K_2	.20	.30	.33
ϕ_0	34.	28.5	35.
w_0	52.	52.	52.
S(Kgf/mm)	72.	60.	73.
A(m/min)	1.55	1.55	1.55

3.2.4 Dynamic Cutting Model for Surface Generation

The relative movement between the tool and workpiece during cutting depends on the different elements of the machine tool. Several vibratory modes generally occur in the turning operation such as tool shank bending, tool post or compound slide bending, workpiece bending and torsion, headstock shaft torsion, headstock bending, and tailstock bending, etc. The tool system, workpiece, headstock, and tailstock are attached to the machine tool bed. In this analysis, the machine tool bed is assumed to be rigid and the three systems which are considered to have the major influence on the machining process are: the spindle structure, the workpiece and tool assembly. Therefore, evaluation procedures for the dynamic characteristics of the spindle structure, the tool assembly and workpiece are needed for developing the dynamic model of surface generation.

3.2.4.1 Evaluation of dynamic characteristics of the system

The workpiece system in the turning operation consists of spindle structure and workpiece. Because the carriage part of the tool assembly is used to support and move the cutting tool, this part is assumed to be included in the dynamic properties of the tool assembly. The spindle structure assembly which consists of spindle, front bearing ,rear bearing and headstock frame is assumed to constitute the machine structure which supports the workpiece. Therefore, the dynamic factors of the headstock assembly are assumed in the reported study to be those of the machine structure when an overhanged workpiece is cut. The dynamic characteristics of the workpiece will be considered separately in the dynamic modelling. The model is schematically shown in Fig. 3.5. The dynamic

characteristics of the machine structure which are represented by M_s, K_s and C_s, are assumed to be those of the spindle assembly which supports the workpiece, since the machine bed is assumed to be rigid.

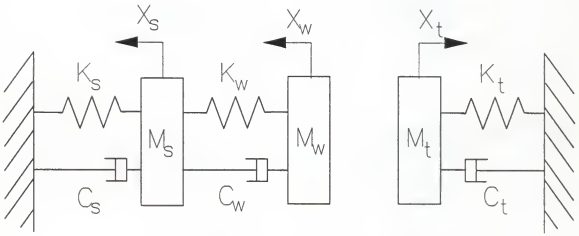

Fig. 3.5 Dynamic model of the system

According to the series of articles published by the Machine Tool Industry Research Association (MTIRA), the spindle-bearing assembly is often the largest single source of flexibility. The following is a summary of their results [69]:

1. For two-bearing spindles the flexibility at the cutting point has components due to bearing deflections and spindle bending. For a given position of the cutting point from the front bearings there is an optimum bearing spacing to give minimum flexibility.
2. The bearings contribute typically some 30-40% of the total flexibility at the cutting point
3. Decreasing the flexibility of the bearings or the cross section of the shaft always decreases cutting point flexibility.
4. For the optimum bearing spacing, decreasing the distance of the cutting point from the front bearing decreases flexibility.

In this analysis, a simple two-bearing spindle system is chosen for the machine tool spindle system as shown in the Fig. 3.6. The model consists of a uniform section shaft, supported at two points by bearings of static stiffness K_f and K_r, a chuck and a spindle overhang. Here, the overhang is assumed to be different from the workpiece, since workpiece is considered to be another dynamic system.

For an unloaded spindle acted on only by a force P, the flexibility factor at the spindle-nose is

$$C_{sp} = \frac{a^3}{3 \cdot E \cdot I_a} + \frac{l \cdot a^2}{3 \cdot E \cdot I} + \frac{1}{K_f} \cdot \left(1 + \frac{a}{l}\right)^2 + \frac{1}{K_r} \cdot \left(\frac{a}{l}\right)^2 \qquad (3\text{-}25)$$

where a = length of overhang,

l = bearing span,

E = elastic modulus of material,

I_a = area moment of inertia of overhang,

I = area moment of inertia of span between bearings and

K_f,K_r = stiffness of front and rear bearing

respectively.

Under the action of a unit force, the first term of eq. (3-25) is the deflection of the overhang beam at its nose; the second is the displacement at the spindle-nose produced by the deflection of the simply supported beam; the third and the fourth are the displacements at the spindle-nose produced by the deflection of the front and rear bearings respectively. These four displacements are all in the same direction and their calculation procedures are given in Appendix B.

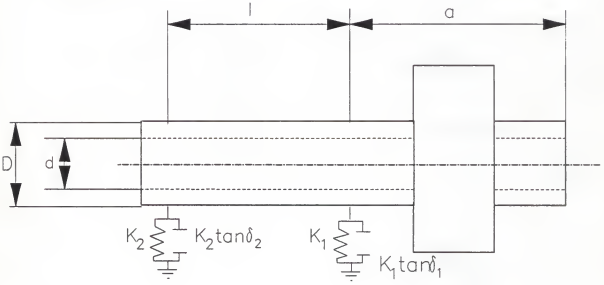

Fig. 3.6 Simple spindle model

In the actual tool system, the workpiece is clamped by the chuck and there should be some relative stiffness and damping between the chuck and the workpiece. However, in the analysis the workpiece is assumed to be clamped to the machine tool spindle structure as a cantilever.

The workpiece which is represented by M_w, K_w, and C_w is assumed to be a cantilever beam when an overhanged workpiece is cut, and a simply supported beam when the workpiece is supported by the headstock and the tailstock. In the modeling of the workpiece, the effects of rotary inertia and shearing deformations are assumed to be negligible.

When the workpiece is supported by the headstock and tailstock, the static compliance is given by

$$C_{wp} = \frac{(L - x)^2 \cdot x^2}{3 \cdot E \cdot I \cdot L} \tag{3-26}$$

where E = Young's modulus,

I = 2nd moment of area of the workpiece,

d = diameter of workpiece,

L = length of workpiece and

x = distance of cutting tool point from the headstock along the workpiece.

When the workpiece is overhanged, the static compliance is given as follows:

$$C_{wp} = \frac{x^3}{3 \cdot E \cdot I} \tag{3-27}$$

The static deflection is highly dependent on the position of the cutting tool point and this factor is very important when the static dimensional accuracy is

considered. When an overhanged workpiece is being cut, the minimum stiffness is given by the following equation.

$$K_w = \frac{3 \cdot E \cdot I}{L^3} \tag{3-28}$$

The effective mass of the workpiece is given as follows:

$$M_w = \frac{33 \cdot m \cdot L}{140} \tag{3-29}$$

where m = mass per unit length of workpiece and

L = total workpiece length from headstock.

The undamped natural frequency of this overhanged workpiece is given by the following equation.

$$\omega = 3.56 \frac{\sqrt{EI}}{L^2 \cdot \sqrt{m}} \tag{3-30}$$

where ω = natural frequency of the workpiece,

L = length of workpiece and

m = mass per unit length.

While stiffness is important for the calculation of the static accuracy, damping is important for the analysis of the dynamic behavior of a machine tool. An increase in stiffness may increase the natural frequency of the system, but damping is significant only near the natural frequencies.

The damping in the workpiece is assumed to be the material damping and is given by

$$C_{wc} = 2\sqrt{M_w K_w} \tag{3-31}$$

$$\S_w = \frac{C_w}{C_{wc}} \tag{3-32}$$

where C_{wc} = critical damping of the workpiece and

$\S_w$ = damping ratio of the workpiece.

The damping of all the elements of spindle structure including the internal damping of the material must be considered in the dynamic analysis of the spindle structure. However, the main source of damping is assumed to be in the bearings which are used to support the spindle. For angular contact and taper roller bearings mounted in a face to face arrangement, the damping is shown to occur internally as well as at the external joints. In other words, damping levels are dependent on the internal geometry of the bearings, outer ring-housing clearance, preload and applied radial load. Experience [59] shows that the overall damping ratio of a conventional machine tool is less than 0.03 and that of a single element is less than 0.002. The term dynamic flexibility can be introduced in considering the stiffness and damping of a bearing at the same time. This term was used by Welbourne and Smith [70] to determine the susceptibility of machine tool to chatter. This value depends on all components of the workpiece system, and assumes that the bearing to be a significant source of damping and flexibility. Therefore, changing the bearing preload can alter both the static and dynamic response characteristics of the workpiece system. For simplicity it is assumed that the bearings are the only source of damping and the damping is hysteretic. The dynamic stiffness of the bearing takes the form:

$$K_D = K + i\, K \cdot \tan \delta \qquad (3\text{-}33)$$

where K is the static stiffness, $\tan \delta$ is the loss tangent, and $i = \sqrt{-1}$.

The damping is included in the system through a damping ratio with an approximate value of ξ_s is 0.03. The mass of the spindle system is considered to be the mass of the chuck.

3.2.4.2 Equations of motion of the dynamic system

The dynamic characteristics of the system components are used in formulating the model for surface generation. An overhanged workpiece configuration is considered and the spindle structure is assumed to be connected in series with the workpiece.

The model which is diagrammatically illustrated in Fig. 3.5 deals with transverse movements only and the axial movement is assumed to be negligible. The spindle structure is defined by M_s, C_s and K_s. The workpiece is defined by M_w, C_w and K_w and the tool assembly is defined by M_t, C_t and K_t. The system response is defined by x_t, x_s and x_w respectively.

The equations of motion for the system can be written as:

$$M_t\cdot\ddot{x}_t(t) + C_t\cdot\dot{x}_t(t) + K_t\cdot x_t(t) = F_x(t)$$

$$M_w\cdot\ddot{x}_w(t) + C_w\cdot(\dot{x}_w(t)-\dot{x}_s(t)) + K_w\cdot(x_w(t)-x_s(t)) = F_x(t)$$

$$M_s\cdot\ddot{x}_s(t) + C_w\cdot(\dot{x}_s(t)-\dot{x}_w(t)) + K_w\cdot(x_s(t)-x_w(t)) + C_s\cdot\dot{x}_s(t) + K_s\cdot x_s(t) = 0 \quad (3\text{-}34)$$

where $x_t(t)$ = tool movement from the equilibrium position,

$x_w(t)$ = workpiece movement from the equilibrium position,

$x_s(t)$ = spindle movement from the equilibrium position and

$F_x(t)$ = dynamic cutting force acting between the tool and the workpiece.

$x_t(t)$, $x_w(t)$ and $x_s(t)$ are defined as positive for the directions shown in Fig. 3.5.

The equations of motion are solved in order to generate the information of the machined surface of workpiece. The results can show the effects of the dynamic characteristics of the system on the surface generation and cutting stability. The surface states depend on the contact states between the tool and

workpiece during cutting. Since the equations can not be solved explicitly, the equations of motion are solved numerically using Runge-Kutta 4th order method.

3.3 Prediction of Surface Roughness and Surface Error from the System Response

It is well known that the relative vibrations between the tool and the workpiece have considerable effect on the quality of the machined surface. The publications in this area are too numerous to review here. Ref. [71] to [73] illustrate the continued interest in this subject and represent some of the excellent contributions to the understanding of the effect of relative vibrations on surface geometry. Rakhit, Osman and Sankar [73] have shown that surface roughness of a machined component is a result of the superposition of a theoretical profile which can be computed from the operational kinematics of the tool-workpiece system, and an oscillatory profile caused by the relative vibrations between the cutting edge and the workpiece. Consequently, the total roughness of the machined components can be evaluated from

$$R = R(f,r) + R(Fx(t)) \tag{3-35}$$

where R = total predicted surface roughness

$R(f,r)$ = kinematic surface roughness derived from feed and tool nose radius

$R(F_x(t))$ = Roughness generated by the dynamic cutting force.

The relative movement is defined as $z(t)$ and is calculated from the solution of equation (3-34) as

$$z(t) = x_t(t) + x_w(t). \tag{3-36}$$

Surface error is defined to be the deviation of the finished machined surface in the transverse direction from the desired surface, that is, the surface which would be produced by a completely rigid machining system. From a static point of view, the entire finished surface has an error in location given by

$$\delta_x = \frac{F_x^m}{K_x} \tag{3-37}$$

where K_x = total static stiffness of machining system,

δ_x = static error due to cutting force and

F_x^m = average transverse directional cutting force.

The total stiffness K_x can be obtained by combining all the stiffness factors of the machining system as explained in chapter 2. Another way of calculating the surface error is solving eq. (3-34) and the steady state value of response would be used as the surface error.

3.4 Results

3.4.1 Numerical Example

In order to check the accuracy of the simulation, a numerical example is considered using the test conditions reported in Ref. [74]. The pertinent test data in this case are given by Table 3.2.

The results from the simulation are listed in Table 3.3. The relationship between response (surface roughness) of the simulation and independent variables can be represented by the following equation.

$$R_{max} = K_0 \cdot V^{K_1} \cdot f^{K_2} \cdot d^{K_3} \cdot r_\beta^{K_4} \tag{3-38}$$

where R_{max} is the response (that is, 'Peak to Valley' height), while V, f and d are the cutting speed, feed rate and tool nose radius, respectively.

Table 3.2 List of test data

Feed rate(f) :	.127	mm/rev
	.508	mm/rev
	.889	mm/rev
Cutting speed(V):	61.	m/min
	183.	m/min
	304.	m/min
Depth of cut(d):	.305	mm
	.508	mm
	.711	mm
Tool nose radius(r_β):	.794	mm
	1.588	mm
	2.381	mm
Tool frequency($1/2\pi\sqrt{K_t/M_t}$):	34.	Hz
Tool mass(M_t):	27.	Kg
Tool damping ratio($\S_t$):	0.07	
Workpiece stiffness(K_w):	2.419×10^8	N/m
Workpiece mass(M_w):	7.829	Kg
Workpiece Damping ratio($\S_w$):	0.003	
Structure Stiffness(K_s):	3.6345×10^9	N/m
Structure damping(C_s):	43071.91	N·sec/m
Chuck mass(M_s):	34.	Kg

Table 3.3 Simulation results

d(mm)	f(mm/rev)	r(mm)	Roughness		
			at 60m/min	183 m/min	304 m/min
0.3050	0.1270	0.7940	21.73	14.60	12.11
0.3050	0.1270	0.5880	16.88	89.96	9.41
0.3050	0.1270	0.3810	14.57	9.77	8.12
0.3050	0.5080	0.7940	67.54	45.28	37.64
0.3050	0.5080	1.5880	52.48	35.18	29.25
0.3050	0.5080	2.3810	45.28	30.36	25.24
0.3050	0.8890	0.7940	106.75	71.57	59.49
0.3050	0.8890	1.5880	82.95	55.61	46.23
0.3050	0.8890	2.3810	71.58	47.99	39.89
0.5080	0.1270	0.7940	24.94	16.72	13.90
0.5080	0.1270	1.5880	19.38	12.99	10.80
0.5080	0.1270	2.3810	16.72	11.21	9.32
0.5080	0.5080	0.7940	77.52	51.97	43.20
0.5080	0.5080	1.5880	60.23	40.38	33.57
0.5080	0.5080	2.3810	51.98	34.84	28.97
0.5080	0.8890	0.7940	122.5	82.14	68.28
0.5080	0.8890	1.5880	95.20	63.82	53.06
0.5080	0.8890	2.3810	82.15	55.07	45.78
0.7110	0.1270	0.7940	27.31	18.31	29.25
0.7110	0.1270	1.5880	21.22	14.23	25.24
0.7110	0.1270	2.3810	18.31	12.28	59.50
0.7110	0.5080	0.7940	84.88	56.91	46.23
0.7110	0.5080	1.5880	65.96	44.22	39.89
0.7110	0.5080	2.3810	56.91	38.15	13.90
0.7110	0.8890	0.7940	134.16	89.94	10.80
0.7110	0.8890	1.5880	104.25	69.89	9.32
0.7110	0.8890	2.3810	89.96	60.31	43.20

However, K_0, K_1, K_2 and K_3 are constants to be determined. This equation can be written in the linear form as:

$$\ln(R_{max}) = \ln(K_0) + K_1 \cdot \ln(V) + K_2 \cdot \ln(f) + K_3 \cdot \ln(d) + K_4 \cdot \ln(r_\beta) \quad (3\text{-}39)$$

which may represent the following mathematic model as continuous function of four independently controlled variables

$$y = f(X_1, X_2, X_3, X_4) \quad (3\text{-}40)$$

where $X_1 = \ln V$,

$X_2 = \ln f$,

$X_3 = \ln d$ and

$X_4 = \ln r_\beta$.

Depending on the accuracy of the system, we can determine the order of model. The equation of the first order is given as follows:

$$y = \ln(R_{max}) = b_0 + \Sigma\, b_j X_j + \in \quad (3\text{-}41)$$

The second order equation can be written as:

$$y = \ln(R_{max}) = b_0 + \Sigma\, b_j X_j + \Sigma\, b_{ij} X_i X_j + \in \quad (3\text{-}42)$$

In order to determine the coefficients, b, Ordinary Least Squares(OLS), Weighted Least Squares(WLS), Maximum Likelihood(ML), and Maximum A Posteriori(MAP) estimation can be applied. Generally, the equation for b is given as follows:

$$b = (X'X)^{-1}X'y \quad (3\text{-}43)$$

where b is the matrix of parameter estimates, X is the calculation matrix, X' is the transpose of X, X'X is the variance matrix, $(X'X)^{-1}$ is the covariance matrix which is the inverse of X'X and y is the matrix of measured response on a logarithmic scale.

The final equation from the regression analysis is obtained as follows:

$$R_{max} = 665.V^{-.364}f^{.818}d^{.27}r_{\beta}^{-.364} \quad (3\text{-}44)$$

From Ref. [74], the equation derived from the experimental analysis is given by

$$R_{max} = 624.2432\ V^{-.4329}f^{.8129}d^{.0335}r_{\beta}^{-.4680} \quad (3\text{-}45)$$

These results obtained from Eq. (3-44) are plotted in Fig. 3.7 versus those obtained from Eq. (3-45) for the different test values. Good correlation can be seen between the simulation results and the experimental data as expressed by Eq. (3-45).

The deviation between the model and the experimental formula can be attributed to the fact that the stylus does not precisely duplicate the actual profile of the roughness and therefore can produce slightly lower peak-to-valley readings than the theoretical expectation. This may explain the difference between the actual and the ideal correlation in Fig. 3.7. By using equation (3-44), the relationship between the surface roughness and cutting parameters are illustrated in Figs 3.8 (a), (b) and (c).

3.4.2 Development of a Generalized Surface Roughness Equations

The simulation was utilized to develop generalized equations for surface roughness based on the output from the vibratory model. An equation of the following form is assumed

$$R^{max} = e^{C} \cdot V^{k1} \cdot f^{k2} \cdot d^{k3} \cdot r_{\beta}^{\ k4} \quad (3\text{-}46)$$

The results as generated from the simulation are used in a regression analysis to obtain the best fit for the equation parameters C, k_1, k_2, k_3, and k_4. A sample of the simulation results for the roughness pattern along the workpiece is shown in Fig. 3.9 for illustration. It should be noted here that case (a) gave identical results (R_{max} = 0.000021 m) to those obtained experimentally in Ref. [74].

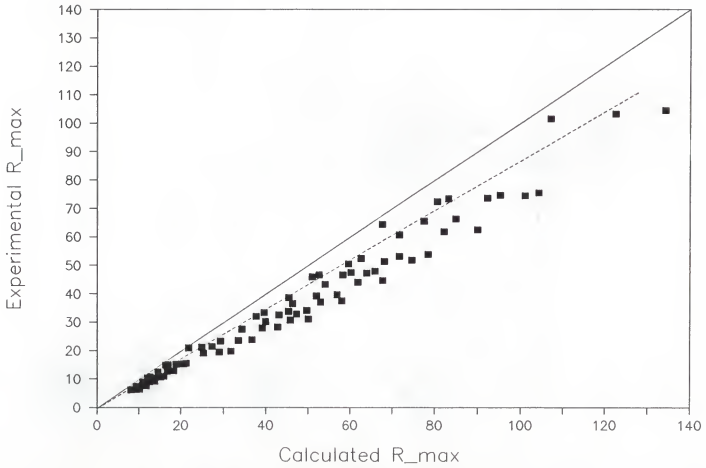

Fig. 3.7 Correlation between values
eqs. (3-45) and (3-44)
—— perfect correlation line - - - correlation line
(solid squares show the correlations)

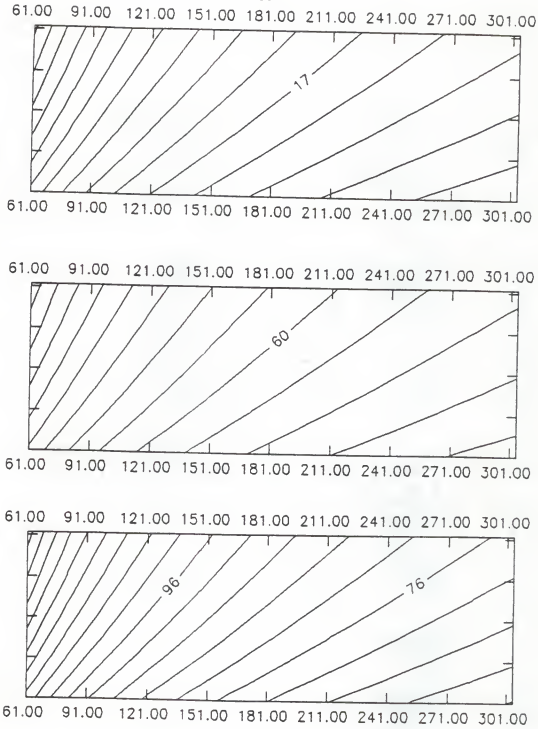

Fig. 3.8 Relationship between the response surface and cutting parameters for turning
a) f= .127 mm/rev b) f= .58 mm/rev c) f= .889 mm/rev
(the slope lines have the equal roughness values)

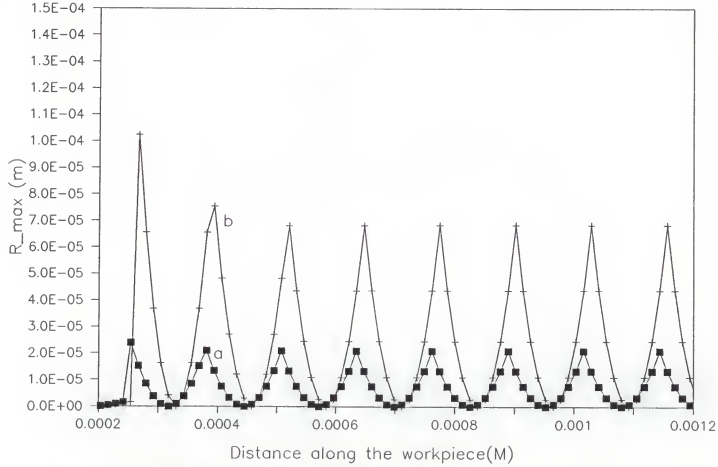

Fig. 3.9 Surface geometry generated from the simulation along the axis of workpiece (V=61 m/min, f=.127 mm/rev, d=.305 mm, r= .794 mm) (a) tool frequency = 34 Hz (b) tool frequency = 24 Hz

The values of the parameters of eq. (3-46) for the case of a chuck mass(M_s) of 34 kg and machine structures with stiffness K_s greater than 10^8 N/m were found to be independent of K_s and are only dependent on the tool natural frequency. The natural frequency of tool assembly is changed from 27 Hz to 250 Hz, and the corresponding surface roughness is calculated. Using the simulation results of 81 cases for each tool natural frequency, the coefficients for equation (3-46) are calculated by regression analysis. The results are plotted in Fig. 3.10 for C and Fig. 3.11 and Fig. 3.12 for K_1, K_2, K_3 and K_4, respectively. It should be noted that these results are not applicable for K_s below 10^8 N/m which represents structures that are too flexible to be practical.

All the simulated results were curve fitted to give the following equations:

$$C = 7.02 - 2.2(1 - e^{-(x-29)/18.3})$$

$$K_1 = -0.3712 + 0.3712(1 - e^{-(x-29)/21})$$

$$K_2 = 0.6302 + 1.3626(1 - e^{-(x-29)/31.3})$$

$$K_3 = 0.5425 - 0.5425(1 - e^{-(x-29)/10.3})$$

$$K_4 = -0.3419 - 0.6523(1 - e^{-(x-29)/51.5}) \qquad (3\text{-}47)$$

where x = tool natural frequency

These equations are plotted as the solid lines in Fig. 3.10, 3.11 and 3.12.

3.5 Conclusions

A dynamic simulation is utilized in this chapter for developing a generalized equation for predicting surface roughness in turning covering the practical range of machine tool dynamic characteristics and cutting conditions. The simulation is shown to give good correlation with the extensive experimental study reported in Ref. [74]. It is interesting to note that the widely used Equation

(2-10) which is based on kinematic considerations gives the same results as the simulation only when the natural frequency of the tool is greater than 150 Hz. In this study where K_s is always greater than 10^8 N/m, which is the situation in most practical conditions, the analysis shows that the tool stiffness (its natural frequency) is the controlling factor for the relative motion between the tool and workpiece. When f_t is greater than 150 Hz (corresponding to $K_t = 2.4 \times 10^7$ N/m), the dynamic movement of the tool is found to be negligible compared to the geometric effect.

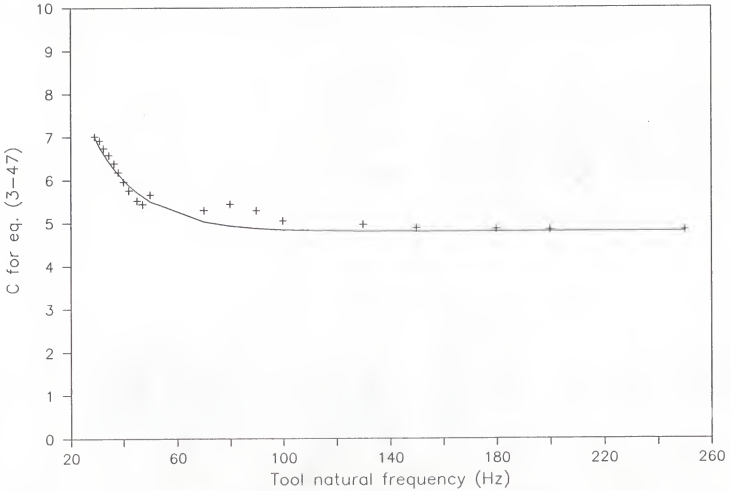

Fig. 3.10 Values for parameter C in eq. (3-47)
___ Curve fit + Simulation

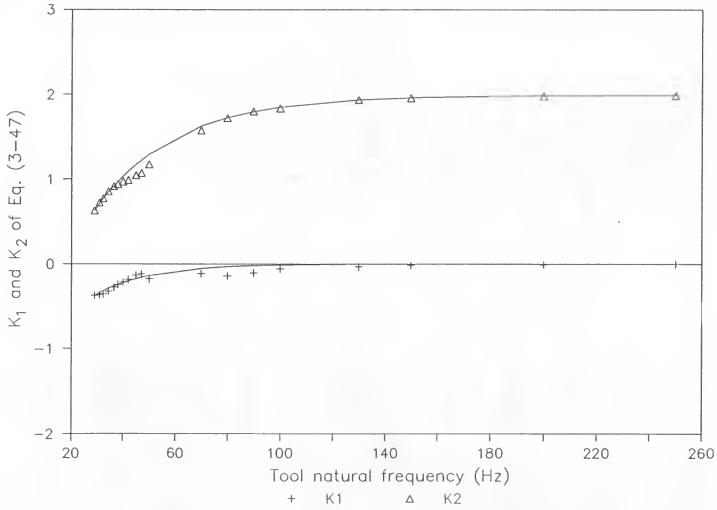

Fig. 3.11 Values for parameter K_1 and K_2 in eq. (3-47)
___ Curve fit + Simulation

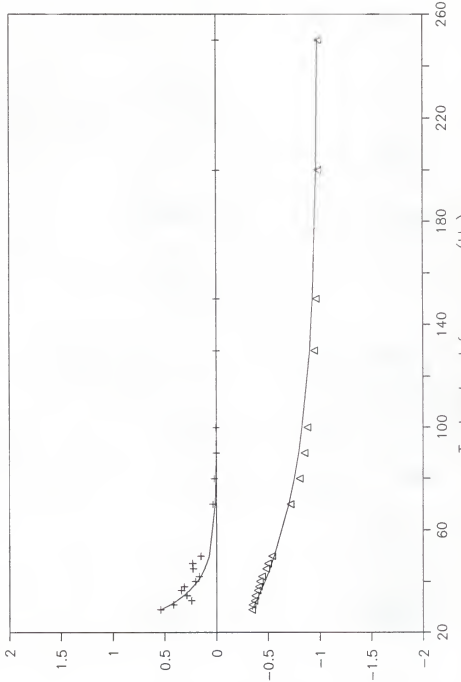

Fig. 3.12 Values for parameter K_3 and K_4 in eq. (3-47)
—— Curve fit + Simulation

CHAPTER 4
PREDICTION OF HEAT GENERATION IN THE CUTTING PROCESS

4.1 Introduction

Cutting tools are subjected to several forms of failure. Some of these are manifested as follows:

1. On the rake face of the tool a crater develops beginning at some distance from the cutting edge.
2. A wear land (flank wear) develops on the clearance face.
3. The tool may distort due to bulk plastic deformation caused by excessive heat.
4. The cutting edge may fracture and/or cracks may develop due to thermal shock or fatigue.

Cutting tool failure such as 4 can be avoided by proper selection of cutting conditions (feed, depth of cut, etc.), by increasing the wedge angle of the tool or by strengthening the cutting edge with land. Under usual conditions of cutting, when the "form stability" of the cutting edge is achieved or failure by fracture is prevented, cutting tools still continue to fail by a process of wear. This is due to the interaction between the chip and the tool or between the workpiece and the tool (1 & 2). The distortion of tool tip may also occur due to plastic deformation (3). These failures are related to the heat generated during the cutting operation.

Previous investigations [75-86] show that the heat generated in the various locations (i.e., tool-workpiece, tool-chip contact, and the deformation zone) produce an assortment of elevated temperatures. These temperatures depend on the machining conditions as well as the physical properties of the tool material and have considerable influence on tool life.

The thermal aspects involved in chip formation and the interaction at the tool-chip contact zone are very complex and are highly sensitive to variation in the cutting parameters. According to previous investigations [75-86], the crater wear is directly related to the tool-chip contact length and more tool-failures occur when high speeds and feeds are used. The more ductile materials yield continuous chips and the longer the contact length, the greater the wear rate.

The wear which appears on the flank of the tool below the cutting edge forms a wear land extending approximately parallel to the cutting edge. This wear is specially harmful to the machined surface. The mechanisms of wear are generally classified into 3 groups, depending on the temperatures in the cutting region[75-86].

1. Mechanical wear due to abrasion and adhesion.
2. Thermochemical wear due to diffusion.
3. Electrochemical wear due to localized galvanic action.

In order to avoid tool failures, the machine tool has to be controlled such that the operating temperature is kept below a certain critical value. In addition, the contact area between the tool and workpiece can have a great effect on the surface quality of the machined part. In other words, the wear-land can be expected to influence the surface finish and cutting forces. The flank contact region also has direct effect on the surface residual stress. Therefore, in order to identify the thermal

effects of the flank contact on the residual stress distribution, the heat generated in this region should be defined.

In this chapter, the literature on the heat generated in the cutting process is reviewed. The published information is critically analyzed for the purpose of developing an appropriate criterion for tool wear and calculating the thermal residual stress distribution generated in the machined surface.

4.2 Heat Generation in the Cutting Process

A large number of investigations dealing with temperatures in metal cutting are available in the literature. Hahn [83] calculated the shear plane temperature by assuming the shear plane to be a uniform band source moving obliquely through an infinite workpiece. Leone [78] and Leowen and Shaw [77] also assumed the shear plane to be an uniform band source but considered that it moved over a semi-infinite workpiece. The proportions of shear plane heat entering the workpiece and chip are determined by applying Block's [84] partition principle. Trigger and Chao [80] and Leowen, and Shaw [77] both used Block's partition principle to calculate the average tool-chip interface assuming that the heat developed at the tool-chip interface was uniformly distributed. Weiner [75] obtained a solution for the shear plane temperature distribution by assuming that the chip velocity is perpendicular to the shear plane and that the heat conduction in the direction of motion and along the chip can be neglected. Using relaxation techniques Rapier [85] calculated the temperature distribution in the workpiece, chip and tool which he treated as three separate systems. He also assumed a constant shear plane temperature and a uniform plane heat source at the tool-chip interface with all the interface heat flowing into the chip and none into the tool. Dutt and Brewer [86] improved the

analysis by treating the workpiece, chip and tool as one system, but after making some approximations found that they were able to dispense with the tool region altogether. In this way they determined the proportion of shear plane heat entering the workpiece and the chip, and the proportion of tool-chip interface heat entering the chip and tool. Chao and Trigger [80] improved their earlier analytical solution for the interface temperature distribution by allowing the fraction of interface heat flowing into the tool to vary along the interface regardless of the uniform heat source and using an iterative analytical procedure involving a grid of real and fictitious point heat sources.

In all the investigated cases they considered simple shear plane models and assumed that the generated heat is confined within the shear plane and the tool-chip interface rather than being spread over finite primary and secondary plastic zones.

In developing the equations of heat generation in the metal cutting process, the following assumptions are made:

(a) The heat flow is steady in the cutting tool and is quasi-steady in the moving chip and workpiece.

(b) Even if a small fraction of work of plastic deformation is retained as latent energy in the strain-hardened chip, all of the mechanical work of plastic deformation is converted into sensible heat.

(c) It is assumed that the primary deformation zone is a plane heat source of uniform strength, that no heat is lost from the free surface of the workpiece and chip, and that the thermal properties of the workpiece are essentially constant under a wide range of working conditions [66].

(d) No heat is conducted in the material in the direction of its motion.

That is, the transfer of heat in the direction of motion is mainly by transport and the conduction term can be neglected.

(e) The thermal distribution at both interfaces is uniform in a direction normal to chip motion, i.e., parallel to the active edge of the orthogonal tool [75,77,78,80].

4.2.1 Heat Generation in the Primary Shear Plane

When a material is deformed elastically, the energy required for the operation is stored in the material as strain energy and no heat is generated. However, when a material is deformed plastically, most of the energy used is converted into heat. In metal cutting the material is subjected to extremely high strains and the elastic deformation constitutes a very small proportion of the total deformation, therefore it may be assumed that all energy is converted into heat.

The rate of energy consumption during machining P_m is given by

$$P_m = F_c \cdot v \tag{4-1}$$

where F_c is the cutting force and v is the cutting speed.

The average temperature increase in the primary shear zone, can be expressed as [79]

$$\delta T_p = \frac{(1 - ß)\cdot q_p}{\rho \cdot c \cdot v \cdot t_1 \cdot w} \tag{4-2}$$

where ß = portion of heat conducted to the workpiece

q_p = rate of heat generated in the primary shear zone

v = cutting speed

t_1 = undeformed chip thickness

ρ = density of workpiece

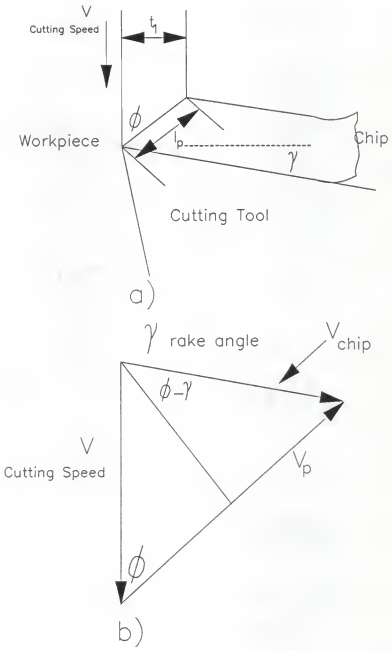

Fig. 4.1 The geometry of orthogonal cutting
a) the geometry of orthogonal cutting
b) the associated hodograph

c = heat capacity of work material

w = width of chip

Fig. 4.1 shows the geometric relation of the cutting process and the velocity relations in the primary shear zone.

$$v_p = \frac{v \cdot \cos \gamma}{\cos(\phi - \gamma)} \tag{4-3}$$

where γ = rake angle and

ϕ = shear angle.

The rate of heat generated in the primary shear zone is

$$q_p = \tau \cdot v_p \cdot l_p \tag{4-4}$$

where l_p = length of the shear plane = $t_1/\sin(\phi)$.

Substituting these relations into equation (4-2), therefore

$$\delta T_p = \frac{(1-ß) \cdot \tau_p \cdot \cos \gamma}{\rho \cdot c \cdot \cos(\phi - \gamma) \cdot \sin \phi} \tag{4-5}$$

The relative constancy of τ_p has led to the use of the term Dynamic Shear Strength [66,80].

Estimates of ß can be made using the following empirical equations based on the experimental data reported by Boothroyd [79].

$$ß = .5 - .35 \cdot \log(R_T \cdot \tan(\phi))$$

$$\text{for } .04 \leq R_T \cdot \tan(\phi) \leq 10.$$

$$\text{and} \quad ß = .3 - .15 \cdot \log(R_T \cdot \tan(\phi)) \tag{4-6}$$

$$\text{for } R_T \cdot \tan(\phi) \geq 10.$$

where R_T is a non dimensional thermal number given by

$$R_T = \frac{p \cdot c \cdot v \cdot t_1}{K} \tag{4-7}$$

where K = the thermal conductivity of the work material.

The heat partition is approximated by an exponential expression using a least square fitting as:[58]

$$(1 - \beta) = 0.51 \cdot \left[\frac{t_1 \cdot v \cdot \tan \phi}{\alpha} \right]^{.21569} \qquad (4\text{-}8)$$

where α = thermal diffusivity of workpiece material.

Many heat partition formulas are published [75-86] and Fig. 4.2 shows a comparison between some of them. The total heat which is generated in the cutting process is transported by the chip, conducted to the workpiece at the primary shear zone, and conducted into the tool through the secondary shear zone. However, the portion of heat which is conducted to the tool is negligible because the chip material near the tool face flows rapidly and has a much greater capacity for the removal of heat than the tool. Therefore, only the first two parts are considered in the formulation of heat partition.

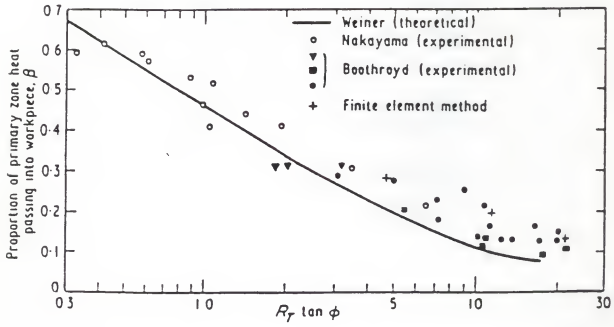

Fig. 4.2 Variation of β with R·tan ϕ where $R = \rho \cdot C_\rho U \cdot t_1 / K$

When the initial temperatures T_w and δT_p are considered, the average temperature in the primary plastic zone where the chip is formed is given by

$$T_{pz} = T_w + \delta T_p \tag{4-9}$$

The tool edge temperature, in a quasi-steady state cutting process, is assumed to be approximately equal to the primary shear zone temperature. Therefore, this temperature will be used as the constraint on the tool plastic deformation.

4.2.2 Heat Generation in the Tool/Chip Interface

It is often considered that diffusion wear plays a major role in crater-wear formation. This is attributed to the fact that high tool-chip interface temperatures occur. Therefore, in order to control this type of diffusion wear occurring in the tool rake face, it is necessary to define the temperature rise in the interface region.

The friction between the chip and the tool can be regarded as a heat source that is moving in relation to the chip and, at the same time, is stationary in relation to the tool. The shear stress is assumed to be constant along the entire tool/chip contact length and it is also assumed that the tool-chip interface acts as a constant heat source.

The total frictional energy, q_c generated along the tool-chip interface will be dissipated at that interface. The heat flux can be expressed as:

$$q_c = \frac{F \cdot v_c}{J \cdot w \cdot h} \tag{4-10}$$

where F = frictional force along the tool-chip interface,

J = mechanical equivalent of heat,

w = chip width,

h = length of contact between the chip and the tool in the direction of motion and

v_c = velocity of chip relative to the tool.

According to Jaeger [88], approximate equations for both the maximum and the mean temperatures at very high sliding speeds (L>10) and very low speeds (L<.5) are given as follows:

L > 10 (high sliding speed)

$$T_{max} = 1.6 \cdot \frac{q_c \cdot l}{k} \cdot \left[\frac{v \cdot l}{\alpha} \right]^{-0.5} \tag{4-11}$$

$$T_{avg} = T_{max} \tag{4-12}$$

where L = dimensionless sliding speed,

$$= \frac{v \cdot l}{2 \cdot \alpha}$$

l = contact length,

q_c = heat generation at the contact,

k = thermal conductivity and

α = thermal diffusivity.

L < 0.5 (low sliding speed)

$$T_{max} = 1.1 \frac{q_c \cdot l}{k} \tag{4-13}$$

$$T_{avg} = .95 \frac{q_c \cdot l}{k} \tag{4-14}$$

The temperature rise due to a stationary heat source can be regarded as the low speed sliding heat source. In the tool-chip contact, the acting force is assumed to be

the frictional cutting force between the tool and the chip and the contact is assumed to be a square asperity contact sliding on a smooth semi-infinite solid. When the heat portion r_2 that flows into the chip is considered, the temperature rise which is derived by Loewen and Shaw [77] is given as:

$$\Delta T_{avg,c} = \frac{.754 \cdot r_2 \cdot q_c (h/2)}{k_c} \cdot \left[\frac{v_c (h/2)}{2 \cdot \alpha_c} \right]^{-0.5} \tag{4-15}$$

where the subscript c designates the chip.

The mean temperature of the chip surface along the tool face will be sum of the temperature rise in the chip at the primary shear zone and the environmental temperature of the workpiece.

$$T_c = \Delta T_{avg,c} + \Delta T_s + T_w \tag{4-16}$$

Loewen and Shaw assumed this case to be a stationary heat source over the semi-infinite solid and a geometric factor $\bar{A}$ which is a function of h/w for a lathe tool and h/2w for an orthogonal tool [77].

$$\Delta T_{avg,t} = \frac{(1-r_2) \cdot q_c \cdot h}{k_t} \cdot \bar{A} \tag{4-17}$$

where k_t = thermal conductivity of the tool material and

$\bar{A}$ = geometric factor of the tool.

The temperature of the tool is the sum of the temperature rise in the tool-chip interface and the original tool temperature which is equal to T_w. Equating the mean surface temperature of the chip and the tool surface temperature, the partition coefficient r_2 is determined and the average tool-chip interface temperature is obtained.

In calculating the temperature rise of the tool-chip interface, we must first determine the friction force, F and the tool-chip contact length, h. In orthogonal cutting, the relation between the shear angle and the friction angle is given by

$$2\phi + \beta - \gamma = \pi/2 \tag{4-18}$$

where ϕ = shear plane angle which is experimentally given in the ch.3,

β = friction angle,

F can be obtained from the cutting force, F_c by $F = F_c \cdot \cos\beta$

γ = rake angle of the cutting tool.

And h is given by Hahn [83].

$$h = \frac{t_1 \cdot \sin(\phi + \beta - \gamma)}{\sin\phi \cdot \cos\beta} \tag{4-19}$$

where t_1 = undeformed chip thickness.

Knowing the mean interface temperature between the tool and the chip, we can calculate the maximum temperature rise in the chip. Assuming a plane heat source at the chip-tool interface, Rapier [85] calculated the maximum temperature rise in the chip. However, he overestimated these values and Boothroyd [79] obtained values which are in good agreement with experimental results using the assumption that the heat source in the tool-chip interface is a distributed heat source of thickness δt_2 and length h. Boothroyd's results can be represented by the empirical equation.[79]

$$\log \frac{\Delta T_{max,c}}{\Delta T_{avg,c}} = 0.06\text{-}0.195\cdot\delta t_2 \left[\frac{L t_2}{h}\right]^{.5} + 0.5\cdot\log\left[\frac{L t_2}{h}\right] \tag{4-20}$$

where $\Delta T_{avg,c}$ = the average temperature rise in the chip given in the above equation,

δ = ratio of thickness of tool-chip interface plastic zone to chip thickness and

t_2 = chip thickness.

It should be noted that equation since Boothroyd [79] did not consider the heat partition between the chip and the tool.

Using dimensional analysis and incorporating the heat partition in eqn. (4-20), the relation between the maximum temperature and the cutting parameters can be formulated as discussed in the Chapter 6.

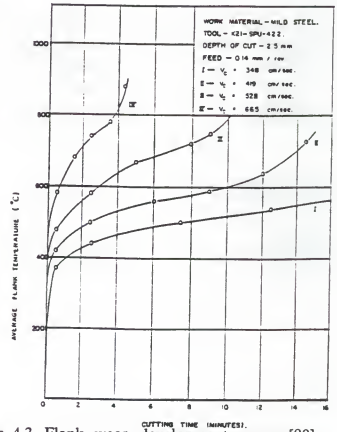

Fig. 4.3 Flank wear development curves [90]

4.2.3 Heat Generation in the Tool-Workpiece Contact

In the cutting operation, the tool rubs against the newly cut surfaces of the work material and the tool flank. The resulting tool wear which is called flank wear can cause the following:

(a) changes in the mechanics of the process,

(b) an increased tendency for chatter, and

(c) changes in the dimensions of the products.

Therefore, when very high accuracy is required in machining, the wear land size may be chosen as the failure criterion of the cutting tool.

A number of analyses of wear in the cutting process have been undertaken over many years [21-36,81,82] and it is well known that there are three temperature conditions which influence flank wear as shown in Fig. 4.3. Adhesive wear or abrasive wear is predominant in the initial and the intermediate steady state stages, but the regenerative effects of wear and temperature make diffusion a considerable factor in the later stages and a predominant factor in accelerating wear. There is a critical temperature which depends on the workpiece, tool materials, and the cutting conditions, at which accelerated wear begins. In other words, there is a critical point where the work-tool interaction becomes temperature sensitive and is generally insensitive below that point. The determination of this critical temperature requires an understanding of the interdependence between the wear, forces, temperature, and contact geometry in the cutting region.

Bowden and Tabor [89] reported that the surface conditions influence the contact resistance and the interface temperature caused by frictional heating and wear. When sliding between two mating surfaces takes place, the asperities of the harder material flow over the softer material causing plastic deformation and wear

of a thin layer of the material. As sliding continues, frictional heat builds up and at a certain temperature, the materials adhere to each other. Further sliding causes separation of built up edge from the parent material, causing plastic lump wear.

The frictional heat generated at the tool-workpiece interface yields a condition characterized by the presence of two heat flows which are different in their magnitude and rate. One, which is in steady state flow goes into the tool. The other is transient and goes into the workpiece. The friction at the tool-workpiece interface generates the heat source which is movable with respect to the workpiece and fixed with respect to the tool. Consequently, two quantitatively different flows occur.

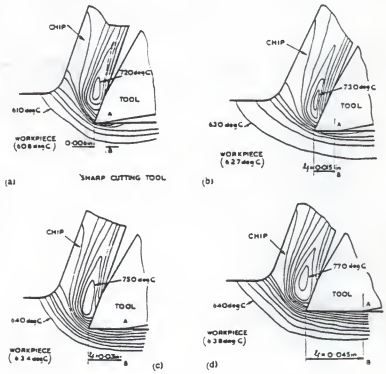

Fig. 4.4 Effect of flank wear land length on temperature distribution in workpiece and chip (isothermal every 10 deg C) [90]

A basic assumption in the development of the temperature calculations of the tool-workpiece interface is that

Hertzian distribution of temperature exists. As shown in Fig. 4.4, the temperature variation along the interface is significant only in the initial stages of the cut, but it then tends to be more uniform with time or as wear progresses.

The total heat quantity generated in the course of the cutting process is defined by the thrust cutting force, the friction coefficient, and the sliding velocity, i.e., the thermal equivalent of the power required to maintain the sliding action over the contact length.

$$q_f = \frac{\mu \cdot p_m \cdot v}{J} \tag{4-21}$$

where μ = frictional coefficient along the interface,

p_m = average pressure along the whole tool-workpiece contact,

v = cutting speed,

J = the mechanical equivalent of heat and

q_f = the rate of frictional heat generation per unit apparent flank area per unit time.

This heat is in fact generated at the real contact spots but is assumed to be generated over the entire flank contact region. It is then partitioned based on the equality of temperature at the contacting surfaces [84]. The temperature distribution in the tool can be assumed to be caused by a stationary heat source and the temperature distribution in the workpiece is assumed to be caused by the moving heat source.

The results in Ref. [90] show that, with a controlled wear land, the tool forces increase linearly with increasing flank wear land length. Even if a sharp cutting tool is used, the results as shown in Fig. 4.5 indicate that there is some contact occurring between the tool flank and the workpiece surface. Thus, it can be seen from both the tool force measurement and the measurement of the temperature distribution given in the figures taken from Ref. [90], that a sharp tool does not correspond to $L_f = 0$. This effect is thought to be due to the actual roundness which exists at the cutting tool tip. Therefore, when the contact length between the tool and the workpiece, L_0, is calculated, an additional length should be included to represent this effect.

Assuming that the wear land length is L_f, then, the total contact length at the tool-workpiece interface will be given by:

$$L = L_0 + L_f \tag{4-22}$$

Theoretically, [30] the cutting force components along and normal to the direction of cut depend on the length of the wear land L_f and are given as follows:

$$F_c = F_{c0} + \mu \cdot p_0 \cdot w \cdot L_f \tag{4-23}$$

$$F_t = F_{t0} + p_0 \cdot w \cdot L_f \tag{4-24}$$

where F_{c0}, F_{t0} are constants for a given tool, workpiece, tool geometry, and cutting conditions. These values are given in chapter 2 and F_c and F_t are linearly related to the wear land despite the fact that the tool temperature is dependent on L_f.[29,91] p_0 is the pressure between the workpiece and the flank wear land. For mild steel cut by H.S.S. it was found, empirically, that $p_0 = Y/3$ where Y is the yield stress of the workpiece material. In other words, the mean stress acting over the apparent area is in the elastic range.

Accordingly, the apparent average contact pressure, p_m, in the tool-workpiece interface can be obtained by dividing the total thrust cutting force by the apparent contact area.

$$p_m = \frac{F_t}{w \cdot L} \tag{4-25}$$

where w = chip width and

L = total apparent contact length including wear land.

As shown in the previous section, the moving heat source due to the friction between the workpiece and the tool at the flank develops a temperature rise at the tool-workpiece interface. The heat partition in this region will be discussed in the Chapter 5.

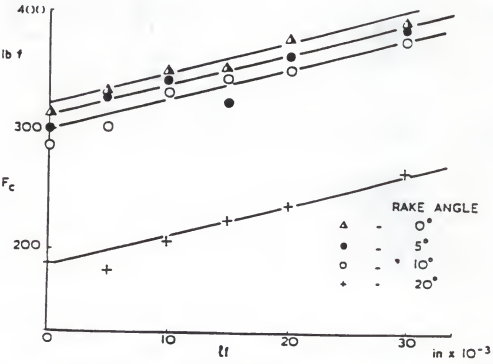

Fig. 4.5 The variation of cutting force with wear land for mild steel at 225 ft/min [90]

The temperature on the flank wear land is generally influenced by the rake-face temperature but this effect will be ignored in this study. As the rate of diffusion wear becomes less than that of adhesive wear, the tool life will increase. Therefore, the crossover point where the wear rate due to diffusion exceeds that due to adhesion can be used as a criterion for tool life as suggested in Ref. [91] In the study, a tool is used until it failed where adhesion and diffusion are the dominant mechanisms of wear. Tolerances were not critical to the process and the machine tool was rigid enough to curtail the chatter arising from excessive wear.

The effect of lubricants and surface coating of the tool can be analyzed easily by using the heat generation model suggested by Bowden and Tabor [89]. Due to these effects, the contact properties such as friction coefficients and heat transfer coefficients will be changed. Using the Bowden and Tabor equation, the heat generation can therefore be calculated [89].

4.3 Numerical Calculations

In order to determine the relation between the cutting parameters such as feed, cutting speed, depth of cut and tool edge radius and temperature rise in the primary deformation zone and tool - chip interface region, the following cutting conditions are used and 81 calculations are carried out.

Workpiece Material: Mild steel with
Ultimate Strength = 500 Mpa
Yield Strength = 210 Mpa

Feed rate(f):	.3 .5 .7	mm/rev
Depth of cut(d):	1 2 3	mm

Cutting speed(V):	50 100 200	m/min
Tool radius(R):	.1 .2 .3	mm
Tool Geometry:		
Rake angle:	10°	
Side angle:	15°	
Carbide tool		
Heat Conductivity:	46.136	N/(sec°C)
Specific Heat:	465	Nm/(kg°C)
Density:	7800	Kg/m^3

The regression model for the mean shear zone temperature as a function of the cutting parameters produces the following equations, respectively.

$$T_{pz} = 452.98 \cdot V^{-.036} \cdot f^{-.0376} \cdot d^{0.0025} \cdot r_\beta^{-.001} \quad (4\text{-}26)$$

$$T_c = 462.14 \cdot V^{0.2761} \cdot f^{.2874} \cdot d^{-.0217} \cdot r_\beta^{0.0085} \quad (4\text{-}27)$$

If the tool forces and the cutting ratio do not vary with changes in cutting speed, the mean shear zone temperature T_{pz} increases slightly with increasing cutting speed and then tends to become constant [50].

However, According to Ref. [92], since the cutting forces decrease with chip thickness and cutting speed, T_{pz} will slightly decrease with the increase of chip thickness and cutting speed. Eq. (4-26) shows that T_{pz} slightly decreases with the increase in feed and cutting speed.

Usually, the temperature, T_c will increase as the feed rate and cutting speed increase as shown in Eq. (4-27) [92]. In real orthogonal cutting operations, the feed rate and the cutting speed play important roles in the heat generation in the primary deformation zone and the tool-chip interface.

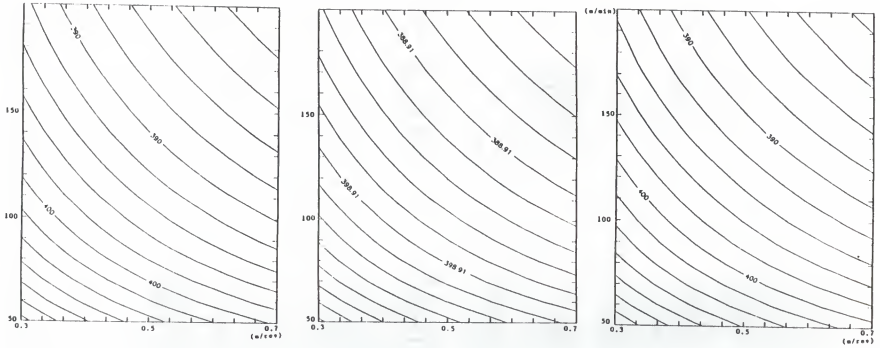

Fig. 4.6 Isothermal curves according to varying feed rate and cutting speed at the primary deformation zone
(feed rate: 0.3-0.7 mm/rev, cutting speed: 50-200 m/min)
a) depth of cut = 1 mm: tool radius = .1 mm
b) depth of cut = 2 mm: tool radius = .1 mm
c) depth of cut = 3 mm: tool radius = .1 mm

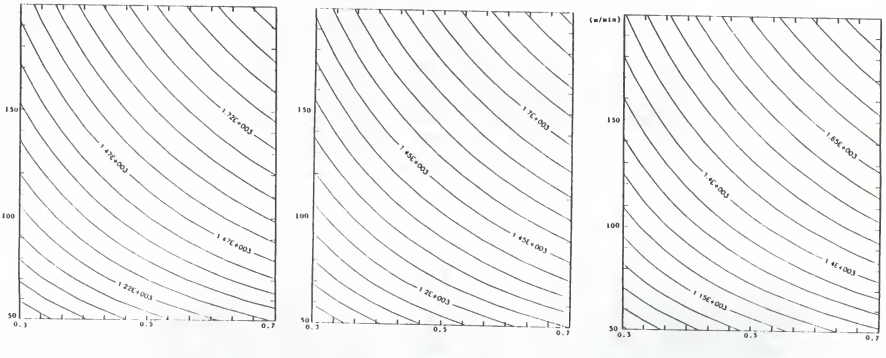

Fig. 4.7 Isothermal curves according to varying feed rate and cutting speed at the tool and chip interface
(feed rate: 0.3-0.7 mm/rev, cutting speed: 50-200 m/min)
a) depth of cut = 1 mm: tool radius = .1 mm
b) depth of cut = 2 mm: tool radius = .1 mm
c) depth of cut = 3 mm: tool radius = .1 mm

Fig. 4.6 shows the isothermal lines of T_{pz} obtained by changing the cutting speeds and feed rates for each depth of cut with a constant cutting tool edge radius (.1 mm)

Fig. 4.7 shows the isothermal lines of T_c for the same condition as Fig. 4.6.

4.4 Conclusions

The following conclusions can be made based on the previous analysis.

1. The heat generation in the primary deformation zone slightly decreases with increasing feed rates and cutting speeds. The depth of cut and tool cutting edge radius have the least effect on heat generation. (Eq. 4-26)

2. The heat generation at the tool-chip interface will increase with increasing feed rate and cutting speed. The depth of cut and tool radius have the least effect on heat generation. (Eq. 4-27)

CHAPTER 5
PREDICTION OF SURFACE RESIDUAL STRESS

5.1 Introduction

Technological developments made it possible that very efficient machining conditions can be implemented for the purpose of increasing productivity. However, such machining conditions may cause undesirable residual stress and damage in the surface region. This is especially the case in high speed machining of high hardness steels. The quality of a machined part can be rated according to its surface integrity. One of the primary aspects of surface integrity is the residual stress distribution because of its direct effect on the life of the part.

Residual stresses are defined as the stress that exist in an elastic body when all external loads are removed. As explained in chapter 2, this stress is classified into two different types, depending on how it is developed. They are called mechanical and contingent residual stress. Although they are generated by different mechanisms, they may be generated simultaneously in the machining process.

Usually, heavy plastic strain and localized heating during sliding contact may generate only mechanical residual stress in some materials. It may also, in some cases, generate additional contingent residual stresses due to the phase change caused by the high frictional heating.

It is important to know the overall pattern of the residual stresses locked in a body. However, in order to better understand the processes that take place when

residual stresses develop, one must first understand the cause-effect relationship of each mechanism.

According to the published literature [5-11], it has been generally accepted that for a given material, the nature of the residual stress distribution in the surface region of a machined workpiece depends on the cutting speed, feed rate, depth of cut, tool geometry, and whether or not a lubricant is used. The residual stresses in a machined surface decay with depth and are all tensile if a perfectly sharp tool is used. A ploughing effect produced by a large radius of the tool edge will generate a compressive residual stress on and near the surface. The magnitude of this compressive residual stress depends on the magnitude of the ploughing force. The absolute value of the residual stress close to the surface is usually high and decreases continuously with depth beneath the machined surface.

Therefore, it is generally accepted that the depth of the stressed region and maximum residual stress tend to increase with an increase in depth of cut, an increase in feed rate, and an increase in cutting speed. At low cutting speeds, the application of a lubricant usually produces a reduction in both the depth of the stressed region and the maximum residual stress, as compared with cutting under dry and unlubricated conditions. At high cutting speeds, the effect of lubrication on the residual stress distribution appears to be negligible.

Although quantitative methods for evaluating the surface residual stress distribution are not fully developed, it is generally accepted that the residual stress may be produced by inhomogeneous plastic deformation induced by the mechanical and thermal events associated with the process of chip formation and interaction between the tool nose region and the freshly machined workpiece surface. Therefore, even though there is a wide variety of metallurgical changes in the machined surface

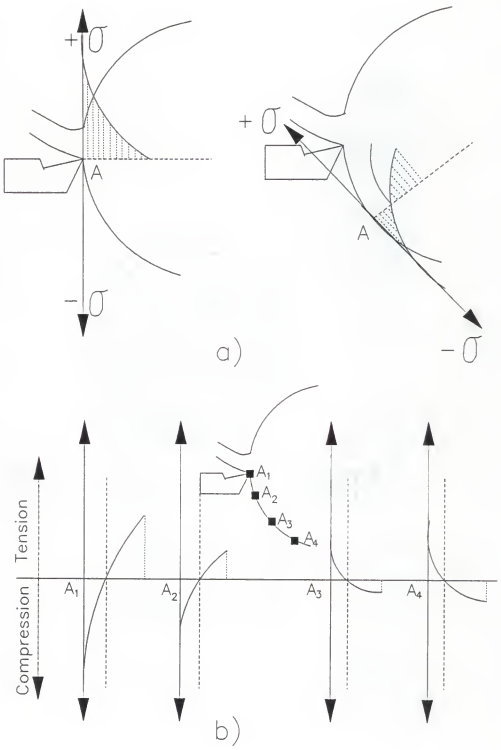

Fig. 5.1 Diagrammatic representation of residual stress
a) mechanical stress
b) thermal stress

region due to the high temperature in the cutting operation, only the residual stress distribution on the machined surface will be examined. The relationship between the amount of residual stress and cutting parameters such as depth of cut, feed rate, speed, and cutting edge roundness will be derived for use in the intended machining optimization procedure discussed in Chapter 6.

The Merwin and Johnson's model [12] which was developed for the analysis of the residual stress production during rolling contact is used in calculating the onset of the plastic deformation generated in the metal cutting process. In this approach, the workpiece is assumed to be elasto-rigid plastic material and the cutting process is simplified as a steady state sliding contact between a rigid stationary plane and an elastic and perfectly plastic half space. The thermal effect in this region is also included in the calculation of residual stress.

5.2 Residual Stress Prediction Model

It is generally accepted that the action of the tool on the workpiece causes plastic deformation in the surface layers where the yield point is exceeded. Below the plastically extended layer are layers of elastic extension. As soon as the tool action ceases, the extended layers will not be expected to return to their original state. Thus the lower layers, which are elastically extended, will exert upon the plastic layer an elastic force which will create in them a state of compression. Consequently, compressive stresses will appear in the upper part of the deformed zone as illustrated in Fig. 5.1.

The machining process also generates, a temperature field which penetrates into the workpiece. The maximum temperature occurs at the contact surface between

the tool and workpiece and decreases with increasing distance from the surface. During dry cutting, the material element near the surface is thermally elongated more than the bulk material. After cutting, the surface element stays hotter than the elements in the bulk, since the cooling occurs from the inside and the air on the surface is a poor conductor of heat. Accordingly, the surface element expands and experiences a compressive stress induced by the bulk material. If this compressive stress exceeds the yield stress, then a tensile residual stress will be induced in the surface element after cooling.

Accordingly, the residual stress distribution in the machined workpiece surface is determined based on knowledge of the cutting forces, tool geometry, workpiece properties, heat generation at the tool/workpiece interface, etc. Thermal stress as well as mechanical deformations during the cutting operation are considered to be the primary sources of residual stress.

The thermal stress on the surface layer is capable of producing only tensile residual stress, and not compressive stress by dry cutting. On the other hand, mechanical deformation can produce both tensile and compressive residual stress. It is also known that residual stress in soft steel is mostly tensile and that in hardened steel is mostly compressive.

In order to completely analyze these phenomena which are illustrated in Fig. 5.1, it is necessary to develop analytical models for the stress distributions caused by the mechanical cutting forces as well as the heat generation at the tool-work interface.

5.3 Stress Analysis During Cutting

5.3.1 Perfectly Sharp Edge Cutting Tool Effect

When a cutting tool with a perfectly sharp edge is used, the stress distribution around the tool tip can be illustrated as shown in Fig. 5.2 where the thrust and cutting directional forces act on the compressed region. According to Connoly and Rubenstein [93], when the tool is perfectly sharp, this effect region can be approximately defined by the lower boundary of the plastic deformation region.

Considering an idealized contour for the lower boundary of the primary deformation as shown in Fig. 5.2, the forces sensed by the workpiece are in equilibrium with the forces acting on the lower boundary of the primary deformation zone. Those ,in turn, are in equilibrium with the forces acting on the tool. Provided that the shape, location and stress system acting on the lower boundary of the primary deformation zone can be specified, the force components acting on the workpiece which are related to the residual stresses on the machined surface can be obtained without information on the upper boundary of the primary deformation zone.

In the Fig. 5.2, there are two intersecting planes; OA, of length L, extending from the tool tip, and, AB, which is tangential to the lower boundary of the primary deformation zone in the cutting process. The line, AB, meets the free surface of the workpiece at 45° and the line OB represents the shear plane with shear angle ϕ. As cutting conditions change, the length of OA (=L) will change. As L decreases, the value of ϕ will approach that of θ, i.e. ϕ will approach 45°. At a given rake angle and a given uncut chip thickness, L decreases as the velocity increases.

$$L = t_1 \cdot (\cot \phi - \cot \theta)$$
$$= t_1 \cdot (\cot \phi - 1) \qquad (5\text{-}1)$$

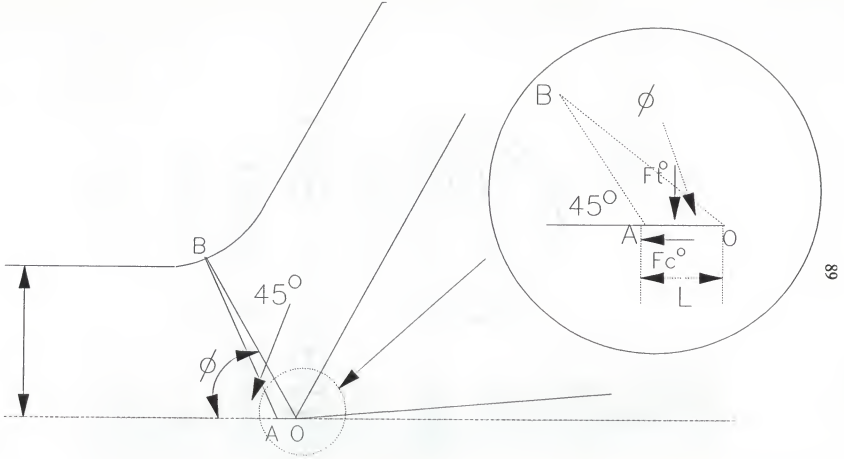

Fig. 5.2 Force components acting in the lower boundary of the primary deformation zone

where t_1 represents the undeformed chip thickness and ϕ is the shear angle of the primary shear plane in the primary deformation zone. It is found empirically that ϕ is relatively lower for brittle workpiece materials than for ductile materials. L reflects, inversely, the degree of ductility of the workpiece material and the variation of L with the cutting speed is consistent with this observation. It may therefore be concluded that L reflects the machinability of the workpiece material [93].

The forces on plane OA with length L is assumed to be the force source for the residual stress. If the shape, location and stress system acting on the lower boundary of the primary deformation zone are specified, the force components acting on the workpiece which influence the generation of residual stress on the machined surface can be obtained without information on the upper boundary of the primary deformation zone. When it is assumed that the shear stress and normal stress along AB are uniform and equal to each other, and the shear stress on the OA is equal to that of AB, the force relations on the lower boundary of the primary deformation zone can be expressed as follows:

$$F_c^{\theta} = W \cdot S \cdot (2 \cdot t_1 + L) \tag{5-2}$$

$$F_t^{\theta} = W \cdot p_1 \cdot L \tag{5-3}$$

Where W = chip width(mm),

S = shear stress in the primary deformation zone(MPa),

t_1 = chip thickness(mm),

p_1 = normal stress in the low boundary region(MPa),

F_c^{θ} = force component of the cutting direction which is assumed to act on the workpiece, L and

F_t^{θ} = force component of the thrust direction.

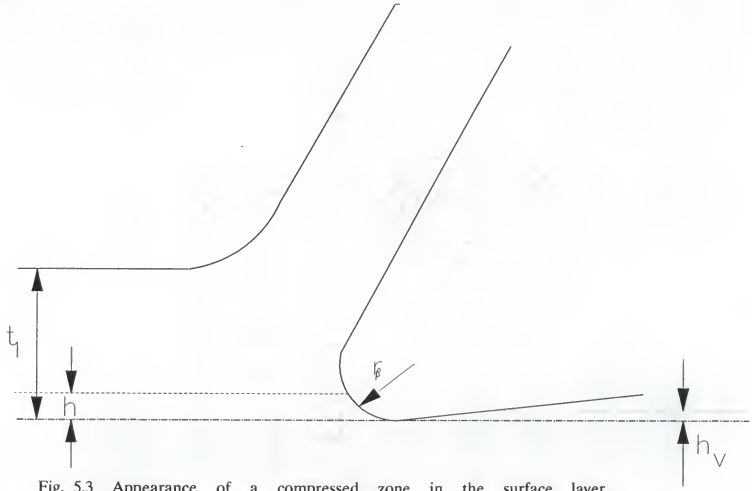

Fig. 5.3 Appearance of a compressed zone in the surface layer

The normal stress on the surface with length L is given in reference [93] and can be expressed as

$$p_1 = S - C\cdot(S+T)\cdot(1+(t_1/L)\cdot(1+\tan\alpha)) \quad (5\text{-}4)$$

where T = tensile strength of the workpiece material,

C = a constant proportion of the chip thickness where the tensile stress acts in front of the tool and

α = rake angle of the tool.

When the cutting tool is assumed to be perfectly sharp, an elliptical load distribution is assumed on OA of the semi-infinite surface workpiece.

5.3.2 Effect of Tool Radius

The cutting edge of a tool is not expected to be perfectly sharp and a tool generally has a particular radius. Fig. 5.3 shows a simplified surface layer formation. The cutting edge with radius r_β is shown and magnified. This radius depends on the sharpening method and on the amount of tool point wear. As a result of this roundness, a part of the undeformed chip, which is plastically strained by the action of the stress field, is pressed in at the depth of h which additionally increases the compression of the material. When this effect is considered, it may be assumed that the imaginary shear surface will start from a certain point O, situated on the curved part of the tool point profile. Fig. 5.3 shows an illustration of the flow pattern of the workpiece material approaching a tool of finite radius. All material below point O must pass below the tool and is compressed. All material above O moves, eventually, parallel to the rake face. When h represents the depth of cut below which no material is removed and with a nominal depth of cut, t_1, the depth of material removed will be $(t_1 - h)$ in a single cut. In other words, as soon as the point O passes

a part of the material which was only elastically deformed the material rebounds to the height h and consequently, the depth of material removed will be (t_1 - h).

If the length of contact between the flank face and the cut surface is assumed to be L_θ, then For any given clearance angle and cutting conditions, the length of contact will be fixed and subjected to a hydrostatic pressure p_m. The contact length for a given nose radius of the tool is given in reference [93] as follows:

$$L_\theta = r_\beta \cdot (\cos \alpha_c + \cot \beta \cdot (1 - \sin \alpha_c)) \tag{5-5}$$

where β = relief angle and

α_c = critical angle of the tool.

Here, when β is 3°, α_c is 70°. Then the cutting edge force components due to tip roundness will arise and can be expressed as: [93]

$$F_t' = p_m \cdot W \cdot L_\theta \tag{5-6}$$

$$F_c' = p_m \cdot W \cdot (h - h_v) + \mu \cdot F_t' \tag{5-7}$$

where μ is the coefficient of friction between the tool and workpiece material and h_v is the height of recovery. Thus, for a given material being cut by a tool of fixed cutting edge radius and with a fixed clearance angle, the cutting edge components F_t' and F_c', should be constant. Values of the coefficient of friction can be obtained from reference [94].

If it is assumed that the material is elastically strained, then $h = h_v$ (i.e. full recovery) and the cutting edge component equation becomes

$$F_c' = \mu \cdot F_t' \tag{5-8}$$

Accordingly, p_m in this case must be less than or equal to 3Y where Y is the yield stress in uniaxial tension or frictionless compression.

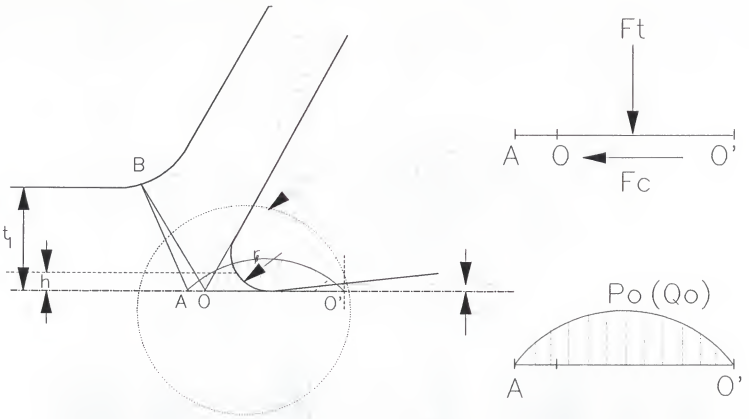

Fig. 5.4 Elliptically distributed stresses in the cutting zone

5.3.3 Effect of Flank Wear on the Cutting Forces

As the flank wear land increases, both Fc′ and Ft′ will increase. Assuming that the length of the wear land is assumed L_f, the cutting forces can be calculated as:

$$Ft'' = p_m \cdot W \cdot L_f \tag{5-9}$$

$$Fc'' = \mu \cdot Ft'' \tag{5-10}$$

where Ft'' = thrust component of the force acting on the wear land and

Fc'' = cutting directional component of the force acting on the wear land.

When the three factors are considered in calculating the components of cutting forces in the cutting operation, part of the action region is stressed by Ft^0 and Fc^0. Then, this stressed region is pressed by the other forces caused by the cutting edge roundness and flank wear land. Therefore, the region in the workpiece which is deformed by the components of the cutting forces which are assumed to be elliptically distributed over L receives another stress which is assumed to be elliptically distributed over the length $L_0 + L_f$. The total forces which act on the deformation zone can therefore be expressed as:

$$Ft = Ft^0 + Ft' + Ft'' \tag{5-11}$$

$$Fc = Fc^0 + Fc' + Fc''. \tag{5-12}$$

These cutting forces are assumed to be elliptically distributed over the length $L_t = L + L_0 + L_f$ and are used in the Merwin and Johnson model. The model utilizes Smith and Liu's [95] solution in calculating the elastic state of stress. In the solution, both normal and tangential loads are assumed to be distributed elliptically over the contact and the maximum value of each load is obtained as: [Fig. 5.4]

$$P_0 = 2 \cdot F_t / (\pi \cdot L_t \cdot W) \tag{5-15}$$

$$Q_0 = 2 \cdot F_c / (\pi \cdot L_t \cdot W) \tag{5-16}$$

5.3.4 Thermal Stresses at the Tool-Workpiece Interface

Experimental evidence [9] strongly suggests that when phase changes are absent in the machined part, the cutting temperature has a significant effect on the stress field by reducing the yield strength of the workpiece material.

The heat generation is assumed to be uniform over the contact length between the tool flank and the machined surface. The stress which results from the heat generation at the interface is assumed to be superimposed on the mechanical stresses and the combined stresses are used to calculate the residual stresses. The temperature at a certain depth into the workpiece is used for calculating the reduction in the yield strength of the workpiece material at that depth.

The heat flux q caused by friction at the tool and workpiece interface is given by a following equation.

$$q = \mu \cdot P_m \cdot V \cdot r \tag{5-15}$$

where r is the heat partition factor given by a following relation.

$$r = \frac{0.946 \cdot K_w \cdot (L/2) \cdot V}{1.046 \cdot K_t \cdot \alpha_w + 0.946 \cdot K_w \cdot (L/2) \cdot V} \tag{5-16}$$

where

K_w = thermal conductivity of the workpiece material,

α_w = thermal diffusivity of the workpiece material,

K_t = thermal conductivity of the tool material,

V = cutting speed and

L = contact length between the tool and the workpiece.

The temperature distribution in the workpiece during the cutting process is generally estimated using the moving heat source theory [88]. The quasi-steady state temperature distribution caused by a plane band source of heat moving along the surface of a semi-infinite body in the x direction at a constant velocity V is given by following equation [88]

$$\Theta(X,Z) = \int_{X-h}^{X+h} e^{-m} \cdot K_0(Z^2 + m^2)^{0.5}\, dm \qquad (5\text{-}17)$$

where

K_0 = the modified Bessel function of the second kind of order zero

$\Theta = \pi \cdot K_w \cdot V \cdot T/(2 \cdot q \cdot \alpha_w)$

$h = V \cdot L/(2 \cdot \alpha_w)$

$X = V \cdot x/(2 \cdot \alpha_w)$

$Z = V \cdot z/(2 \cdot \alpha_w)$

It is generally accepted that the thermal effect is more significant when there are no phase changes in the material of the machined part. The analysis developed here assumes that no phase changes occur with temperature. It is further assumed that tensile residual stress is created in the machined surface when the thermal stress caused by cutting is dominant, and that residual compressive stress is created when the burnishing effect of the cutting tool is dominant. This is expected to be the case for a grinding operation when most of the grinding energy is absorbed in the workpiece as heat. However, in machining as compared to grinding, the heat absorbed in the workpiece is relatively small (10-15 % of total cutting energy in the primary shear zone) and the penetration depth of the heat is much smaller due to

the higher speed of the workpiece. In the flank contact zone, the contact pressure and the heat generation are lower than the corresponding values in the primary cutting zone and heat partition between the tool and workpiece occurs. Therefore, it is less likely that the heat absorbed in the workpiece during cutting is the major source for the tensile residual stress. It is accepted that the temperature rise produced during cutting reduces the yield strength of the workpiece material significantly, and thus the stressed zone is enlarged.

Using the temperature rise at the machined surface, the thermal tensile stress is calculated using the following equation [98].

$$\sigma_{th}^{surface} \approx -\alpha_w \cdot E \cdot q / (\pi \cdot \rho_w \cdot c \cdot (1-\nu) \cdot K_w) \qquad (5\text{-}18)$$

The temperature gradients give rise to thermal stress which can be evaluated from:

$$\sigma_{th} = - E \cdot \alpha \cdot \Delta T \; / \; (1 - 2 \cdot \nu) \qquad (5\text{-}19)$$

where

E = Young's modulus,

α = thermal expansion coefficient and

ν = Poisson ratio.

The distortions are large only in the vicinity of the tool contact region where the actual surface is approximately plane and the temperature gradients in the bulk material are relatively low which lead to approximately uniform expansion or contraction. Neither of these introduces thermal stresses or significantly changes the profile in the contact zone. Although the thermally induced stress effect on the stress distribution in the workpiece is small, it is nontheless calculated and used in obtaining the residual stress in the machined workpiece.

5.4 Calculation of Residual Stresses in the Machined Surface

5.4.1 Procedure of Residual Stress Formation

As mentioned in the previous section, a part of the workpiece surface is plastically strained by the action of stress field in front of the cutting tool. As a result of the roundness of the cutting edge, this part is pressed-in again at the depth h which additionally increases the compression of the material. (Fig. 5.3)

Liu and Barash [9] explained the surface layer deformation and residual stress formation using Fig. 5.5 as follows:

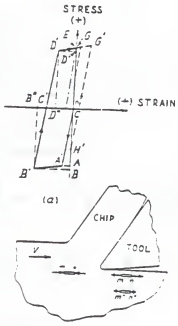

Fig. 5.5 Loading and unloading process

It is assumed that in an orthogonal cutting model, the geometric constraint is that the length of a material element remains unchanged before and after generation of a new surface. In an assumed uniaxial stress strain curve, a small line element of material, MN is subjected to a compression until it yields and then it is subjected to stress unloading, satisfying the condition of compatibility (elongation = 0). Therefore, element MN of the subsurface layer material will follow ABCDE on

the y-axis of the figure. When a pseudo-line, OA'B'C'D'E is assumed for the elastic-perfectly plastic material, the final stage reaches E due to zero elongation. The stress OE is the residual stress developed in this line element after cutting and OF is the corresponding elastic strain of the strain-hardened element. FB" and B"F are the plastic strain which MN experiences during the loading and unloading process. The final residual stress is different at different depths and is modified by the conditions of equilibrium and compatibility. Due to the roundness of the cutting edge, M'N' is further subjected to stretching by friction when it is behind the tool edge. The stress-strain state will move to G before unloading and the residual stress will be OH. If M'N' is stretched to G', then the residual stress will be OH'. A line element M"N", deeper than the machined surface, M'N' may not experience the stretching and the residual stress will be consequently different.

5.4.2 Calculating Procedure of Residual Stress

As explained in section 5.3.3, the cutting surface is assumed to be initially stressed by the cutting force components over L and is stressed again by the friction over the length $L_0 + L_f$ while unloading. As the cutting speed increases, the length L will decrease. Beyond a certain cutting speed, L may be negligible. In other words, it is not necessary to calculate the residual stress distributions twice in order to determine the residual stress at a point in the machined surface. Since the loaded region is limited only to the interface between the tool and workpiece, the total loads, F_t and F_c are assumed for simplicity to act on this region, L_t. Therefore, the maximum stresses induced by the thrust and cutting forces, P_0 and Q_0, are given by Eqs. (5-13) and (5-14).

Fig. 5.4 shows the load exerted on a semi-infinite solid surface in the cutting process. For convenience, the cutting tool is considered to be stationary and the semi-infinite solid which represents the workpiece is assumed to be moving with speed V. The superimposed stresses caused by the thermal and mechanical effects are then used to check the plastic yielding criterion of the workpiece material and Merwin-Johnson's model [12] is used in calculating the stress distribution in the plastically deformed region.

A plane strain condition (i.e. $\sigma_{yy} = 0$ and $\partial/\partial y = 0$) is assumed in the analysis. In order to find the stresses in the plastically deformed region, it is necessary to trace the loading cycle at each point as it passes under the load. In the Merwin-Johnson's model, during plastic deformation, it is initially assumed that the plastic strains are equal to the elastic strains. The stresses at each point in the plastic region are then found by employing the Prantl-Reuss equations [97] for an elastic-perfectly plastic material. During plastic deformation the von Mises flow rule (i.e., the rule for determining the locus of yield points) is chosen as the yield criterion. The basic assumption in the Merwin-Johnson method is that the total strain is identical to the elastic strains obtained by solving elastic stress-strain relations, even when the materials yield plastically. As a result of plastic deformation, each point must have a state of residual stress since the unloading displacement is different from the loading displacement. A step-by-step numerical method, the Runge-Kutta-Gill method [97], is used in solving the stress-strain equations in the plastically deformed region and the related equations in Merwin-Johnson's model are given in Appendix A. The elastic states of stress in the machined surface under the elliptically distributed load are calculated based on Smith and Liu's solution. [95]

The analysis is performed according to the following steps:

1. Initially, the steady state residual stresses and strains in the x-y plane are assumed to be zero.
2. A fixed point in the plane is considered (initially at $x = \infty$ and $y = y_0$). Since the contact is far away from this point, the state of stress is calculated by superimposing the elastic and thermal stresses. The stresses are recalculated at this point as it moves towards the contact with a speed V and increments of dx. The elastic stress fields are calculated using Smith and Liu's solution.
3. When the state of stress at the point satisfies the von Mises yield criterion, the Prantl-Ruess equations are used to calculate the state of stress for the successive deformation movement of the point, assuming that the total strains are the same as that given by elastic behavior. During plastic deformation, Von Mises flow rule requires that the second invariant of the stress deviator, J_2' remains constant and equal to K^2, where K is the yield strength in shear. This is given as follows:

$$J_2' = \Sigma\,\Sigma\,(\sigma_{ij}'\sigma_{ij}') = (1/3)\cdot\bar{\sigma}^2 = K^2 \qquad (5\text{-}20)$$

The total strain rate, ε_{ij}, is the summation of the elastic strain rate, ε_{ij}^e, and the plastic strain rate, ε_{ij}^p, or

$$\varepsilon_{ij} = \varepsilon_{ij}^e + \varepsilon_{ij}^p \qquad (5\text{-}21)$$

The plastic strain rate can be related to the applied stress using the Prantl-Reuss equations as:

$$\varepsilon_{ij}^p = (W^p/(2K^2))\cdot\sigma_{ij}' = (3/2)\cdot\frac{d\varepsilon^p}{\sigma}\cdot\sigma_{ij}' \qquad (5\text{-}22)$$

where $W^p = \Sigma\,\Sigma\,(\varepsilon_{ij}^p\sigma_{ij}') = \sigma\cdot\varepsilon^p$. This equation can be written as follows:

$$\varepsilon_{ij} = \sigma_{ij}'/(2G) + W_p\cdot\sigma_{ij}'/(2K^2) \qquad (5\text{-}23)$$

$$\sigma'_{ij} = 2G\cdot(\varepsilon_{ij} - W_p\cdot\sigma_{ij}/(2K^2)) \tag{5-24}$$

4. The Prantl-Ruess equations are integrated using Gill's modification of the Runge-Kutta method to the fourth order.

   In order to integrate Eq. (5-24), it is convenient if the time rate of change can be transformed to gradients with respect to x as follows:

$$\frac{d}{dt}(\sigma'_{ij}\varepsilon_{ij};W) = U\cdot\frac{\partial}{\partial t}(\sigma'_{ij}\varepsilon_{ij};W) \tag{5-25}$$

   where U is the steady sliding speed of the lower plane. Therefore, by substituting Eq. (5-25) into (5-24), the time rate of change will be replaced by derivatives of x. U is cancelled out of the equation.

5. When the von Mises yield criterion is no longer satisfied or the rate of plastic work becomes negative, then the plastic deformation terminates. For successive movements of the point, the state of stress is found from the elastic equations according to Smith and Liu's solution.

6. In order to satisfy the equilibrium condition, at the end of calculations, the stresses are relaxed elastically. This procedure may give non-zero residual stress and strains.

7. The same procedure is followed for points at different depths to approximate the total state of stress. The final residual stress equations are given as follows:

$$(\sigma_{xx})_r = (\sigma_{xx})'_r - \frac{\nu}{(1-\nu)}(\sigma_{zz})_r \tag{5-26}$$

$$(\sigma_{yy})_r = (\sigma_{yy})'_r - \frac{\nu}{(1-\nu)}(\sigma_{zz})_r \tag{5-27}$$

   The detailed equations used in the analysis are given in Appendix A.

In order to determine the plastic deformation of a surface region that can influence variations in hardness, microstructure, and residual strain, the depth of the plastically deformed region is important. It is generally known that the depth increases with an increase in cutting speed and an increase in the chip-tool contact length and appears to be unaffected by the method of tool preparation such as grinding and polishing. Here, only the plastic deformation induced by the cutting forces and thermal stresses is considered. In order to calculate the thermal effects on reducing the yield strength of the workpiece, the temperature distribution in the workpiece is calculated.

Because the maximum depth of the plastically deformed region is important, the depth where the residual stress vanishes inside the workpiece is used as the maximum depth of the plastically deformed region.

5.5 Numerical Examples

Case 1. Comparison with published experimental data

It can be seen from the previous discussion that the nature of the residual stress distribution in the surface region of a machined workpiece depends on the cutting conditions such as cutting speed, feed rate, depth of cut, tool geometry , and whether or not a lubricant is used.

Although there are many published results on the measurement of residual stress very few give complete information on the cutting conditions involved. One of the cases where such information is given is the study by P. Leskovar and J. Peklenik [100]. It will therefore be used to check the validity of the developed model. The conditions reported in this example are

Material: 42CrMoS4 steel with

Ultimate Strength = 930 MPa

Yield Strength = 610 MPa

Feed rate = .132 mm, and .314 mm

Depth of cut = 1 mm

Cutting Speed = 200 m/min

A sharp tool with a pointed edge is used in this case. Fig. 5.6 shows that a plot of the calculated residual stress pattern for the same conditions The published experimental data are also plotted for comparison.

It can be seen that the theoretical and experimental results are in excellent agreement up to a depth of .09 mm. Below this depth, there appears to be a difference in the compressive stresses which can reach up to 14 % of the value of the maximum tensile stresses. It should be noted in this case, that the residual stress on the surface are tensile which is to be expected when a sharp edge is used. [9]

Case 2.

In order to illustrate the results which can be obtained from the model for a tool with a rounded edge, an orthogonal turning operation is investigated under the following material and cutting conditions:

Workpiece Material: Mild steel

Ultimate Strength = 500 Mpa

Yield Strength = 210 Mpa

Feed rate(f): .3, .5 .7 mm/rev

Depth of cut(d): 1, 2. and 3 mm

Cutting speed(V): 50, 100 and 150 m/min

Tool radius(R): .1, .2 and .3 mm

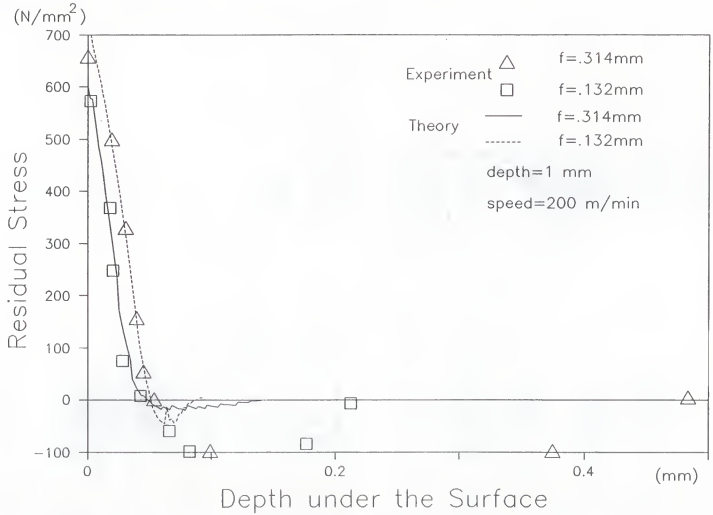

Fig. 5.6 Residual stress distribution compared with experimental data from Ref. [100]

Tool:	Carbide material
Tool Geometry:	
Rake angle:	10°
Side angle:	15°

Without considering tool wear (i.e. $L'' = 0$), 81 calculations were carried out. The surface residual stresses, the maximum tensile stresses and the plastically deformed depths are chosen as the parameters for defining the residual stress condition.

Figures 7, 8, 9, and 10 show the residual stress distributions on and beneath the machined surface. The following can be deduced from the calculated results:

1. The maximum residual stresses occur at the surface, are compressive and decrease with depth beneath the machined surface. The stresses then become tensile, reach a maximum, then asymptotically vanish with further increase in depth.
2. The values of maximum compressive stresses increase with increasing feed and decrease with increasing cutting speed and tool radius. However, the depth of cut appears to have little effects on the maximum stress.
3. The maximum tensile residual stress below the surface increases with cutting speed and tool radius. The feed rate appears to have an opposite effect.
4. The maximum depth of the plastically deformed region increases with increasing feed rate, cutting speed and tool radius. The depth of cut shows the least effect.
5. The maximum depth of the region with compressive residual stress increases with feed rate and tool radius and decreases with increasing depth of cut. Although this value increases with the cutting speed, the effect is relatively small.

Curve fitted relationships are obtained for the maximum compressive surface stresses, maximum tensile stresses and the maximum plastically deformed depth as a function of the cutting parameters by a regression analysis. The obtained relationships for the considered example based on the calculated 81 cases are as follows:

$$\sigma_c = -2284.32 \cdot f^{.7525} \cdot d^{-.01797} \cdot v^{-.3962} \cdot R^{-.3828}$$

$$d_c = .1739 \cdot f^{.67205} \cdot d^{-.05849} \cdot v^{.0909} \cdot R^{.31652}$$

$$\sigma_t = 25.752 \cdot f^{-.6611} \cdot d^{.07607} \cdot v^{.3057} \cdot R^{.9858}$$

$$d_{th} = .4854 \cdot f^{.4221} \cdot d^{-.01153} \cdot v^{.1938} \cdot R^{.7158} \qquad (5\text{-}28)$$

These equations are only applicable for mild steel machined with a carbide tool with .1 mm < R < .3 mm, 50 m/min < V < 150 m/min, 1 mm < d < 3 mm and .3 mm/rev < f < .7 mm/rev

5.6 Conclusions

A model for predicting the residual stress is developed which takes into consideration the mechanical and thermal aspects of the problem. The results from the model show good agreement with the experimental data published in Ref. [100]. It is interesting to note that the sharpness of the tool influences the magnitude and type of the maximum stress at the surface. Compressive residual stress is expected to occur when a tool with rounded edge is used. A perfectly sharp tool can be expected to produced tensile stress.

In the latter case, only the front cutting region will act as the main source force for the tensile residual stresses.

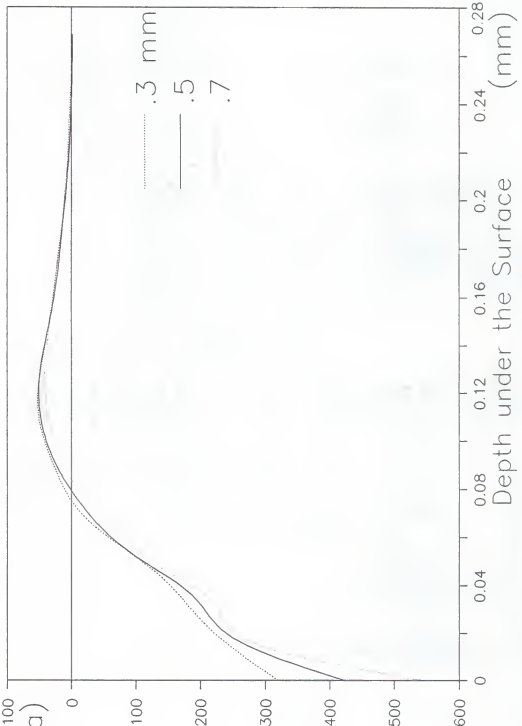

Fig. 5.7 Residual stress variation with feed depth of cut=3 mm speed=50 m/min radius=.3 mm

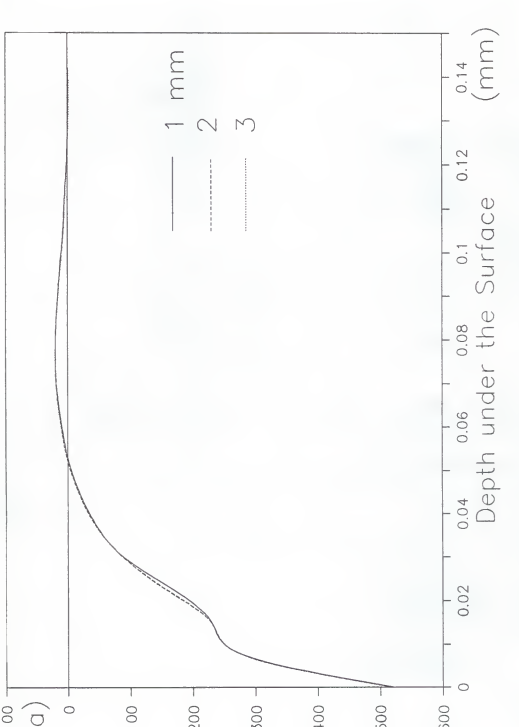

Fig. 5.8 Residual stress variation with depth of cut feed = .3 mm/rev speed = 50 m/min radius = .3 mm

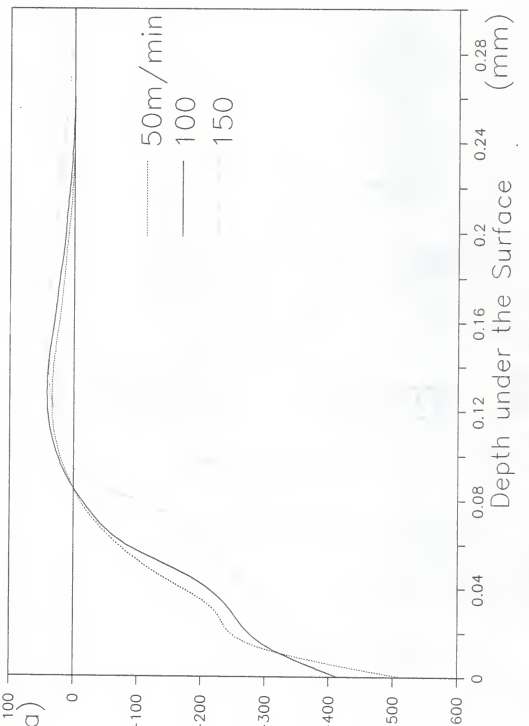

Fig. 5.9 Residual stress variation with cutting speed feed = .3 mm/rev depth of cut = 3 mm radius = .3 mm

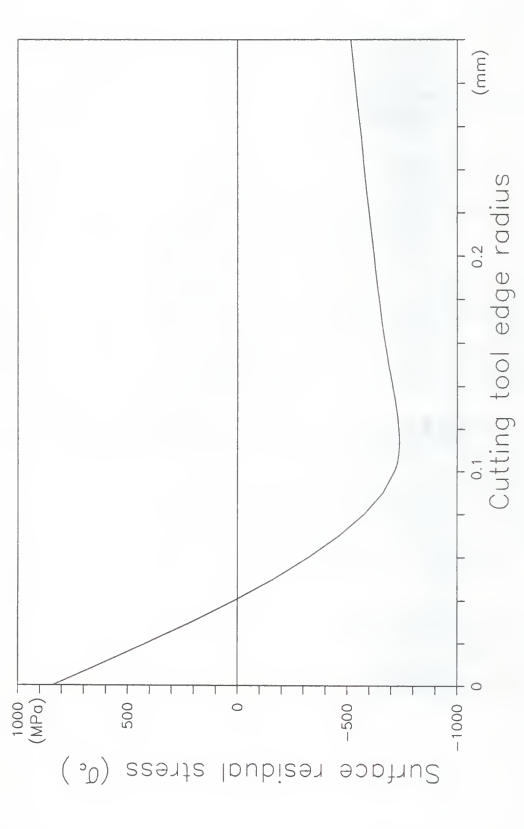

Fig. 5.10 Residual stress variation with tool radius feed = .3 mm/rev depth of cut = 3 mm cutting speed = 50 m/min

According to references [9] and [11], a tool with a finite cutting edge radius will cause a ploughing effect which may generate a stretching force in the process of relieving the plastically deformed material and compressive residual stress will occur on the machined surface.

CHAPTER 6
OPTIMIZATION ALGORITHM FOR USE IN ADAPTIVE CONTROL OF THE MACHINING PROCESS

6.1 Introduction

Since the advent of the first Numerically Controlled (NC) machine in 1952, the full automation of machine tools has been the primary goal of production research. Recently, the expansion of computing power and computer networks have made possible the full integration of DNC (Direct Numerical Control) and CNC (Computer Numerical Control) in a hierarchical manufacturing system with distributed control. Within such a system the individual machine tool should ideally be able to carry out the machining activities independently and adaptively without human intervention at the machine hardware.

Randau [37] defined an adaptive system as follows:

> "An adaptive system measures a certain index of performance (IP) using the inputs, the states, and the outputs of the adjustable system. From the comparison of the measured index of performance and a set of given ones, the adaptation mechanism modifies the parameters of the adjustable system or generates an auxiliary input in order to maintain the index of performance close to the set of given ones (i.e., within the set of acceptable ones)."

An adaptive control process is illustrated in Fig. 6.1. In the process, the adjustable system must be understood to be a system capable of adjusting its performance either by modifying its parameters (internal structure) or by modifying its input signals. The measurement of the index of performance can be done in several ways, sometimes directly, sometimes indirectly, as for example, through the identification of the dynamic parameters of the system.

The comparison-decision block makes the comparison between the given set of the IP's and the measured IP and decides if the measured IP is within the acceptable IP set. If not, the adaptation mechanism will act accordingly by modifying the system or by changing the system control inputs. In the general case, the comparison decision block makes a class separation as well as an evaluation of the distances to the separation boundary.

As reviewed in Chapter 2, the adaptive control system in the machining process is defined as a system that allows machine tools equipped with sensors to detect a changing environment (e.g., tool wear, working material hardness, and chattering...) and then to take adaptive actions (e.g., change speed or feed). Many investigations in the Adaptive Control of Optimization (ACO) and Adaptive Control of Constraint (ACC) are focused on the purpose of minimizing production cost, maximizing the profit and maximizing the production rate. However, in addition to this purpose, the satisfaction of the surface quality and surface integrity requirements is important, since they determine the useful life of the machined part. The residual stress distribution is one of the important factors in this regard. To date few researchers have addressed this problem in the context of controlling the machining process.

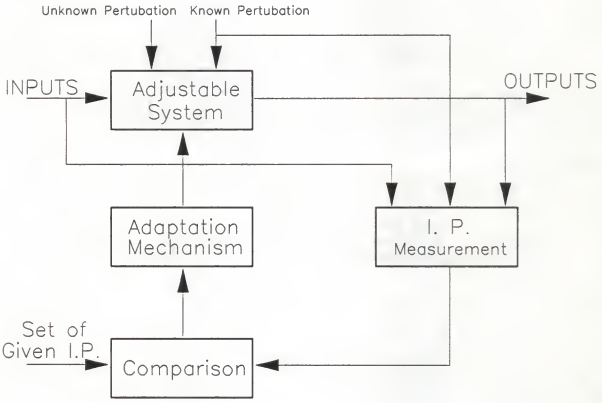

Fig. 6.1 Basic model of adaptive system [37]
(I. P. means the index performance)

In this chapter, an optimization algorithm is developed for use in adaptive control of Advanced ACC system. The algorithm determines the machining parameters which maximize the productivity of the system, while providing the functional specifications for the machined parts. Accordingly, by operating the machine within specified physical constraints, catastrophic tool failure can be avoided and better quality machined surfaces can be obtained.

The objective of this chapter is to develop a rational adaptive metal cutting model which utilizes the results of an algorithm defining the requirements and constraints of the process. The algorithm takes into consideration tool wear and surface integrity based on the physical behavior of the machining process.

6.2 Formulation of the Optimization Model

To construct the frame work of the methodology for the proposed ACC optimization, the first task is to identify the most important physical parameters governing the process. The second task is to map the constraints onto the optimization space of control variables, and subsequently, determine the optimum condition in terms of the control variables.

In this approach to adaptive control, many constraints are chosen to set the limits on the control variables such as speed, feed, and depth of cut. These constraints can be divided into parameter constraints and behavioral constraints. Tool failure, surface residual stress distribution, surface finish condition, and stability of the dynamic cutting are among the important behavioral constraints.

The objective of the optimization is to determine the cutting speed, feed rate, and depth of cut which maximize the production rate without violating the constraints imposed on the process [58,101].

6.2.1 Constraints Identification and Mapping onto the Decision Space

6.2.1.1 Parameter constraints

For a given tool-workpiece material combination and for a certain machine tool, there are minimum and maximum values of the cutting parameters, depending on the machine tool capability. These constraints can be stated as follows:

$$f_1 < f < f_2$$
$$V_1 < V < V_2$$
$$d_1 < d < d_2 \qquad (6\text{-}1)$$

6.2.1.2 Operation constraints and mapping

In this section,tool life, surface condition of the machined workpiece, and stability of the machine tool in the dynamic cutting process are considered as the operation constraints. The machining parameters should satisfy these operation constraints

[1] Tool failure constraints. Plastic deformation, tool flank wear, crater wear, and tool fracture are constraints which control the life of the tool.

Tool fracture. The brittle failure of the tool is defined as the break-away of the tool edge. The fracture occurs when the normal stresses reach the ultimate stress value in the so-called "dangerous" point. This value is equal to the ultimate strength of the tool at uniaxial tension (σ_B) or compression (σ_{-B}). Based on published theoretical and experimental works [25,102] there exist two different stress zones in the working part of cutting tool during the machining. These are the zone of compression ($\sigma_2 \leq 0$, $\sigma_3 \leq 0$) and the zone of tension (σ_1) where (σ_1, σ_2, σ_3) are the principal normal stresses at a given point. The border of these two zones is the neutral surface where the principal stresses is zero. [Fig. 6.2]

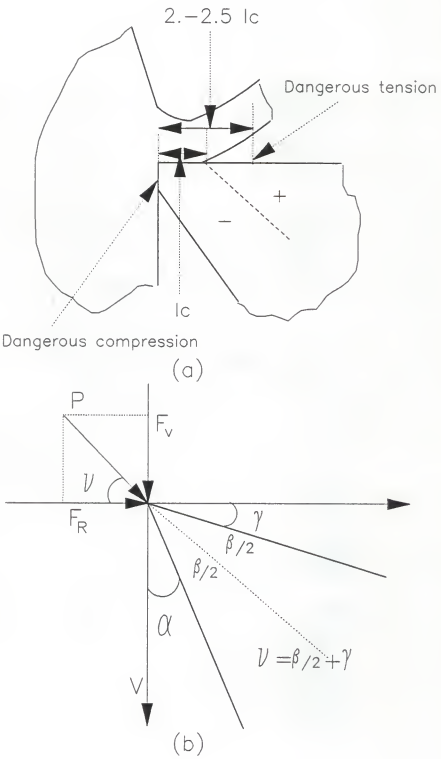

Fig. 6.2 Acting force diagram in the tool face [102]
(a) Stress distribution in the tool
(b) Resultant force in the wedge
(l_c means the length of contact between tool and chip)

According to Loladze [25] and Chandrasekaran [102], the "dangerous" point where tensile principal stress (σ_1) has its maximum value occurs in the tensile zone located at a rake surface ($\sigma_3 = 0$) at the distance of approximately double the contact length of the chip along the rake. Consequently, the most probable area where cracking and brittle failure begins is the rake surface region. According to Loladze [25], the maximum tensile stress on the rake face is proportional to the feed rate.

$$\sigma_1 = c_1 \cdot f \tag{6-2}$$

where c_1 can be determined experimentally and theoretically [102].

The theoretical approach for calculating the maximum tensile radial stress on the rake face of the tool was proposed by Chandrasekaran and Nagarajan [28] The relations is shown in Fig. 6.2. The maximum tensile stress, σ_{max} is given as:

$$\sigma_{max} = \frac{P}{b \cdot h} \left[\frac{\sin \beta/2 \cdot \sin(\nu - (\beta/2 + \gamma))}{\beta - \sin \beta} + \frac{\text{Cos } \beta/2 \cdot \text{Cos}(\nu - (\beta/2 + \gamma))}{\beta + \sin \beta} \right] \tag{6-3}$$

where β = wedge angle of tool,

P = resultant cutting force,

h = tool and chip contact length,

b = width of cut and

ν = inclination of the resultant force P with respect to the radial cutting force.

This relation will be used for estimating the maximum radial tensile cutting force on the rake face in terms of the cutting parameters.

Therefore, for a given tool and work materials and a given tool geometry there exist limits on feed rate (breaking feed) and other cutting parameters at which

the stresses at the dangerous point reaches the rupture values. Near this dangerous point, cracking of the tool material can occur.

Depending on the type of operation (turning, boring, milling, etc.), the nature of tool loading changes considerably. Changes in the nature of loading during the entrance and exit phases of the cutting tip are other factors which reduce the value of limiting feed rate for different machining operations.

During the turning and boring operations, the tool is generally subjected to fluctuating load (of constant sign), whereas in milling, it is subjected to cyclic alternating load.

Thermal stresses can play a significant role in the brittle failure of the working part of the tool. During interrupted cutting (milling, hobbing, etc.), the value of thermal stress is higher than that generated in continuous cutting (turning, boring, etc.). Often during milling thermal cracks appear at the flank surface of the tool perpendicular to the cutting edge.

Tool plastic deformation. A tool material must have sufficiently high thermal strength to maintain its shape under the cutting temperatures. The melting point of the workpiece material sets an absolute limit on the cutting temperature that can not be exceeded, regardless of the cutting speed.

Plastic deformation has been identified as a major mode of failure for high-speed steel and carbide tools [27,34]. The plastic deformation stress of the tool edge can reach some critical value at which the yield strength of the tool is lower than the normal stress on the rake face. This phenomenon is caused by the loss of form stability and can cause a "bulge" on the clearance face by shearing of a thin films of the tool material. This flank wear further increases the temperature and

weakens the tool strength until total failure occurs. As the cutting speed increases, the stress near the edge doesn't increase and may fall. However, as the temperature rises, the yield stress of the tool material is reduced causing plastic deformation to start.

To avoid plastic deformation, the temperature at the tool tip should ideally be kept lower than some critical value as the cutting parameters are increased.

The tool edge temperature, which is assumed to be equivalent to the temperature at the primary shear zone, will reach a steady state value asymptotically, for each combination of work material and cutting conditions.

If the steady state value is less than the critical temperature for the plastic deformation, then plastic deformation will not occur. The temperature increase in the primary shear zone is given by Eq. (4-2) and the average temperature in the primary plastic deformation zone is given by Eq. (4-9).

The maximum normal stress on the rake face in the primary deformation zone should be known. According to the Loladze's expression [25], based on the plasticity conditions, we can determine the maximum normal stress on the rake face which is high enough to cause plastic yielding for the given condition.

$$\sigma_{max} = 2 \cdot \tau_p \cdot (1.3 - \gamma) \qquad (6\text{-}4)$$

where τ_p = shear strength of the work material in the primary shear zone and

γ = the rake angle (radian).

Using Fig. 6.3 generated by Trent and Wright [27], we can determine the critical temperatures corresponding to σ_{max} which will cause the yielding of the cutting tool.

[2] Tool wear failure. Tool failures due to fracture or deformation are sudden and catastrophic. Such tool failures are disruptive in a conventional factory and can not be tolerated in an automated machining system. After the requirements for adequate fracture and deformation resistance are met, failure of the cutting point is determined by the progressive development of characteristic wear scars in the areas of contact between the tool and the workpiece. Typically, a wear land forms on the flank of the tool where the tool contacts the newly machined workpiece surface and a crater depression forms on the rake face of the tool in the chip-tool contact region.

A combination of flank wear and crater wear criteria may be used, although this is not often convenient. Takeyama [103] used cemented carbide tools to machine 18-8 stainless steel and suggested that for low speed and high feed, the wear land failure criterion should be adopted, but for high speed and low feed, the crater depth is a better criterion.

Flank wear criterion. A wear land develops on the flank face of the cutting tool. This flank wear is important because it has a direct effect on the quality of the product. The onset of crater wear results in a change in the mechanics of the cutting process (the effective rake angle and the chip tool contact length change). It also reduces the amount of force that the tool can withstand. Flank wear has a three fold influence [31]:

(a) Change in the mechanics of the process,

(b) An increased tendency for chatter, and

(c) Changes in the dimensions of the product.

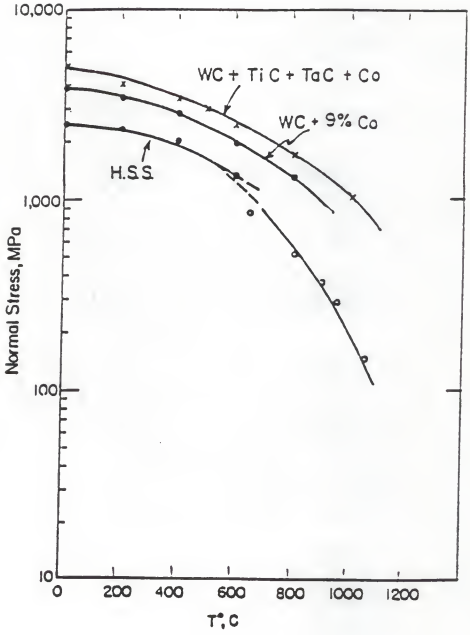

Fig. 6.3 Compressive yield strength of tool materials against the temperature [27]

A number of analyses [29,30,82,91] on this type of wear have been undertaken over the years. In general, abrasion will be the dominant wear mechanism only when the cutting temperature is relatively low. Adhesive wear predominates in the intermediate steady state stages, but the regenerative effects of wear and temperature make diffusion a considerable factor in the later stages and definitely the predominant factor in the accelerated wear region. There is a critical temperature at which accelerated wear begins (this is called "burn-out"temperature). Below that temperature, flank wear increases uniformly with time. Above that temperature, the wear increases exponentially with temperature. The exponential rise in wear above the critical temperature is due to the dominating influence of diffusion.

In the optimization of the cutting process, the tool life that will optimize the process is not known beforehand and another aspect which is essential for optimization is the rate of tool wear that can be suitably used. According to Kannatey-Ashibu [91], the recommended criterion for tool life is essentially the same as the crossover point where the wear rate by diffusion becomes greater than that by adhesive wear.

Therefore, it may be expected that the time at which the rate of wear due to diffusion exceeds that due to adhesion can be used as a criterion for tool life.

The wear rates due to adhesion and diffusion can be expressed as follows:

$$L_1 = K_2 \cdot v \cdot (T_f + T_w)^a \cdot L^{-5} \qquad (6\text{-}5)$$

$$L_2 = K_3 \cdot \sqrt{v} \cdot \exp(-Q/(2R \cdot (T_f + T_w + 273)) \cdot L^{-5} \qquad (6\text{-}6)$$

where L_1 = adhesive wear rate,

L_2 = diffusive wear rate,

v = cutting speed,

Q = activation energy for diffusion,

K_2, K_3 = constants related to the cutting geometry and work-tool combination,

T_f = temperature increase in the wear land given Eq. (4-26),

T_w = environmental workpiece temperature,

L = wear land length and

a = constant exponent.

When L_2 becomes greater than L_1, that is, when diffusion dominates for wear, the tool enters a rapid deterioration stage. This condition will be used as the constraint on the tool flank wear.

Crater wear criterion. It has been considered that diffusion wear plays a major role in crater wear formation [31]. This is attributed to the fact that high tool-chip interface temperature occurs. Evidence by Dawihl [32], Trent [34], Venkatesh [34], and others confirm that diffusion wear occurs on the tool rake face. Colding [36] showed that a larger crater can weaken the tool and lead to total failure.

High tool-chip temperature dominates at higher speeds, which is considered as another limit on the cutting speed. In carbides the predominant mechanism of wear is diffusion, which is also temperature sensitive [32,34].

Although there is a wide range of working conditions between slight and severe craters, it will be assumed that there is a specific temperature, above which rapid wear will be initiated.

According to Loewen and Shaw [77], the tool-chip interface temperature rise can be calculated from Eqn. (4-20). Using the relation developed by Loewen and Shaw, [77] a dimensional analysis relation can be formulated between the

temperature T_c and the cutting speed, feed rate as well as specific cutting energy, and the thermal quantity $k\rho c$. This relation is expressed as follows:

$$T_c = C_0 \cdot (v \cdot f/(k\rho c))^{0.5} \cdot u \qquad (6\text{-}7)$$

where u = specific cutting energy = $C_1 \cdot f^n$,

k = thermal conductivity,

C_0= nondimensional constant,

n = Kronenburg suggests a value of -0.2 for n [1],

c = heat capacity and

ρ = density.

In many cases, c increases while k decreases at a similar rate. Thus, the product $k\rho c$ remains constant. In order to avoid catastrophic failure, T_c should be kept below the softening temperature of the tool material. Some of these are listed in table 6.1.

Table 6.1

Softening points of Tool Materials and
Melting Points of Workpiece Materials [108]

Tool Material (Softening Point)	Workpiece Material (Melting Point)
High Speed Steel (600°C)	Aluminum (600-660°C)
Cemented WC (1100°)	Superalloy (13-1400°C)
Aluminum Oxide (1400°C)	Steel (1450-1500°C)
Cubic Boron Nitride (1500°C)	Titanium (16-1650°C)
Diamond (1500°C)	Zirconium (18-1850°C)

[3] Surface integrity constraints. The quality of a machined surface can be determined by such properties as surface roughness, hardness variation, structural changes, waviness, residual stress, and dimensional tolerances, etc. The combination of these properties is generally called Surface Integrity. The residual stress distribution is a major factor in evaluating surface integrity since it can greatly affect material stability and fatigue life [6-12].

Residual stress constraint. Most surface failures are the result of high tensile stresses on the surface of the part. The criterion used for rating the surface quality of the machined part is considered to be the maximum compressive residual stress. The depth of the region d_c where compressive residual stress is induced is dependent on the depth of the plastically deformed region. Accordingly, the depth d_c is also used as a measure of the surface integrity especially for situations where high tensile stress gradients occur on the surface. This conditions can be described by

$$d_c \geq d_{given} \tag{6-8}$$

where d_{given} is the necessary depth for improving the stress field for the particular part under the expected loading conditions.

Surface roughness constraint. The surface finish conditions in the machining operation will depend on the type of chip formation, the cutting-tool profile and the process geometry. Discontinuous chip formation can cause cracks which may extend into the finished work surface and create force fluctuations which deflect the tool causing ridges to form on the machined surface. This type of chip formation can also cause vibration which affect the surface finish. A continuous chip with a built-up edge leads to similar problems since the built-up edge is unstable and fractures

periodically, depositing built-up edge particles on the workpiece. In general, the continuous chip with no built-up edge is the most desirable, since steady state cutting conditions prevail with little or no force fluctuations and their associated difficulties. To a certain extent the discontinuous chip can be changed to a continuous chip by increasing the rake angle or using cutting fluids. Similarly the built-up edge, which is associated with friction and forces on the rake face, can be reduced or eliminated by using cutting fluids, or increasing the cutting speed.

Nigm [104] proposed the criterion for the continuous chip by using a dimensional analysis of the steady state orthogonal cutting data. The peak to valley height is the root to crest value of roughness. Theoretically, this value can be approximately obtained from the feed and cutting edge radius.

In the optimization process, the permitted value of the surface roughness will be chosen as the constraint. The condition for the continuous chip can be expressed as follows:

$$f \cdot v^n \geq C_3 \tag{6-9}$$

where f = feed rate,

v = cutting speed and

C_3 = constant of tool-workpiece and geometry.

As explained in the Chapter 3, when the natural frequency of tool assembly is over 150 Hz, the surface roughness equation is similar to the kinematic values. The theoretical kinematic peak to valley height of the surface roughness is given as follows:

$$h = f^2 / r_\beta \tag{6-10}$$

where r_β = cutting edge radius and

f = feed rate.

The constraint on the surface roughness can be expressed as follows:

$$h \leq h_{given} \tag{6-11}$$

[4] Dimensional accuracy constraint. Deflection of the tool and workpiece produces inaccuracies in the dimensions of the part produced, and have to be limited to acceptable tolerances. In the case of the turning operation, the part produced would have been a perfectly accurate cylinder if the processing system was absolutely rigid. However, it is virtually impossible to achieve this absolute rigidity and if an attempt is made to approach it the cost involved would be too high.

After establishing the optimum distribution of stiffness of the tool (headstock, tailstock and carriage system) and the workpiece through the optimization process, the deflection can be given by equation (3-27). As mentioned in chapter 3, the dimensional error would be defined by the steady state displacement of dynamic cutting system as shown in Fig. 3.1. The constraint on this dimensional accuracy can be expressed as follows:

$$\delta \leq \delta_{given} \tag{6-12}$$

6.3 Optimization Procedure

With the knowledge of constraints in terms of control variables, we can carry out the optimization procedure. The total optimization procedure can then be expressed as follows:

$$\text{Objective function} : F = f\, d\, v \tag{6-13}$$

$$\text{Constraints} : \quad \sigma_1 \leq \sigma_{max}$$

$$T_{pz} \leq T_{max}$$

$$L_2 \leq L_1$$

$$T_c \le T_{softening}$$

$$\sigma_c \ge \sigma_{given}$$

$$d_c \ge d_{given}$$

$$f \cdot v^n \ge C_3$$

$$h \le h_{given}$$

$$\delta \le \delta_{given}$$

$$f_1 \le f \le f_2$$

$$V_1 \le V \le V_2$$

$$d_1 \le d \le d_2 \qquad (6\text{-}14)$$

This optimization problem can be regarded as a constrained optimization with inequality constraints. Due to the complexities of the constraints, it is almost impossible to find out gradient of each constraint function in terms of cutting parameters. Therefore, procedures which do not require the derivatives of functions would be desirable such as the Feasible Search Methods. There are two types, the direct method and the indirect method, depending on the treatment of constraints. Due to the inconvenience of the direct method, which was developed by Box [105], the Powell's unconstrained method with the exterior penalty function will be used in this research [106,107].

The exterior penalty function of this problem will have the following form:

$$\begin{aligned}\Phi \quad = & - f \cdot d \cdot V + \\ & \Re \cdot (<f - f_2>^2 + <d - d_2>^2 + <V - V_2>^2 + \\ & <\sigma_1 - \sigma_{max}>^2 + <T_{pz} - T_{max}>^2 + <T_c - T_{softening}>^2 + \\ & <d_c - d_{given}>^2 + <\sigma_{given} - \sigma_c>^2 + <C_3 - f \cdot v^n>^2 + \\ & <h - h_{given}>^2 + <\delta - \delta_{given}>^2 + <f_1 - f>^2 + <d_1 - d>^2 \\ & + <V_1 - V>^2) \end{aligned} \qquad (6\text{-}15)$$

This penalty function will be used as the objective function in the Powell's optimization algorithm [106].

6.4 Numerical Calculations

In order to illustrate the use of this adaptive control cutting model, which takes into consideration the surface integrity of the machined component and tool failures, the following cutting conditions were used and the optimization procedure was carried out for each set of conditions.

6.4.1 Cutting Conditions

Mild steel is used as the workpiece material and a carbide tool material is chosen in the simulation. The related parameter constraints are given as followings:

$$0.3 \leq f \leq 0.7 \quad (\text{mm/rev})$$
$$40 \leq v \leq 110 \quad (\text{m/min})$$
$$1 \leq d \leq 3 \quad (\text{mm}) \qquad (6\text{-}16)$$

The objective of this simulation is to maximize the production rate within the given parameter constraints. Only one type of cutting tool is used with the following specifications:

Side cutting edge angle = 15°
Tool edge radius = 0.3 mm
Rake angle = 10 °
Clearance angle = 5 °
Carbide cutting tool

6.4.2 Tool Fracture Constraints

Using Eq. (6-2), 81 values of the maximum tensile radial force component on the rake face of the cutting tool were obtained and the corresponding regression

relation was calculated. The same cutting conditions as those of chapter 5 were used. The final relation is given as follows:

$$\sigma_{max} = .3875 \cdot f^{1.3466} \cdot V^{1.3610} \tag{6-17}$$

From this equation, we can see that σ_{max} depends on feed rate and cutting speed. However, the depth of cut and the tool radius have no effect on σ_{max}, which is similar to the estimation suggested Loladze [25]. The fracture stress of the carbide tool is approximately 550 - 800 N/mm^2 [25] and this value will be used as the limit on the rake tensile stress.

6.4.3 Tool Plastic Deformation Constraint

The temperature at the primary shear zone is assumed to be related to the tool edge plastic deformation. According to Loladze, the maximum normal stress causing plastic yielding for the given condition is given by Eq. (6-3). In this example, the rake angle is 10° and the shear strength of the mild steel in the primary shear zone is 588 N/mm^2. Therefore, σ_{max} is 1300 N/mm^2 and from Fig. 6.3, the corresponding temperature for the carbide tool is approximately 830°C.

The temperature in the primary shear zone is given by equation (4-26) and the constraint equation can therefore be written as:

$$T_{pz} = 453.53 \cdot V^{0.036} \cdot f^{0.0376} \cdot d^{0.0025} \leq 830 \tag{6-18}$$

6.4.4 Tool Wear Failure Constraints

Flank wear constraint. According to Ref. [91], when a carbide tool is used in cutting steel, the wear rate caused by adhesion is given by

$$L_1 = 0.0792X10^{-6} \cdot V \cdot (25 + 13\ V \cdot L^{0.25})^{0.055} \tag{6-19}$$

The wear rate caused by diffusion is given as follows:

$$L_2 = 0.137X10^6 \cdot V \cdot \exp(-20000/(298+13 \cdot V \cdot L^{0.25})) \cdot L^{-0.5} \quad (6\text{-}20)$$

Here, L is assumed to be the maximum permissible wear land length, that is, .3 mm [50]. The constraint is therefore,

$$L_2 \leq L_1 \quad (6\text{-}21)$$

Crater wear constraint. The temperature generated in the tool-chip interface is given by Eq. (4-27). This temperature should be kept below the softening temperature of the tool material. For the case of a carbide tool, it is 1100°C. Therefore, the constraint is formulated as:

$$457.44 \cdot V^{0.2761} \cdot f^{.2874} \cdot d^{-.0217} \leq 1100. \quad (6\text{-}22)$$

6.4.5 Surface Integrity Constraints

There are three types of constraints which are considered in defining surface integrity. These are: the amount of surface residual stress, the plastically deformed depth with compressive residual stress and the permissible surface roughness. The permissible magnitude of each constraint will be given inputs.

Residual stress constraint. The depth with the compressive residual stress is calculated by Eq. (5-28). When the prescribed depth with compressive residual stress is assumed to be d_{given} cm, the related constraint can be expressed as follows:

$$0.1188 \cdot f^{0.6720} \cdot d^{-0.05849} \cdot V^{0.0909} \geq d_{given} \quad (6\text{-}23)$$

The amount of compressive surface residual stress, σ_c is calculated by Eq. (5-28) and the value is limited by the desired values.

$$-3621.72 \cdot f^{.7525} \cdot d^{-.01797} \cdot V^{-.3962} \geq \sigma_{given} \quad (6\text{-}24)$$

Surface roughness constraint. From ch3, when the tool frequency is higher than 150 Hz, the roughness is given by the following equation.

$$h = 381.85 \cdot f^2 \tag{6-25}$$

The roughness in this cutting procedure is assumed to be limited by the permissible roughness and the related equation is as follows:

$$381.85 \cdot f^2 \leq h_{given} \tag{6-26}$$

When the natural frequency of tool assembly is assumed to be 34.5 Hz, the surface roughness equation in terms of cutting parameters is given by Eq. (3-44) and when the tool edge radius, r_β is .3 mm, the related equation can be written as:

$$604.43 \cdot f^{.818} \cdot d^{-.27} \cdot V^{-.364} \leq h_{given} \tag{6-27}$$

Dimensional accuracy constraint. When the tool natural frequency is assumed to be 150 Hz, the regressional relation between the roughness and the cutting parameters can be written as:

$$\delta = 100.6558 \cdot f^{0.9709} \cdot d^{0.4905} \cdot V^{-0.2848} \tag{6-28}$$

The maximum permissible deflection of the workpiece during the cutting process is assumed to be δ_{given} micrometer. Then, the constraint can be expressed as follows:

$$100.6558 \cdot f^{0.9709} \cdot d^{0.4905} \cdot V^{-0.2848} \leq \delta_{given} \tag{6-29}$$

The equation related to the surface roughness are valid only for cutting in the absence of the built-up-edge which is the case when the cutting conditions V and f satisfy the following condition [104]:

$$f \cdot V^{0.9} \geq 0.8184 \tag{6-30}$$

Using all the constraint equations from (6-16) to (6-30), the overall penalty function maximizing the metal removal rate can be written as follows:
(the natural frequency of tool assembly is assumed to be 150 Hz)

$$\Phi = f\cdot d\cdot v + \Re(<0.3-f>^2 + <f-0.7>^2 + <40-V>^2 + <V-110>^2 + <1-d>^2 + <d-3>^2 + <0.3875\cdot f^{1.3466}\cdot V^{1.361}-550>^2 + <453.53\cdot V^{-0.036}\cdot f^{-0.0376}\cdot d^{0.0025}-830>^2 + <L_2-L_1>^2 + <457.44\cdot V^{0.2761}\cdot f^{0.2876}\cdot d^{-0.0217}-1100>^2 + <d_{given}-0.1188\cdot V^{0.0909}\cdot f^{0.672}\cdot d^{-0.05849}>^2 + <381.85\cdot f^2-h_{given}>^2 + <3621.72\cdot f^{.7525}\cdot d^{-.01797}\cdot V^{-.3962}-\sigma_{given}>^2 + <100.6558\cdot f^{0.9709}\cdot d^{0.4905}\cdot V^{-0.2848}-\delta_{given}>^2 + <0.8184\cdot f\cdot V^{0.9}>^2) \quad (6\text{-}31)$$

The bracket function $<\cdot>$ means that $<g> = g$ when $g \geq 0$ and 0 when $g \leq 0$. Therefore, such function can be expressed by the following equation.

$$<g> = (g + |g|)^2/2 \quad (6\text{-}32)$$

This exterior penalty function is used as the objective function and by changing the values of $\Re$, this function is optimized for the maximum removal rate.

Case 1. When the constraints on tool wear are imposed, equations (6-18), (6-21) and (6-22) are used in this case. The result is summarized in the first part of Table 6.2. When the temperature of tool plastic deformation is reduced to 800°C and T_c is also reduced to 1000°C, the optimum solution is different from the result of the first case. The result is listed in the second part of Table 6.2.

Case 2. When surface integrity constraints are imposed, the related equations are (6-23), (6-24) and (6-26). The natural frequency of tool assembly is assumed to be 150 Hz and the optimization is performed for the following conditions.

(a) σ_{given} is -500 MPa and -600 MPa

(b) σ_{given} is -500 MPa and d_c is 0.1 mm

(c) σ_{given} is -500 MPa and d_c is 0.11 mm

(d) σ_{given} is -600 MPa and d_c is 0.1 mm

(e) σ_{given} is -600 MPa and d_c is 0.11 mm

(f) σ_{given} is -500 MPa and d_c is 0.1 mm and R_{max} is 100 μm

(g) σ_{given} is -400 MPa and d_c is 0.1 mm and R_{max} is 100 μm

The calculation results show that cases (b), (c), (d) and (e) have the same optimum solution as case (a), which specifies the amount of surface residual stress.

The results are summarized in the Table 6.3.

Table 6.2 Results of case 1

	Case 1.a	Case 1.b
Feed rate:0.3 mm/rev:	0.3 mm/rev	0.35 mm/rev
Cutting speed :	91 m/min	55 m/min
Depth of cut :	3 mm	3 mm
Tool edge radius :	0.3 mm	0.3 mm
Tool frequency :	150 Hz	150 Hz
T_{pz} :	404°	409.5°
T_c :	1098°	998.8°
L_1 :	9.364×10^{-6}	5.6×10^{-6}
L_2 :	1.24×10^{-16}	5.65×10^{-18}
σ_{max} :	35.39 MPa	21.96 MPa
d_c :	0.075 mm	0.079 mm
σ_c :	-240.27 MPa	-329.4 MPa
Roughness :	1.45 μm	1.97 μm
δ(deflection) :	14.83 μm	19.89 μm

Table 6.3 Results of case 2

Cases	(a)-500 MPa	(b)-600 MPa	(b)&(c)	(d)&(e)
f (mm/rev)	0.7	0.7		
V (m/min)	71	45		
d (mm)	3	3		
r_β(mm)	0.3	0.3	same as	same as
f_t(Hz)	150	150	case (a)	case (a)
T_{pz} (°C)	395.4	401.9	500MPa	600MPa
T_c (°C)	1307.4	1153.2		
L_1	7.27×10^{-6}	4.56×10^{-6}		
L_2	2.57×10^{-17}	1.85×10^{-18}		
σ_{max} (MPa)	79	42.5		
d_c (mm)	0.129	0.124		
σ_c (MPa)	-501.	600.9		
R_{max} (μm)	187.1	187.1		
δ (μm)	36.18	41.27		

Cases	(f)	(g)
f (mm/rev)	0.51	0.51
V (m/min)	40	71
d (mm)	1.9	1.2
r_β(mm)	0.3	0.3
f_t(Hz)	150	150
T_{pz} (°C)	407.9	402.7
T_c (°C)	1029.	1180.
L_1	4.05×10^{-6}	6.954×10^{-6}
L_2	9.87×10^{-19}	1.98×10^{-17}
σ_{max} (MPa)	23.6	48.65
d_c (mm)	0.102	0.104
σ_c (MPa)	-500.2	402.
R_{max} (μm)	99.24	99.24
δ (μm)	25.08	26.98

Case 3. In the case the constraints imposed in case 1 and case 2 are considered simultaneously and the surface integrity conditions are specified as follows:

σ_{given} = -400 MPa

d_{given} = .1 mm

R_{max} = 100 μm

The result is shown in the Table 6.4.

Table 6.4 Result of case 3

Feed rate	:	0.51 mm/rev
Cutting speed	:	52 m/min
Depth of cut	:	3. mm
Tool edge radius	:	0.3 mm
Tool frequency	:	150 Hz
T_{pz}	:	404.6°
T_c	:	1095.8°
L_1	:	5.29×10^{-6}
L_2	:	4.10×10^{-18}
σ_{max}	:	33.78 MPa
d_e	:	0.101 mm
σ_t	:	-447.1 MPa
Roughness	:	99.24 μm
δ(deflection)	:	29.12 μm

Case 4. The tool natural frequency is assumed to be 150 Hz and all of the constraints defined by Eq. (6-31) are used.

Here, the constraint values are given as follows:

h_{given} = 100 μm

σ_{given} = -400 MPa

d_{given} = .1 mm

δ_{given} = 20 μm

The result in this case is listed in the Table 6.5.

Table 6.5 Result of case 4

Feed rate	:	0.47 mm/rev
Cutting speed	:	54 m/min
Depth of cut	:	1.6 mm
Tool edge radius	:	0.3 mm
Tool frequency	:	150 Hz
T_{pz}	:	404.65°
T_c	:	1096.8°
L_1	:	5.49×10^{-6}
L_2	:	5.08×10^{-18}
σ_{max}	:	31.85 MPa
d_c	:	0.1 mm
σ_c	:	-418.92 MPa
Roughness	:	84.28 μm
δ(deflection)	:	19.55 μm

Here, the maximum metal removal is 40610 mm^3 / min. and the cutting conditions satisfy all of the cutting constraints considered in this study.

In order to illustrate the sensitivity of the constraints, the following cases are considered and the results are summarized in the following tables and figures. The results obtained from the calculations of case 1 through 4 are included in the Tables 6.6, 6.7, 6.8 and 6.9 and Figures 6.4, 6.5, 6.6 and 6.7.

Case 5. From the results of case 1, the important component among three different temperature components is found to be T_c. Therefore, only three different values of T_c are imposed.

The obtained results are listed in the Table 6.6 and plotted in the Fig. 6.4.

Case 6. 3 different values of compressive surface residual stress are imposed as the constraints and the obtained results are listed in the Table 6.7 and plotted in the Fig. 6.5.

Table 6.6 Results of case 5

T_c(°C)	950	1000	1100	1150
V(m/min)	40	44	48	48
d(mm)	2.1	2	1.9	1.9
f(mm/rev)	0.38	0.4	0.42	0.42
T_f(°C)	86	88.82	91.7	91.7
T_{pz}(°C)	413	410.4	408	408
σ_c(MPa)	400	400.8	402	402
R_{max}(μm)	55.1	61.05	67.31	67.31
δ(μm)	19.79	19.77	19.72	19.72
fdv (x1000mm^3/min)	31.92	35.2	38.304	38.304

Table 6.7 Results of case 6

σ_c(MPa)	250	420	430
V(m/min)	78	43	40
d(mm)	3	1.8	1.7
f(mm/rev)	0.35	0.42	0.42
T_c(°C)	1100	995	975
T_{pz}(°C)	404	410	410.8
T_f(°C)	91.7	88.1	85.8
R_{max}(μm)	46.7	67.3	67.3
δ(μm)	18.	19.8	19.67
fdv (x1000mm^3/min)	81.9	32.51	28.56

Case 7. The values of surface roughness are imposed as the constraint. The obtained results are listed in the Table 6.8 and summarized in the Fig. 6.6.

Case 8. In order to show the case of the high precision machining operation, the lower limit value of the feed rate is extended up to 0.01 mm/rev and 3 values of the surface roughness are imposed for the constraints. The obtained results are listed in the Table 6.9 and plotted in the Fig. 6.7.

6.5 Conclusions

An optimization procedure for adaptive control of machining with constraints is presented and used for obtaining the optimum cutting conditions which satisfy the given constraints. This procedure emphasizes the surface integrity and tool wear. In all the considered examples, an unique solution is obtained which maximizes the metal removal rate while satisfying the specified constraints. This model can be particularly useful in cases of high precision machining with specified surface quality requirements for the machined part.

Table 6.8 Results of case 7

R_{max}(μm)	60	65	70	75
V(m/min)	42	46	48	53
d(mm)	2	2	1.9	1.8
f(mm/rev)	0.39	0.41	0.42	0.44
T_c(°C)	964	1003	1023	1067
T_{pz}(°C)	411	409	408	406
T_f(°C)	87	90	92	95
σ_c(MPa)	400	400	400	400
δ(μm)	19.55	19.99	19.72	19.53
fdv (x1000mm^3/min)	32.76	37.72	38.304	41.976

Table 6.9 Results of case 8

R_{max}(μm)	0.098	0.673	1.563
V(m/min)	110	110	110
d(mm)	3	3	3
f(mm/rev)	0.016	0.042	0.064
T_c(°C)	498.3	657.6	742.2
T_{pz}(°C)	448.6	432.6	425.8
T_f(°C)	126	126	126
σ_c(MPa)	24.6	50.76	69.7
δ(μm)	0.82	2.08	3.14
fdv (x1000mm^3/min)	5.18	13.86	21.12

Results from the analysis showing the influence of the different constraints on the machining productivity, the cutting parameters, and the resulting surface properties are given for different cases. A summary plot for all the considered cases illustrating the sensitivity of the results to the constraints is given in Figs. 6.4, 6.5, 6.6 and 6.7. The latter is an illustration of applying the procedure to high precision machining conditions.

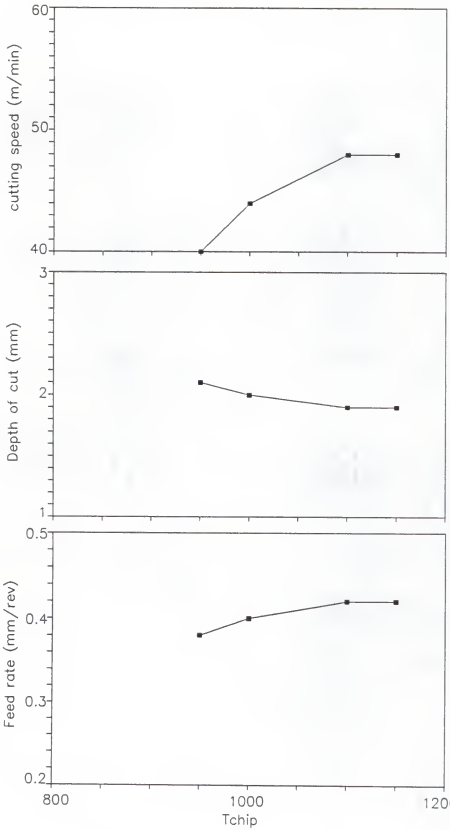

Fig. 6.4 Results of case 5
(a. Cutting condition variations: x axis unit= °C)

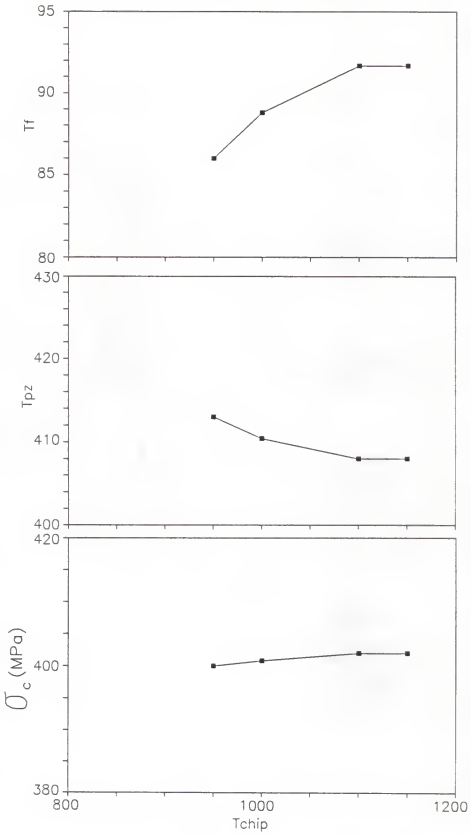

Fig. 6.4 Results of case 5
(b. temperature and stress variations: x axis unit = °C)

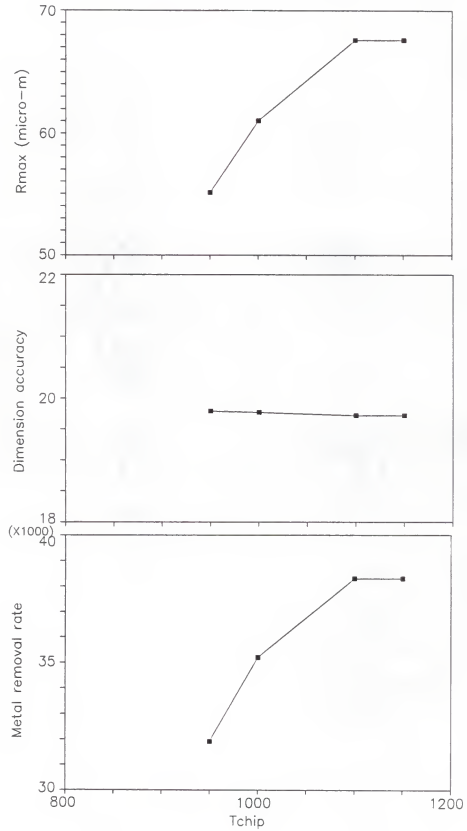

Fig. 6.4 Results of case 5
(c. other constraint variations: x axis unit= °C)

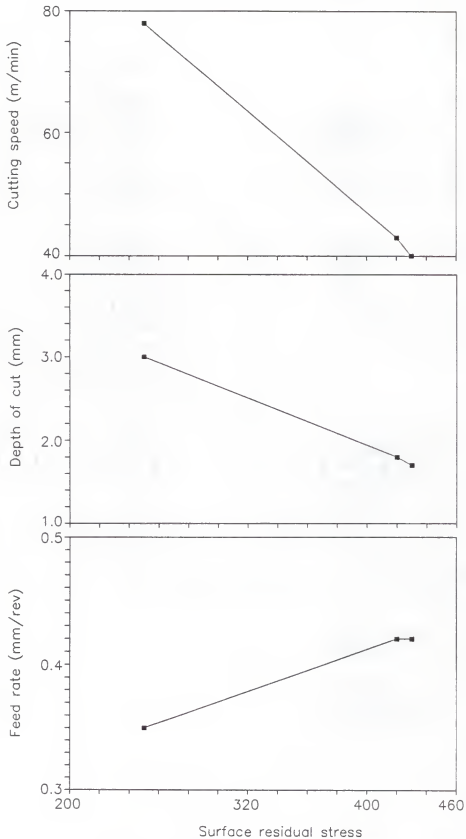

Fig. 6.5 Results of case 6
(a. cutting condition variations: x axis unit= MPa)

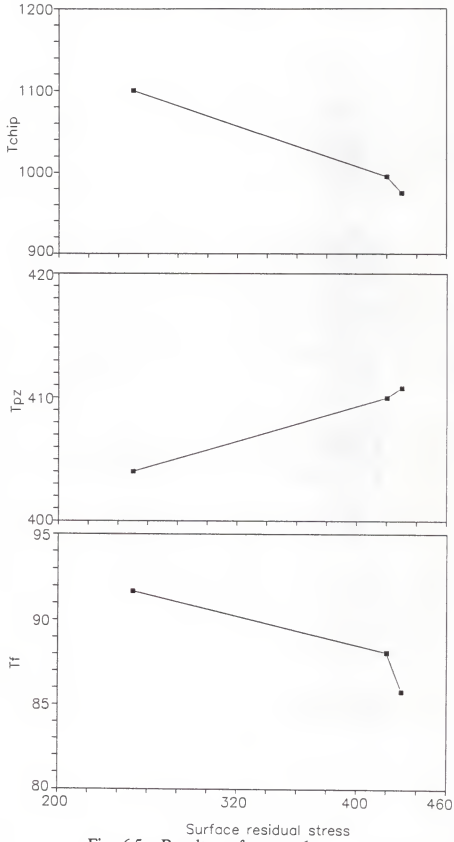

Fig. 6.5 Results of case 6
(b. temperature variations: x axis unit = MPa)

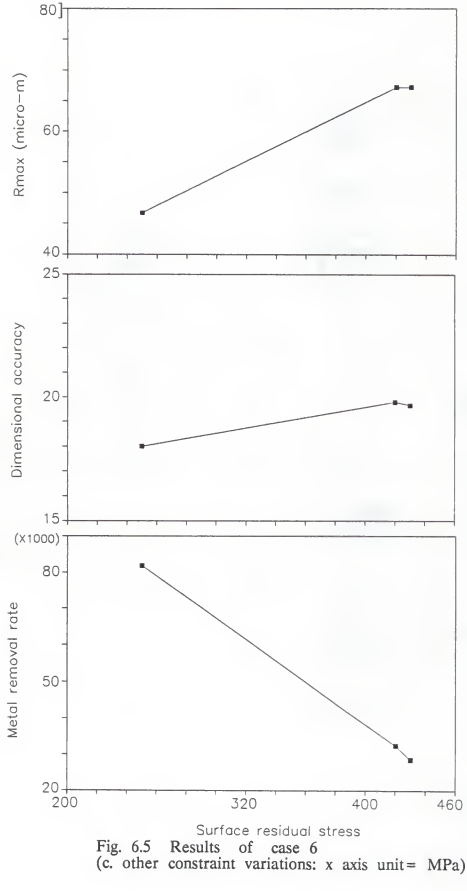

Fig. 6.5 Results of case 6
(c. other constraint variations: x axis unit= MPa)

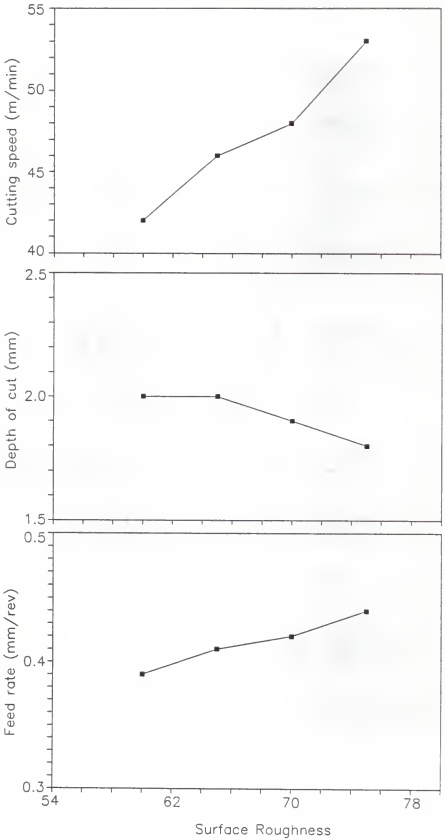

Fig. 6.6 Results of case 7
(a. cutting condition variations: x axis unit= μm)

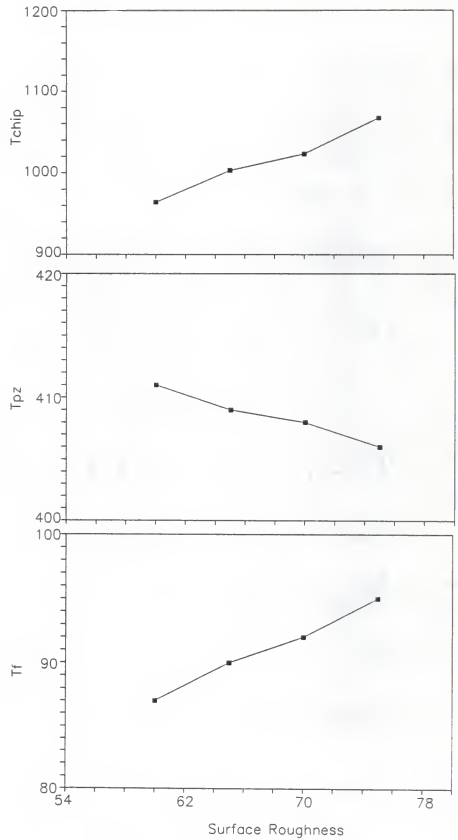

Fig. 6.6 Results of case 7
(b. temperature variations: x axis unit = μm)

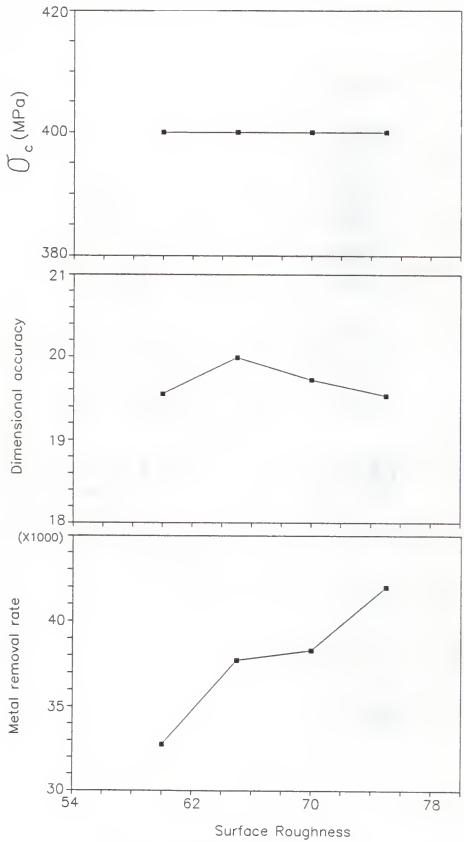

Fig. 6.6 Results of case 7
(c. other constraint variations: x axis unit= μm)

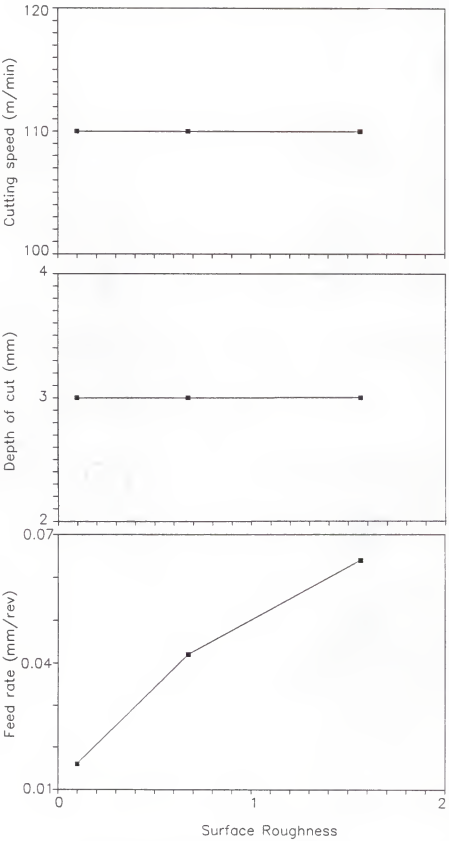

Fig. 6.7 Results of case 8
(a. cutting condition variations: x axis unit= μm)

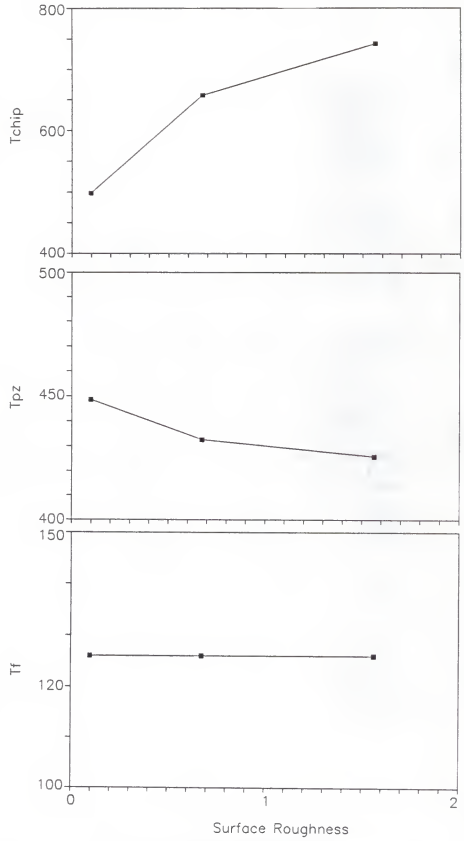

Fig. 6.7 Results of case 8
(b. temperature variations: x axis unit= μm)

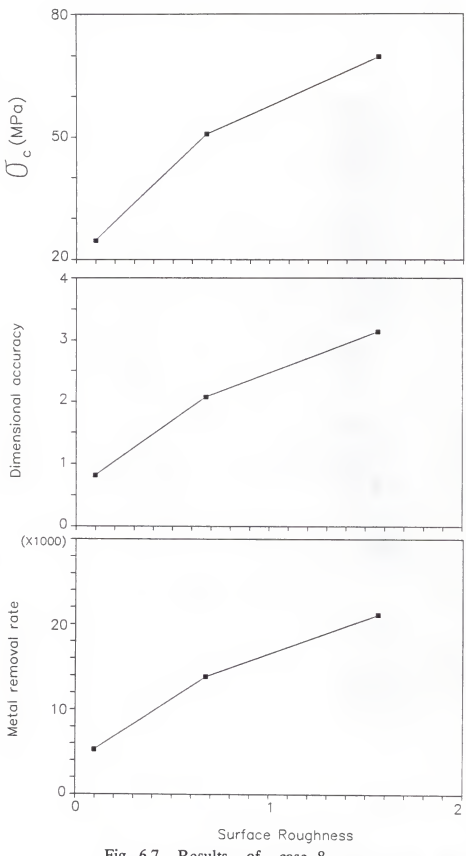

Fig. 6.7 Results of case 8
(c. other constraint variations: x axis unit = μm)

CHAPTER 7
SUMMARY, CONCLUSIONS AND RECOMMENDATIONS

7.1 Summary

The study reported in this thesis can be summarized in the following:

Surface roughness prediction

A computer based dynamic simulation model for estimating the surface roughness in the turning process has been developed. This model takes into consideration the dynamic characteristics of the tool assembly, the workpiece and the spindle structure. In estimating the surface roughness, the kinematic behavior of the cutting tool and the relative dynamic motion between the tool and the workpiece are combined. The generalized dynamic cutting forces used in activating the system considers the regenerative effect as well as damping in the cutting process. The simulation results show good correlation with the experimental results and indicate that when K_s is greater than 10^8 N/m, which is the situation in most practical conditions, the tool stiffness becomes the major factor in controlling the dynamic motion between the tool and the workpiece. A generalized equation for predicting the surface roughness in turning is formulated which can be used in calculating the surface roughness when the stiffness of structure is greater than 10^8 N/m. The surface roughness is expressed as a function of the cutting parameters and the natural frequency of the tool assembly. For rigid systems where the natural frequency is greater than 150 Hz (corresponding to $K_t = 2.4 \times 10^7$ N/m), the surface roughness

equation gives the same results as the well known equation which is based on the kinematic consideration only.

Prediction of heat generation in the cutting process

The heat generation in the plastic deformation zone and at the interface between the tool and the chip is formulated in terms of the cutting parameters for use in the optimization procedure. The published information on the subject is utilized in developing an appropriate criterion for the tool wear based on a regression relationship between the temperature and the cutting parameters.

Predicting the surface residual stress

A computer based model for predicting the surface residual stress is developed. The model takes into consideration the mechanical and thermal aspects of the machining process. The cutting force used in the model includes the force component acting in front of the cutting tool edge and the component existing under the cutting tool. The contact between the tool and the workpiece is assumed to be Hertzian and the force is assumed to be distributed elliptically over the region between the tool and workpiece. Merwin-Johnson's theory is used in calculating the stress distribution in the plastically deformed region. Regression equations are developed to relate the cutting parameters to the maximum surface residual stress, the maximum tensile stress in the subsurface layers, the maximum depth of plastically deformed region with compressive residual stress and the maximum plastically deformed depth under the surface. The numerical example shows good agreement with published experimental results. It is interesting to note that the sharpness of the tool influences the magnitude and type of the maximum stress at the surface. The front cutting region acts as the main source for the tensile residual

stress. Compressive residual stress is expected to occur when a tool with rounded edge is used.

Optimization algorithm for use in adaptive control

An optimization algorithm is developed which can be used in on and off-line adaptive control systems. While avoiding the catastrophic tool failure, the machining conditions for maximum cutting rate can be obtained for any specified surface conditions such as surface residual stress, surface roughness and dimensional accuracy. The algorithm takes into consideration tool wear, tool fracture, surface integrity and dimensional accuracy based on the physical behavior of the machining process.

7.2 Conclusions

The following can be concluded from the reported study:

1. Models have been developed for predicting the surface roughness and surface residual stress distribution in the turning process. These models are incorporated in an optimization algorithm for use in the adaptive control of the machining process. The algorithm insures the surface integrity of the machined components and maximizes the metal removal rate while satisfying the tool life constraints.

2. From the model predicting the surface roughness, the powers of the machining parameters in the generalized equation depend on the natural frequency of the tool assembly only when the stiffness of the spindle structure is greater than 10^8 N/m. Also, when the natural frequency is greater than 150 Hz which is equivalent to $K_t=2.4x^7$ N/m, the dynamic movement of the tool is found to be

negligible and the geometric effect of the cutting tool edge becomes dominant. In other words, when the natural frequency is over 150 Hz, the generalized surface roughness equation becomes the same as the well known kinematic relationship.

3. The residual stress study shows that the maximum residual stresses on the surface are compressive when the part is machined with a rounded tool. The maximum values occur at the surface and decrease with depth beneath the machined surface. The stresses become tensile, reach a maximum, then asymptotically vanish with further increase in depth. The value of the maximum compressive stress increases with increasing feed and decreases with increasing speed and tool radius. The depth of cut appears to have little effect on the maximum stress. The roundness of the tool cutting edge has considerable effect on the compressive residual stress formation. The plastically deformed depth inside the workpiece increases with feed rate, cutting speed and tool radius.

4. An optimization algorithm which can be used in on and off-line adaptive control system provides an unique solution for providing the maximum metal removal rate subjected to the constraints imposed on the process and the machined surface.

One of the significant contributions of this research is that practical models has been established for surface quality based on physical understanding of the turning processes. The models provide the basic background for actual implementation in adaptive control systems for optimum machining.

7.3 Recommendations

The models used in this thesis can be extended for different cutting materials and cutting tools. By analysis of the cutting forces and the process dynamics, it is

possible to generate the general machinability chart for different machining process and material. The charts can be applied to optimize the cutting parameters for a specified surface condition of machined components. Because the surface conditions and tool failures are emphasized, the developed system can be extended for the control of automated manufacturing and precision machining. In addition, by taking into consideration the time dependency of tool wear, the dynamic optimum conditions can be calculated and implemented on line during the cutting process.

The most important issue in the adaptive control of manufacturing is the real time control of the process. The success of an adaptive control system, especially in time varying situations will depend on accurate sensors for measuring the cutting force and temperature. The measured data can be used in the optimization procedure for real time control. Tool wear and surface integrity considerations can be incorporated into the optimal control algorithm in order to achieve the highest productivity while insuring the desired quality for the machined part.

Although only the turning process is considered in this thesis, the dynamic simulation modelling approach can be extended to other manufacturing processes by appropriate formulation of the process dynamics as well as the mechanical-thermal behavior of the tool and workpiece.

APPENDIX A
MERWIN-JOHNSON METHOD

Fig. 5.2 illustrates the load exerted on a semi-infinite solid by an asperity. It is assumed that the asperity is stationary and the semi-infinite solid is moving with velocity U. The contact length is 2a. A plane strain condition is assumed and the y axis is perpendicular to the plane of the paper.($\sigma_{yy} = 0$ and $\partial/\partial y = 0$) During plastic deformation it is initially assumed that the plastic strains are equal to the elastic strains by applying Liu and Smith's equations[11] and Hook's law.

The stresses in the plastic region are found by employing Prantl-Reuse equations for an elastic-perfectly plastic material. During plastic deformation the von Mises flow rule requires that the second invariant of the stress deviator, J_2' remain constant and equal to K^2, where K is the yield strength in shear. This is given as follows:

$$-J_2' = \Sigma\,\Sigma\,(\sigma_{ij}'\sigma_{ij}') = (1/3)\bar{\sigma}^2 = K^2 \qquad \text{(A-1)}$$

The total strain rate, ε_{ij}, is the summation of the elastic strain rate, ε_{ij}^e and the plastic strain rate, ε_{ij}^p or

$$\varepsilon_{ij} = \varepsilon_{ij}^e + \varepsilon_{ij}^p \qquad \text{(A-2)}$$

The plastic strain rate can be related to the applied stress by using the Prantl-Reuss equations as follows:

$$\varepsilon^{p}_{ij} = (W^{p}/(2K^{2}))\cdot\sigma'_{ij} = (3/2)\cdot\frac{d\varepsilon^{p}}{\sigma}\cdot\ \sigma'_{ij} \qquad \text{(A-3)}$$

where $W^{p} = \Sigma\,\Sigma\,(\varepsilon^{p}_{ij}\sigma'_{ij}) = \sigma\cdot\varepsilon^{p}$. This equation can be written as follows:

$$\varepsilon_{ij} = \sigma'_{ij}/(2G) + W_{p}\cdot\sigma_{ij}/(2K^{2}) \qquad \text{(A-4)}$$

$$\sigma'_{ij} = 2G\cdot(\varepsilon_{ij} - W_{p}\cdot\sigma_{ij}/(2K^{2})) \qquad \text{(A-5)}$$

Since the rate of work done to deform the material plastically is much larger than the rate of elastic energy stored,

$$W^{p} \approx W \qquad \text{(A-6)}$$

where W is the rate of total work done. Therefore,

$$\sigma'_{ij} = 2G\cdot(\varepsilon_{ij} - W\cdot\sigma_{ij}/(2K^{2})) \qquad \text{(A-7)}$$

where ε_{ij} is the total strain rate. The basic assumption of the Merwin-Johnson method is the total strain is identical to the elastic strains obtained by solving Eqs. (A-1) through (A-7), even when the materials yield plastically. Plastic deformation occurs as long as J'_{2} equals to $-K^{2}$ and W is positive. Otherwise , the solid is in an elastic state.

The stress field of the plastically deforming solid can be determined by integrating Eq. (A-7). In order to integrate Eq. (A-7), it is convenient if the time rate of change can be transformed to gradients with respect to x as follows:

$$\frac{d}{dt}(\sigma'_{ij}\varepsilon_{ij};W) = U\cdot\frac{\partial}{\partial t}(\sigma'_{ij}\varepsilon_{ij};W) \qquad \text{(A-8)}$$

where U is the steady sliding speed of the lower plane. Therefore, by substituting Eq. (A-8) into (A-7), the time rate of change will be replaced with derivatives of x. U is cancelled out of the equation.

The stresses that are found by Eqs. (A-1) through (A-8) do not satisfy the

equilibrium during the loading cycle. Therefore, it is necessary to restore the condition of equilibrium at the end of the loading cycle by considering elastic unloading phenomena.

Had the loading been entirely elastic the stresses would approach zero when the asperity contact moved away from the point of interest. However, as a result of plastic deformation, each point must have a state of residual stress because the unloading path is different from the loading path. Since every point at a given depth experiences exactly the same loading history, residual stress, $(\sigma_{ij})_r$, and strains must be independent of x; that is,

$$\begin{aligned} (\sigma_{xx})_r &= f_1(z) \\ (\sigma_{zz})_r &= f_2(z) \\ (\sigma_{yy})_r &= \nu(f_1 + f_2) \\ (\sigma_{xz})_r &= f_3(z) \end{aligned} \tag{A-9}$$

The equilibrium condition requires that these residual stresses satisfy the equilibrium condition,

$$\begin{aligned} \frac{\partial(\sigma_{xx})_r}{\partial x} + \frac{\partial(\sigma_{xz})_r}{\partial z} &= 0 \\ \frac{\partial(\sigma_{xz})_r}{\partial x} + \frac{\partial(\sigma_{zz})_r}{\partial z} &= 0 \end{aligned} \tag{A-10}$$

Substituting Eq. (A-9) into (A-10), we obtain

$$\begin{aligned} df_3/dz = 0 \text{ or } f_3 &= c_1 \\ df_2/dz = 0 \text{ or } f_2 &= c_2 \end{aligned} \tag{A-11}$$

The boundary conditions $\sigma_{zz} = 0$ and $\sigma_{xz} = 0$ at $x = \infty$ and $z = 0$ yield $c_1 = c_2 = 0$. Therefore, the only permissible state of residual stress is

$$(\sigma_{xx})_r = f(z)$$

$$(\sigma_{yy})_r = \nu f(z)$$

$$(\sigma_{zz})_r = 0$$

$$(\sigma_{xz})_r = 0 \qquad \text{(A-12)}$$

The stress field obtained by solving (A-7) does not satisfy the condition specified by (A-12); that is σ_{zz} and σ_{xz} are not zero. To satisfy Eq. (A-12) opposing stresses $-(\sigma_{zz})$ and $-(\sigma_{xz})$ must be applied to cancel out $(\sigma_{zz})_r$ and $(\sigma_{xz})_r$, which is equivalent to unloading the material elastically. The residual strains at the end of a loading and unloading cycle are

$$(\varepsilon_{zz})_r = -\frac{1 - 2\nu}{2(1-2\nu)\ G}(\sigma_{zz})'_r \qquad \text{(A-13)}$$

$$(\gamma_{xz})_r = -\frac{(\sigma_{xz})'_r}{G} \qquad \text{(A-14)}$$

where $(\sigma_{zz})'_r$ and $(\sigma_{xz})'_r$ are the pseudoresidual stresses and $(\gamma_{xz})_r$ is the residual engineering shear strain. Furthermore, the residual stresses $(\sigma_{xx})_r$ and $(\sigma_{yy})_r$ become

$$(\sigma_{xx})_r = (\sigma_{xx})'_r - \frac{\nu}{(1 - \nu)}(\sigma_{zz})_r \qquad \text{(A-15)}$$

$$(\sigma_{yy})_r = (\sigma_{yy})'_r - \frac{\nu}{(1 - \nu)}(\sigma_{zz})_r \qquad \text{(A-16)}$$

APPENDIX B
STATIC ANALYSIS OF SIMPLE SPINDLE MODEL

The static flexibility of the simple spindle model shown in Fig. 3.6 is derived in this appendix. The model consists of a uniform single diameter shaft of outside diameter D and bore d supported by two bearings, a chuck and a workpiece. The bearings have static stiffness K_f and K_r. Bearing spacing is 'l' and the overhang distance of the cutting point from the front bearing is 'a'. The spindle diameter D and bore d are assumed to be effective over the width of the chuck and workpiece so that the cutting point flexibility can be entirely accounted for by simple bending of a uniform shaft and bearing deflections. For simplicity shear deflections are neglected while the usual assumptions of homogeneity, linearity and isotropy are considered.

For a force F applied at the cutting point, bearing reactions are

$$R_f = (l+a)/l \cdot F \quad \text{and} \quad R_r = (-a/l) \cdot F \tag{B-1}$$

and the corresponding deflections are

$$\Delta_f = (l+a)\cdot F/(l\cdot K_f) \text{ and } \Delta_r = -\,a\cdot F/(l\cdot K_r) \tag{B-2}$$

Due to the bearings alone the deflection at the cutting point is

$$\Delta_c = \Delta_f + (a/l)\cdot(\Delta_f - \Delta_r) = (l+a)/l\cdot\Delta_f - a/l\cdot\Delta_r \tag{B-3}$$

The component of deflection due to spindle bending can be found by integration of

the differential equation.

$$EI \cdot d^2y/dx^2 = M \qquad \text{(B-4)}$$

where E is Young's Modulus and I is the second moment of area of the spindle and M is the bending moment.

Using the notation shown in Fig. 3.6 this equation can be written as

$$EI \cdot d^2y/dx^2 = [F \cdot x]_0^{(l+a)} - [R_f(x-a)]_a^{(l+a)} \qquad \text{(B-5)}$$

where the limits shown outside the square brackets denote the region of validity of the terms inside the brackets.

Integrating twice with respect to x and using the boundary conditions y = 0 at x=a and y = 0 at x=a+l gives, for x=0

$$y_{(x=0)} = \Delta_s = (a^3 + l \cdot a^2)/(3 \cdot EI) \cdot F \qquad \text{(B-6)}$$

The net spindle deflection at the cutting points is

$$\begin{aligned} \Delta &= \Delta_s + \Delta_B \\ &= F \cdot ((a^3 + l \cdot a^2)/3EI + (l+a)^2/(l^2 \cdot K_f) + (a/l)^2/K_r) \end{aligned} \qquad \text{(B-7)}$$

and the cutting point static flexibility is hence given as follows:

$$C_{sp} = \frac{a^3}{3 \cdot E \cdot I_a} + \frac{l \cdot a^2}{3 \cdot E \cdot I} + \frac{1}{K_f} \cdot \left(1 + \frac{a}{l}\right)^2 + \frac{1}{K_r} \cdot \left(\frac{a}{l}\right)^2 \qquad \text{(B-8)}$$

where a = length of overhang

l = bearing span

E = elastic modulus of material

I_a = area moment of inertia of overhang

I = area moment of inertia of span between bearings

$K_f K_r$ = stiffness of front and rear bearing respectively

REFERENCE LIST

1. Kronenberg, M., Machining Science and Application, Pergamon, London, 1965.

2. Nakayama, K.,"Studies on the Mechanism of Metal Cutting," Bull. Fac. Eng. Yokohama Nat. Univ., 8, 1956, pp.1-9.

3. Usui, E., and Hirota, A.,"An Energy Approach to Mechanics of 3 Dimensional Metal Machining," Proc. Inst. Conf. on Prod. Eng., Tokyo, 1974.

4. Nakayama, K., and Ari, M.,"On the Storage of Data on Metal Cutting Forces," C.I.R.P. , Vol. 25, 1976, pp.1-18.

5. Osgood,"Residual Stress in Machined Surfaces," Trans. A.S.M.E., Vol. 73, 1951, pp.69-76.

6. Heniksen, E.K.,"Residual Stress in Machined Surfaces," Trans. A.S.M.E., Vol. 73, 1951, pp.69-76.

7. Okushima, K., and Kakino, Y.,"The Residual Stress Produced by Metal Cutting," C.I.R.P., Vol. 20, No.1, 1971, pp.13-14.

8. Lojczok, M.R.,"A Study of Some Aspects of Metal Machining Using the Finite Element Method," Ph.D. Dissertation, North Carolina University, 1980.

9. Liu, C.R., and Barash, M.M.,"The Mechanical State of the Sublayer of a Surface Generated by Chip Removal Process, Part 1 & 2," Trans. A.S.M.E., Vol. 98, Nov.,1976,pp.1192-1208.

10. Barash, M.M., and Schoech, W.J.,"A Semi-Analytical Model of the Residual Stress Zone in Orthogonal Machining," Proc. 11th Int. Mach. Tool Design & Res. Conf., Sept., 1970, Pergamon Press, London.

11. Field, M., Kahles, J.F., and Cammett, J.T.,"A Review of Measuring Method for Surface Integrity," Proc. Inst. Mech. Engrs., Vol. 177, 1976, pp.236-245.

12. Merwin, J.E., and Johnson, K.L.,"An Analysis of Plastic Deformation in Rolling Contact," Proc. Inst. Mech. Engrs., Vol. 177, 1976, pp.676-690.

13. Albrecht, A.B., "How to Secure Surface Finish in Turning Operations," American Machinist, Vol.100, 1956, pp.133-136.

14. Chandiramani, K.L., and Cook, N.H.,"Investigations on the nature of Surface Finish and its Variations with Cutting speed," Trans. A.S.M.E., Vol.86, No 3, Ser. B., 1970, pp.134-140.

15. Olsen, K.V., "Surface Roughness in Turned Steel Components and the Revant Mathematical Analysis," The Production Engineer, December 1968, pp.593-606.

16. Sata, T., "Surface Roughness in Metal Cutting," C.I.R.P., Ann Alen Band, Heft, 4., 1964, pp.190-197.

17. Solaja, Vladimir, "Wear of Carbide Tools and Surface Finish Generated in Finish Turning of Steel," Wear, Vol.2, 1958-1959, pp.40-58.

18. Ansell,C.T., and Taylor J.,"The Surface Finish Properties of a Carbide and Ceramic Tool," Advances in Machine Tool Design and Proc. of 3rd Int. M.T.D.R. Conf., Pergamon Press, New York, 1962, pp.235-243.

19. Armarego,E.J.A., and Brown, R.H., The Machining of Metals, Prentice Hall, New York, 1969,p.78.

20. Taraman, K., "Multi Machining Output-Multi Independent Variable Turning Research by Response Surface Methodology," Int. J. Prod. Res., Vol.12, No 2, 1974, pp.233-245.

21. Wu, S.M., "Tool Life Testing by Response Surface Methodology," Parts I and II, Trans. A.S.M.E., Vol.86, 1964, p.105.

22. Chandrupatha, T.R.,"Dimensional Accuracy in Tuning Cylindrical Shafts," A.S.M.E. Paper, No 82-Prod-14.

23. Bajpai, S.,"Optimization of Workpiece Size for Turning Accurate Cylindrical Parts," Int. J. M.T.D.R., Vol. 12, 1972, pp.221-228.

24. Rao, P.N., Rao, U.R.K., and Rao, J.S.,"Toward Improved Design of Boring Bar, Part 2," Int. J. M.T.D.R., Vol. 28, No. 1, 1988, pp.33-44.

25. Loladze, T.N.,"Nature of Brittle Failure of Cutting Tool," C.I.R.P., Vol. 24, 1955, pp.13-16.

26. Trent, E.M., Metal Cutting , Butterworths, London, 1977.

27. Wright, P.K., and Trent. E.M.,"Metallurgical Appraisal of Wear Mechanisms and Processes on High Speed Steel Cutting Tools," Metals Technology, Jan.,

1974, pp.13-23.

28. Huet, J.F., and Kramer, B.M.,"The Wear of Ceramic Tools", Proc. 10th NAMRC, Mamaster University, Hamilton, Ontario, 1982, SME, p.297.

29. Bhattacharyya, A. and Ham, I.,"Analysis of Tool Wear, Part 1: Theoretical Model of Flank Wear", A.S.M.E., J. Eng. Ind., Vol. 91, 1969, pp.790-798.

30. Rubenstein, C.,"An Analysis of Tool Life Based on Flank Wear, Part 1:Theory," A.S.M.E., J. Eng. Ind., Vol. 98, 1976, pp.221-226.

31. Bhattacharyya, A., and Ghosh, A.,"Diffusion Wear of Cutting Tools," Proc. 5th M.T.D.R. Conf., 1964, pp.225-242.

32. Usui, E., and Shrakashi, T.,"Analytical Prediction of Cutting Tool Wear," Wear, Vol. 100, 1984, pp.129-151.

33. Dawihl, W.,"Study of the Wear of Cemented Carbide Tools," Sahl unf Eisen, Vol. 61, 1941, p.210.

34. Trent, E.M.,"Some Factors Affecting Wear on Cemented Carbide Tools," Proc. Inst. Mech. Engrs., Vol. 166, p. 192.

35. Venkatesh, V.C.,"Diffusion Wear of High Speed Steel Tools," Advances in Machine Tool Design and Research, Vol. 401, 1966.

36. Colding, B.N.,"Testing of Machinability by Radioactive Methods," Acta Polytechnia Scandinavia Me., Vol. 1, 1958, p127.

37. Landau, Y.D., Adaptive Control: The Model Reference Approach, Marcel Dekker, New York, 1979.

38. Centner, R.,"Final Report on Development of Adaptive Technique for N.C. Milling Machines," Bendix Research Lab., Technical Documentary Report No. ML-TDR-64-279.

39. Davis, R.P., Wsyk, R.A., Agee, M.H., and Kimbler, D.L.,"Optimizing Machining Parameters in a Frame-Work for Adaptive Computer Control," Computers and Industrial Engineering, Vol.4, 1980, pp.143-151.

40. Optiz, H.,"Adaptive Control - Fundamental Principles for Numerical Optimization of Cutting Conditions," ASME Proc. Int. Conf. on Manufacturing Technology, Sept., 1967, pp.25-28.

41. Yonetsu, S., Inasaki, I., and Kijima, T.,"Optimization of Turning Operation," 6th NAMRC, 1978, pp.17-23.

42. Jaeschke, J.R., Zimmerly, R.D., and Wu, S.M.,"Automatic Cutting Tool Temperature Control," Int. M.T.D.R., Vol.7, No.4, Dec., 1967, pp.465-475.

43. Koren, Y., and Masory, O.,"Adaptive Control with Process Estimations," Annals of C.I.R.P., Vol.30, No.1, 1981, pp.373-380.

44. Tlusty and Elbestawi, M.,"Constraints in Adaptive Control with Flexible End Mills," Annals of C.I.R.P., Vol.28, 1979, pp.417-421.

45. Defilippi, A., and Ippolito, R.,"The Influence of Constraints on Cutting Condition Optimizations," Annals of C.I.R.P., Vol.24,1975, pp.417-421.

46. Cook, N.H.,"Adaptive MAchining Parameter Selection," 5 th NAMRC, 1977, pp.344-356.

47. Kaminskaya, V.V.,"Trends in the Development of Adaptive Control," Machines and Tools, Vol. 45, No.8, 1974, pp.66-70.

48. Koren, Y.,"Dynamic and Static Optimization of the Cutting Process," 1st NAMRC, Hamilton, May, 1973, Vol.3, pp.67-94.

49. Schlueter, R.A., Retford, E.T., and Van Wieren, S.,"The Optimal MAchine Tool Control Problems," Trans. A.S.M.E., J. Dyn. Sys. Meas. Control, Vol.100, 1978, pp.191-200.

50. Boothroyd, G., Fundamentals of Metal Machining and Machine Tools, McGraw-Hill, New York, 1971.

51. Wu, S.M., and Ermer, D.S.,"Maximum Profit as the Criterion in the Determination of the Optimum Cutting Conditions," Trans. A.S.M.E., J. Eng. Ind., Vol.88, 1966, pp.435-442.

52. Ermer, D.S.,"Optimization of the Constrained Machining Economics Problems by Geometric Programming", Trans. A.S.M.E., J. Eng. Ind., Vol.93, 1971, pp.1067-1172.

53. Papalambros, P.,"Monotonicity in Goal and Geometric Programming," A.S.M.E. Paper No. 80-Det-48.

54. Ermer. D.S., and Kromodihardjo, S.,"Optimization of Multipass Turning with Constraints," Trans. A.S.M.E., J. Eng. Ind., Vol.103, 1981, pp.462-468.

55. Kops, L.,"Economical Aspects of Cutting Speed Slection When Turning Stepped Parts," Trans. A.S.M.E., J. Eng. Ind., Vol. 93, 1971, pp.1067-1172.

56. Bedini, R., and Pinitti, P.C.,"Experiments on Adaptive Constrained Control of CNC Lathe," Trans. A.S.M.E., J. Eng. Ind., Vol.104, 1982, pp.139-150.

57. Ulsoy, A.G., Koren, Y., and Rasumussen, F.,"Principal Developments in the Adaptive Control for Batch Manufacturing", A.S.M.E. WAM, Dynamic Systems and Control Division, Hart, D.E., 1982, pp.105-119.

58. Yen, D.W., and Wright, P.K.,"Adaptive Control in Machining - A New Approach Based on the Physical Constraints of Tool Wear Mechanisms," Trans. A.S.M.E., J. Eng. Ind., Vol.105, 1983, pp.31-38.

59. Tobias, S.A., Machine Tool Vibration, Blackie and Son Ltd., London, 1965.

60. Sisson, T.R., and Kegg, R.L.,"An Explanation of Low Speed Chatter Effects," A.S.M.E. Journal of Engineering for Industry, Vol. 91, Nov. 1969.,pp.951-955.

61. Tlusty, J.,"A Method of Analysis Machine Tool Satbility," M.T.D.R. Conf., 1965.

62. Kondo, Y., Kawano, O., and Sato, "Behavior of Self Excited Chatter Due to Multiple Regenerative Effect," A.S.M.E. Journal of Engineering for Industry, Vol.103, Nov. 1965, pp.447-454.

63. Tlusty, J., and Ismail, F.,"Special Aspects of Chatter in Milling," Trans. A.S.M.E., J. of Mech. Design, 1981, pp.1-9.

64. Piispanen, V.,"Lastunmoudostimisen Teoriaa," Teknillen Aika Kauslehti, Vol. 27, 1937, p.315.

65. Merchant, M.E.,"Mechanics of the Cutting Process," J. Appl. Phys., Vol. 16, 1945, pp.267-318.

66. Kobayashi, S., and Thomsen, E.G.,"Some Observations of the Shearing Process in Metal Cutting," Trans. A.S.M.E., J. Eng. Ind., Vol. 81, 1959, p.251.

67. Palmer, W.B., and Oxley, P.L.B.,"Mechanics of Orthogonal Machining," Proc. Inst. Mech. Engrs., Vol. 173, 1959, p. 623.

68. Okushima, K., and Hitomi, K.,"An Analysis of the Mechanics of Orthogonal Cutting and its Application to Discontinuous Chip Formation," Trans. A.S.M.E., J. Eng. Ind., Vol. 83, 1961, p.68.

69. Wardle, F.P., Lacey, S.J., and Poon, S.Y.,"Dynamic and Static Characteristics of a Wide Speed Range Machine Tool Spindle," Precision Engineering, Vol. 141, 1982, pp.175-183.

70. Welbourn, D.B., and Smith, J.D., Machinne Tool Dynamics: Introduction, Cambridge Univ. Press, Cambridge, 1970.

71. Rakhit, A.K., Sankar, T.S. and Osman, M.O.M.,"The Influence of Metal

Cutting Forces on the Formation of Surface Texture in Turning," M.T.D.R., Vol.16, 1970, pp.281-292.

72. Sankar,T.S., and Osman,M.O.M.,"Profile Characterization of Manufactured Surfaces using Random Function Excursive Technique," A.S.M.E. Journal of Engineering for Industry, Vol.97, Feb. 1975,pp.190-195.

73. Rakhit, A.K., Osman, M.O.M., and Sankar, T.S.,"Machine Tool Vibrations: Its Effect on Manufactured Surfaces," Proc. 4th Canadian Congress Appl. Mech., Montreal, 1973, pp.463-464.

74. Hasegawa, M., Seireg, A.A., and Lindberg, R.A., "Surface Roughness Model for Turning," Tribology International, Dec. 1976, pp.285-289.

75. Weiner, J.H., "Shear Plane Temperature Distribution in Orthogonal Cutting," Trans. A.S.M.E., Nov. 1955, pp.1331-1341.

76. Chao, B.T., and Trigger, K.J.,"The Significance of the Thermal Number in Metal Machining," Trans. A.S.M.E., Feb,1954,p.109.

77. Loewen, E. G., and Shaw,M.C.,"On the Analysis of Cutting Tool Temperature," Trans. A.S.M.E., Feb., 1954, p.217.

78. Leone, W.C.,"Distribution of Shear Zone Heat in Metal Cutting," Trans. A.S.M.E., Jan. 1954, p.121.

79. Boothroyd,G.,"Temperatures in Orthogonal Cutting," Proc. Inst. Mech. Engrs, Vol. 77, No. 29, 1963, p.789.

80. Chao,B.T., and Trigger,K.J.,"Temperature Distribution at the Tool-Chip Interface in Metal Cutting," Trans. A.S.M.E., Oct. 1955, p.1107.

81. Levy, E.K., Tsai C.L., and Groover M.P.,"Analytical Investigation of the Effect of Tool Wear on the Temperature Variations in a Metal Cutting Tools," Trans. A.S.M.E., J. Eng. Ind., Feb., 1976, pp.251-257.

82. Koren,Y., and Lenz,E.,"Mathematical Model for the Flank Wear While Turning Steel with Carbide Tools," Proc. CIRP Seminars on Manufacturing Systems, Vol. 1, No. 2, 1972, pp.127-137.

83. Hahn,R.S.,"On the Temperature Developed at the Shear Plane in the Metal Cutting," Proceedings of the First U.S. National Congress of Applied Mechanis, 1951, pp.661-666.

84. Block,H.,"Theoretical Study of Temperature Rise at Surface of Actual Contact Under Oiliness Lubricating Condition," Proceedings of General Discussion Lubrication and Lubricants, 1955, Vol.2, p.222.

85. Rapier, A.C.,"A Theoretical Investigation of Temperature Distribution in the Metal Cutting Process," Br. J. Appl. Phys.,1954, Vol. 5,No. 11,p.400.

86. Dutt, R.P., and Brewer, R.C.,"On the Theoretical Determination of the Temperature Field in the Orthogonal Machining," Int. J. Prod. Res.,1964,Vol.4, pp.91-114.

87. Trent,E.M.,Metal Cutting, Butterworths, London, 1977.

88. Carslaw, H.S., and Jaeger, J.C., Conduction of Heat in Solids, Oxford Press, Oxford, 1959.

89. Bowden, F.P., and Tabor, D.,"Area of Contact Between Solids," The Friction and Lubrication of Solids, Oxford University Press, London,1954, pp.5-32.

90. Boothroyd, G., Eagle, J.M., and Chisholm, W.J.,"Effect of Flank Wear on the Temperatures Generated During Metal Cutting," M.T.D.R., 1969, pp.669-679.

91. Kannatey-Asibu, E.Jr.,"A Transport-Diffusion Equation in Metal Cutting and Its Application to Analysis of the Rate of Flank Wear," A.S.M.E., J. Eng. Ind., Vol.107, 1985, pp.81-89.

92. Tlusty, J., Lecture Note for Production Engineering, U. of Florida, 1987.

93. Connoly, R.,and Rubenstein, C.,"The Mechanics of Continuous Chip Formation in Orthogonal Cutting," Int. J. Mach. Tool. Des. Res., Vol. 8, 1968. pp.158-187.

94. Bailey,J.A.,"Friction in Metal Machining-Mechanical Aspects," Wear, Vol. 31, 1975, pp.245-275.

95. Smith,J.O., and Liu,C.K.,"Stress Due to Tangential and Normal Loads on an Elastic Solid with Application to Some Contact Stress Problems," Trans. A.S.M.E., J. of Appl. Mech. Vol.20, No.2, 1953.

96. Kaczmarck,J.,Principles of Machining by Cutting, Abrasion and Erosion, Peter Peregrinus Limited, Stevenage, England, Oxford, 1950.

97. Hill,R., The Mathematical Theory of Plasticity, Clarendon Press, Oxford, 1950.

98. Barber,J.R.,"Thermoelastic Displacement & Stresses Due to a Heat Source Moving over the Surface of a Half Plane," Trans. A.S.M.E., 1984, pp.636-640.

99. Gill,S.,"A Process for the Step by Step Integration of Differential Equations in an Automatic Digital Computing Machine," Proc. Camb. Phil. Soc., Vol.47, 1951, pp.90-108.

100. Leskovar, P., and Peklenik, J.,"Influence Affecting Surface Integrity in the Cutting Process," C.I.R.P., 1981, pp.245-248.

101. Balakrishnam, P., and Devries, M.F.,"Sequential Estimation of Machinability Parameters for Adaptive Optimization of Machinability Data Base Systems," Trans. A.S.M.E., J. Eng. Ind. Vol. 107, 1985, pp.159-166.

102. Chandrasekaran, H., and Nagarajan, R.,"On Certain Aspect of Transient Stresses in Cutting Tools," Trans. A.S.M.E., J. Eng. Ind., Vol. 102, 1980, pp.133-141.

103. Takeyama, N.,"Performance of Carbide Tools in Machining 18-8 Stainless Steel," Trans. A.S.M.E., Vol. 83, 1961, pp.572-579.

104. Nigm, M.M., Sadek, M.M., and Tobias, S.A.,"Dimensional Analysis of the Steady State Orthogonal Cutting Process," M.T.D.R., Vol. 17, 1976, pp.1-18.

105. Box, M.J.,"A New Method of Constrained Optimization and Comparison with Other Methods," The Comp. J., Vol. 8, 1965, pp.42-52.

106. Fox, R.L., Optimization Methods for Engineering Design, Addition-Wesley, Massachusetts, 1971.

107. Rao, S.S., Optimization: Theory and Applications, Wiley-Eastern, India,1979.

108. Pipkin, N.J., Roberts, D.C., and Wilson, W.I., "Amborite-- A Remarkable New Cutting Tool Material from DeBeers," Industrial Diamond Review, Vol.40, June, 1980, p. 203.

BIOGRAPHICAL SKETCH

The author was born January 20, 1956, in Bee-In, the middle part of Korea. He moved to Seoul when he was 11 years old and graduated from Shil-Il Middle and High School. He entered the Seoul National University and spent most of his time there until he came to America, earning his B.S. and M.S. from that university. He continued his study in the Ph.D program, and he was awarded a Westinghouse Fellowship for continued research at the University of Florida. He met his lovely wife, Hyemin, in 1982 and married in 1983. Their lovely son, Kukjin was born in 1983. After he finishes his studies, he plans to start his career in the industry for the world prosperity.

I certify that I have read this study and that in my opinion it conforms to acceptable standards of scholarly presentation and is fully adequate, in scope and quality, as a dissertation for the degree of Doctor of Philosophy.

Dr. Ali A. H. Seireg, Chairman
Ebaugh Professor of Mechanical Engineering

I certify that I have read this study and that in my opinion it conforms to acceptable standards of scholarly presentation and is fully adequate, in scope and quality, as a dissertation for the degree of Doctor of Philosophy.

Dr. George N. Sandor
Research Professor of Mechanical Engineering

I certify that I have read this study and that in my opinion it conforms to acceptable standards of scholarly presentation and is fully adequate, in scope and quality, as a dissertation for the degree of Doctor of Philosophy.

Dr. Ulrich H. Kurzweg
Professor of Aerospace Engineering, Mechanics, and Engineering Science

I certify that I have read this study and that in my opinion it conforms to acceptable standards of scholarly presentation and is fully adequate, in scope and quality, as a dissertation for the degree of Doctor of Philosophy.

Dr. Gary K. Matthew
Associate Professor of Mechanical Engineering

I certify that I have read this study and that in my opinion it conforms to acceptable standards of scholarly presentation and is fully adequate, in scope and quality, as a dissertation for the degree of Doctor of Philosophy.

Dr. Bruce H. Edwards
Associate Professor of Mathematics

This dissertation was submitted to the Graduate Faculty of the College of Education and to the Graduate School and was accepted as partial fulfillment of the requirements for the degree of Doctor of Philosophy.

May, 1990

for Dr. Winfred M. Phillips
Dean, College of Engineering

Dr. Madelyn M. Lockhart
Dean, Graduate School